Dissertation
submitted to the
Combined Faculties for the Natural Sciences and for Mathematics
of the Ruperto-Carola University of Heidelberg, Germany
for the degree of
Doctor of Natural Sciences

Put forward by

Hossein Ebadi

born in Khomein, Iran

Oral examination: 29th June 2011

Stabilization and interference in high-frequency laser driven atoms

Referees: **Prof. Dr. Christoph H. Keitel**
Prof. Dr. Thomas Gasenzer

Zusammenfassung

Die grundlegende Dynamik von Modell-Atomen unter dem Einfluss intensiver XUV-Laser wird theoretisch mit Hilfe der nicht-relativistischen Schrödinger Gleichung und den klassischen Bewegungsgleichungen untersucht. Hierbei ist das Hauptziel den genauen Mechanismus von Rückstreuung und den Einfluss von Interferenzen auf die finale Elektronenenergieverteilung zu verstehen. Diese Arbeit baut Untersuchungen von ATI Photoelektronenspektren von Modell-Atomen weiter aus und findet Spuren von Starkfeldrückstreuung sowie deutliche Abweichungen der sogenannten Starkfeldapproximation durch Kopplung von gebundenen Zuständen bei hohen Frequenzen. In der Phasendarstellung sind die Photoelektronenspektren dem niedrigen Frequenz Fall (IR) bemerkenswert ähnlich und deutliche klassische Trajektorien können für hoch energetische Photoelektronen beobachtet werden. Die Energieanalyse der Photoelektronenspektren zeigt Starkfeldeffekte (Ionisation und Rückstreuung) aus den gebundenen Kramers-Henneberger Zuständen. Eine Zeitanalyse der ATI-Spektren weißt eine deutliche Stabilisierungsdynamik sowie eine Ionisationsverstärkung durch den Drift des Wellenpaketes im Stabilisationsregime auf. Es wurde festgestellt, dass die Kramers-Henneberger Zustände im Stabilisationsregime kohärent koppeln, was zu einer totalen destruktiven Interferenz der emittierten elektronischen Wellenpakete aus den beiden benachbarten gebundenen Zuständen in denselben Kontinuumszustand führt.

Abstract

Fundamental dynamics of a model atoms exposed to intense XUV lasers are studied theoretically by means of the non-relativistic Schrödinger and classical equations of motion. The main goal was to understand the detailed mechanism behind the rescattering and the influence of the interferences on the final electron energy distribution. This work advances the studies of above-threshold ionization photoelectron spectra from model atoms and finds strong field rescattering signatures and clear deviation from the strong field approximation due to the coupling of bound states at high frequencies. The photoelectron spectra are remarkably similar to the low frequency (IR) case in the phase-space representation and clear classical trajectories can be observed for high energy photoelectrons. The energy analysis of photoelectron spectra demonstrates strong field effects (ionization and rescattering) from the multiple bound Kramers-Henneberger states. A time-analysis of ATI spectra shows a clear stabilization dynamics and ionization enhancement due to the drift of the wavepacket in the stabilization regime. It has been found that the Kramers-Henneberger states in the stabilization regime are coupled coherently which results in a fully destructive interference of the emitted electronic wave packet from the two adjacent bound states to the same continuum state.

Contents

Chapter 1

Introduction

Light has been a topic of interest in the history of physics and was studied where it is visible by human eye. In addition to its interaction with medium, as an electromagnetic wave light can travel through medium and vacuum with diffraction or interference effects. The nature of light fueled a lot of investigations that led to the verification of quantum theory. However, relativistic theory of quantum mechanics is entangled to the light. The study of light-matter interactions is helpful to understand of matter in the microscopic size and history of the universe. The radio-frequency sources are used in the magnetic-resonance and its application in medical science. The electromagnetic wave with infrared frequencies are used to identify the functional groups in material science. The chemical scientists utilize the light of visible and ultraviolet frequencies to consider the electronic structure of molecules. The shorter wavelengths in x-ray regime have enormous application in the condensed matter and solid state science.

Technological advances have led to the development of lasers with a duration of a few optical cycles and intensity of pettawats in a wide variety of frequencies. Thus, the light-matter interaction can be studied from the linear regimes where the light is a perturbation compare to the atom field, right through to where the light-field is so strong that the atom field can be considered as a perturbation compared with the light field.

The discovery of the laser in 1960 [1] provided scientists with an exceptional tool that had a wide variety of applications. With the progression of technology, by 1961 the intensity of the lasers was enough high to generate second-harmonic radiation [2]. In the development of laser technology a pronounced progress has been achieved by Q-switching technique which delivered pulses to the nano-second domain with a laser intensity of megawatts. Mode-locking and chirped pulse amplification (CPA) are technologies which allowed one to achieve a laser intensity up to $10^{20}\,\mathrm{Wcm}^{-2}$ in the femtosecond domain [3]. Due to the application of short pulses in science, the main part of the technological development has been devoted generating of intense pulsed lasers. Nowadays, a few femtosecond ($10^{-15}\,\mathrm{seconds}$) pulse in the visible and near-infrared frequencies can be produced experimentally. To reduce the pulse duration the facilities should be extended to higher

frequencies which is feasible today with high harmonic generation (HHG) [4, 5] and excellent free electron facilities in the world such as FLASH, SCSS and LCLS [6]. By these new light sources, the experimentalists are able to use frequencies in the extreme ultraviolet (XUV) or soft X-ray regime entering the research area of the attosecond (10^{-18} seconds) time scale, so called attophysics. The short pulses enable one to consider ultrafast phenomena such as molecular vibration or electron dynamics in atoms and molecules which cannot be achieved by normal light sources.

With these high intensity light sources many non-linear and non-perturbative processes were discovered, such as multiphoton ionization, coherent radiation of multiple frequencies of deriving laser by atoms and molecules, laser-assisted electron-atom collisions and other collective dynamics in complex systems.

Atomic physics in an intense laser pulse was started with multi-photon ionization of Xenon gas with a ruby laser by Delone *et al.* in 1965 [7]. Multiphoton ionization (MPI), however, was predicted by Göppert-Mayer, where an atom can ionize by absorbing of many photons if the energy of a single photon is even much smaller than the ionization potential [8]. However, she was awarded Nobel prize for her contribution in the theoretical studies of nuclear structure.

The next important phenomenon, which has been called above threshold ionization (ATI), was discovered by Agostini *et al.* in 1979 [9]. It has been found that, at sufficient high intensities (of about $10^{13}\,\mathrm{Wcm}^{-2}$), an electron is able to absorb more photons than the minimum required for MPI.

Another intense field effect related to ATI is high-order harmonic generation (HHG), where an atom or molecule responds nonlinearly to a strong laser field to emit radiation with harmonics of the laser frequency [10, 11]. This phenomenon is a very important tool for developing table-top high-frequency XUV lasers with duration in the attosecond domain. The fundamental intense field processes are schematically explained in Fig. 1.1. Here the frequency of the light, ω, is assumed to be much smaller than the ionization potential. Intense field studies start with near-IR frequency i.e. 800 nm is called low frequency regime. In low frequency strong laser fields, when the electric field component of an electromagnetic field competes with Coulomb field of an atom, the ionization process happen via static electric field ionization, i.e. tunneling through an effective potential resulting from Coulomb and electric field. In the tunneling ionization the time that the electron needs to escape through the potential barrier is small compared to the period of the laser field. The ionization mechanism, however, can be different with respect to the intensity and frequency of the laser pulse. The theoretical approach for the quasistatic ionization for the first time was considered by Popov [13] and further developed by Amosove, Delone and Krainov, the so-called ADK theory [14]. The new high-intensity radiation sources at XUV frequencies give access to the interaction regimes which are far from the ADK tunneling condition, such as over-the barrier suppression and high frequency nontunneling

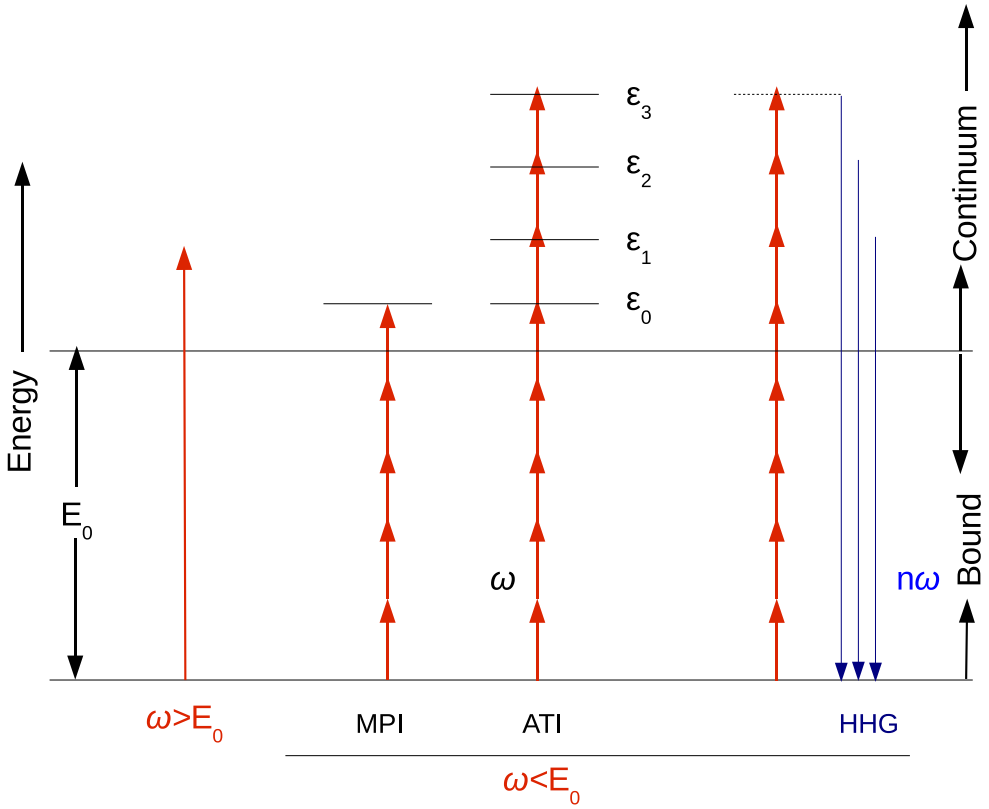

Figure 1.1: Fundamental intense field processes of a single active electron atom with ionization potential E_0. The absorption of a number of photons to the threshold is multiphoton ionization (MPI). Absorption of more photons than necessary for the threshold ionization is called, above threshold ionization (ATI). Ionized electrons can recombine to the ground state or excited states to produce high order harmonics (HHG) of driving laser's frequency (adapted from Fig.(1.1) in ref. [12]).

ionization.

Stabilization of atoms in a super-intense laser field is another phenomenon, which has been intensively studied since 1990. Initially, it was predicted theoretically by Gavrila [15]. The two main mechanisms of stabilization are the Kramers-Henneberger (KH) [16, 17] or adiabatic stabilization [18] and interference stabilization (IS) of Rydberg atoms [19]. The interference stabilization was observed in experiments by Noordam *et al.* [20, 21]. The adiabatic (KH) stabilization can be theoretically treated by two formalism, quasi-energy stabilization (QS) [15] and dynamic stabilization (DS) [22]. In QS it is assumed that the strong field is a continuous monochromatic wave. The situation in pulsed laser, however, is very different and the strong fields are usually produced in a form of very short time with different shape. Hence, to prob the response of an atom in a pulsed laser, one has to consider a fully time-dependent dynamical problem including the pulse shape. The first investigation that the atom could survive in the strong pulse, was done by Su *et al.* [22]. The early investigations of stabilization were based on the time-dependent Schrödinger equation of the model atoms [23]. The stabilization of a three-dimensional model atom

was considered classically by Lewenstein *et al.* [24] and quantum mechanically by Kulander *et al.* [25]. Other studies based on the one and two dimensional short range model potentials have been reported by other authors [26,27]. The results of the stabilization dynamics from different authors were partly in agreement and partly in disagreement [25–27]. It is noted that the stabilization of an atom in a strong laser pulse is classical in nature. There is no unified classical and quantum mechanical study to clarify the classical and quantum signatures of the stabilization dynamics. A comprehensive classical and quantum mechanical investigation is desirable in different dimensions in an unified picture. Moreover, the stabilization dynamics, which have been intensively studied, from the theoretical point of view, for the lowest ionization potential (hydrogen atom) needs a high frequency laser pulse in the XUV regime. This can be accessed today and the near future.

The subject of the present work is to theoretically investigate the response of a single active electron in an intense laser field in the XUV frequency regime with different approaches such as the time-dependent Schrödinger equation (TDSE), classical simple man's model (SM) and classical-trajectory Monte Carlo (CTMC). The combination of different approaches allows one to investigate the ionization, rescattering , interferences in the stabilization regime at high frequencies and compare to the low frequency condition in the tunneling regime. The following questions for high frequency case in strong fields have been addressed within this work:

- Rescattering of photoelectrons in high frequency domain;
- Time-analysis of ionization in strong laser fields;
- The mechanisms of interferences in the stabilization regime.

Chapter 2

Fundamentals of strong field dynamics

Interaction of matter with light is one of the fundamental subjects of physics. Optical spectroscopy is an important tool to study the structure of matter and has enormous application in all area of science. However, in its early times the aim of linear optical spectroscopy was focused on the emission or absorption of light. To obtain spectral properties of matter, the sample had to be excited by a non-radiating process such as thermal sources and collision with an accelerated particles or absorption a broad band of normal light. However, in some special cases, emitted light from some other atoms or molecules could be used to excite the sample, but the light could not be tunable. The situation changed dramatically with the invention of the lasers. The advances in electrical devices today allow to study the light-matter interaction in order to understand the dynamical processes in atomic level. In non-linear optical spectroscopy, experimental scientists are able to choose a light source with different frequencies, intensities and pulse lengths. With these new technologies, many new kinds of experiments are possible which are required a theoretical studies for the better understanding of physical and chemical processes. The topic processes described in this work are within the area of nonlinear processes in strong fields.

Note, that this chapter is intended to give an overview of well-known results in the field of this thesis and that major parts of this chapter have been adapted from the dissertations by Randerson [12], Ni [28], Bauch [29] and review by Protopapas *et al.* [30].

2.1 Interaction of light with free electron

The light as an electromagnetic wave is the solution of Maxwell's equations in free space [31]. The wave equation can be written in term of electric field as

$$\nabla^2\mathbf{E} - \frac{1}{c^2}\frac{\partial^2}{\partial t^2}\mathbf{E} = 0. \tag{2.1}$$

The simplest solution of Eq. (2.1) is the plane wave solution

$$\mathbf{E}(\mathbf{r},t) = \mathbf{E}_0 \cos(\mathbf{k}.\mathbf{r} - \omega t + \phi) \tag{2.2}$$

where $\omega = \frac{|k|}{c}$. The wave-vector $\mathbf{k}$ gives the direction of propagation, ω gives the frequency, and ϕ is a phase. The electric force, $\mathbf{F}$, acts on a charged particle with charge $q = -1$ a.u. as an electron has, given by

$$\mathbf{F} = -\mathbf{E}. \tag{2.3}$$

Given that the magnetic field is smaller than the electric field by a factor of $1/c$, the magnetic force is given by

$$\mathbf{F}_{\text{mag}} = \frac{\mathbf{v}}{c} \times \mathbf{B}. \tag{2.4}$$

Then the magnetic field effect on the particle's motion will be negligible if $|\mathbf{v}| << \mathbf{c}$, that is to say in the non-relativistic limit. In this work all fields are in the non-relativistic regime. Starting with Eq. (2.3), we can determine the equations of motion of a free electron in a sinusoidal plane wave of infinite duration. If the electron is initially at the origin with zero velocity, the problem is 1D along the polarization of the electric field (denoted x). Conceptually, the motion is oscillatory or quivering with the electric field. Using Newtons equations one arrives at

$$F = \ddot{x} \tag{2.5}$$

$$\ddot{x} = E_0 \cos(\omega t) \tag{2.6}$$

$$\dot{x} = \frac{E_0}{\omega} \sin(\omega t) \tag{2.7}$$

$$x = -\frac{E_0}{\omega^2} \cos(\omega t). \tag{2.8}$$

This model is called simple man's model (SM) which have been first introduced by Muller *et al.* [32] and it was frequently used to explain ionization dynamics in low frequency intense field regime. For an electric field of $E_0 = 0.007$ a.u. the maximum electron displacement is 2 a.u.. This is two times larger than the atomic size (a_0) of the hydrogen atom in the ground state according to the Bohr theory. For all examples in this chapter, radiation with a wavelength of 800 nm (Ti:Sapphire laser) is assumed. The electrons with a small initial velocities, however, cannot move far away from the origin. For larger intensities, the electron can oscillate within a long distance from the atomic core up to several nanometers. Thus, in intense laser fields the infinite plane wave approximation is valid, where the electron motion can be described by above equations.

The second important feature of the simple man's model is the time averaged kinetic energy of an electron in a laser field so called ponderomotive potential, U_P, given by

$$U_P = \frac{1}{2}\langle v_x^2 \rangle = \frac{E_0^2}{4\omega^2}. \tag{2.9}$$

For a relatively small electric field $E_0 = 0.007$, the ponderomotive potential of a free electron is $U_P = 0.004$ a.u.. The ponderomotive energy which is proportional to the

intensity, gives a scale how much extra energy a part from the binding potential, I_P, an electron needs to be considered free. Later it will be shown that the effective ionization potential increases by U_P in laser field. Note that U_P is directly proportional to the intensity.

2.2 Interaction of electromagnetic field with atom

The time-dependent Schrödinger equation (TDSE) is a quantum mechanical theoretical tool for the investigation of the ionization processes of atoms and molecules in the non-relativistic regime. In atomic physics with super-strong lasers, the electromagnetic field is mostly treated classically and is also applied in this work without quantum electrodynamic effects due to the fact that the intensity of the light is high. By this assumption some phenomena like Lamb shift, spontaneous emission and the width of the the quantum states cannot be described [33]. On the other hand, classical treatment of the intense external field explains and predicts the response of a system to the external fields quite well. The stationary quantum effects like spontaneous emission are negligible compared to the stimulated and light induced effects, such as emission or absorption of many photons. Quantum electrodynamic effects can be considered in the relativistic domain which is not the subject of this work.

In the classical representation of the electromagnetic field the electric field, $\mathbf{E}(\mathbf{r},t)$, and the magnetic field $\mathbf{B}(\mathbf{r},t)$ are illustrated by a vector potential $\mathbf{A}(\mathbf{r},t)$ and a scalar potential $\phi(\mathbf{r},t)$ [31]:

$$\mathbf{E}(\mathbf{r},t) = -\nabla\Phi(\mathbf{r},t) - \frac{1}{c}\frac{\partial \mathbf{A}(\mathbf{r},t)}{\partial t} \quad \text{and} \quad \mathbf{B}(\mathbf{r},t) = \nabla \times \mathbf{A}(\mathbf{r},t) \tag{2.10}$$

which are determined from the solution of Maxwell's equations. Another formulation of Maxwell's equations are based on the the vector and scalar potentials,

$$\nabla^2\phi + \frac{1}{c}\frac{\partial}{\partial t}(\nabla.\mathbf{A}) = 0 \tag{2.11}$$

$$\nabla^2\mathbf{A} - \frac{1}{c^2}\frac{\partial^2 \mathbf{A}}{\partial t^2} - \nabla(\nabla.\mathbf{A} + \frac{1}{c}\frac{\partial \phi}{\partial t}) = 0, \tag{2.12}$$

with gauge freedom associated with the potentials, A and ϕ. The formulation of quantum mechanics in the external fields are also based on potentials rather than fields. Similarly, the time-dependent quantum dynamics are formulated in two common gauges so-called length and velocity gauges.

The TDSE of one particle in an external potential $V(\mathbf{r})$ interacting with a vector potential $\mathbf{A}(\mathbf{r},t)$ and a scalar potential $\phi(\mathbf{r},t)$ via minimal coupling reads in atomic units,

$$\frac{1}{2}(\hat{\mathbf{p}} + \frac{1}{c}\mathbf{A}(\mathbf{r},t))^2\Psi(\mathbf{r},t) - \phi(\mathbf{r},t)\Psi(\mathbf{r},t) + V(\mathbf{r})\Psi(\mathbf{r},t) = i\frac{\partial}{\partial t}\Psi(\mathbf{r},t) \tag{2.13}$$

in which $\hat{\mathbf{p}} = -i\nabla$ is the momentum operator and $V(\mathbf{r})$ is a one particle potential, like ionic Coulomb potential [34]. By the vanishing scalar potential ($\phi(\mathbf{r}, t) = 0$), only the vector potential $\mathbf{A}$ is coupled to the system in Eq. (2.13). This potential is included in a one-electron Hamiltonian by replacing the classical momentum operator with the canonical momentum operator Π;

$$\mathbf{\Pi} = \mathbf{p} + \frac{1}{c}\mathbf{A}. \tag{2.14}$$

This brings the Hamiltonian of (2.13) to

$$\hat{H} = \frac{1}{2}\mathbf{\Pi}^2 + V(\mathbf{r}) \tag{2.15}$$

$$= \frac{1}{2}\left[\mathbf{p}^2 + \frac{1}{c}(\mathbf{p}.\mathbf{A} + \mathbf{A}.\mathbf{p}) + \frac{1}{c^2}\mathbf{A}^2\right] + V(\mathbf{r}). \tag{2.16}$$

This can be grouped into a field-free zeroth-order Hamiltonian, $\hat{H}_0$, and an interaction term, $\hat{H}_{\text{int}}$ which are given by

$$\hat{H}_0 = \frac{1}{2}\mathbf{p}^2 + V(\mathbf{r}) \tag{2.17}$$

and

$$\hat{H}_{\text{int}} = \frac{1}{2c}(\mathbf{p}.\mathbf{A} + \mathbf{A}.\mathbf{p}) + \frac{1}{2c^2}\mathbf{A}^2. \tag{2.18}$$

Now, the whole interaction with the electromagnetic field is included in $\hat{H}_{\text{int}}$. We note that the canonical momentum $\mathbf{\Pi}$ and $\mathbf{P}$ are physically different. The equation of motion up to this point is exact in an external field. Although, there is no exact analytic solution of TDSE with Hamiltonian $\hat{H}_0 + \hat{H}_{\text{int}}$, nowadays, with advances in computer technology, it is possible to solve TDSE numerically. With further approximations such as the dipole approximation, one is able to solve the TDSE numerically up to two electrons in a combined Coulomb and laser field at the moderate intensities. As the dipole approximation is used in this work for the interaction Hamiltonian, it is briefly explained here.

Dipole approximation

The interaction Hamiltonian, $\hat{H}_{\text{int}}$, contains the scalar products $\hat{\mathbf{p}}.\mathbf{A}$ and $\mathbf{A}.\hat{\mathbf{p}}$ [34]. The expression has simpler form and its implementation in numerical techniques is easier, if the dipole approximation is applied. Generally according to Maxwell's equations, the vector potential $\mathbf{A}(\mathbf{r}, t)$ depending on space and time is given by

$$\mathbf{A}(\mathbf{r}, t) = \mathbf{A}_0 \cos(\eta), \quad \eta = \mathbf{k} \cdot \mathbf{r} - \omega t \tag{2.19}$$

where $\mathbf{k}$ is the wave vector. If the interaction region is small and the vector potential is uniform within this range ($\mathbf{k} \cdot \mathbf{r} << 1$), its spatial dependence can be neglected. A Taylor

expansion of the vector potential (up to first order) with respect to the first argument gives

$$\mathbf{A}(\mathbf{r},t) = \mathbf{A}_0\cos(\mathbf{k}_0\mathbf{r}_0 - \omega t) - \mathbf{A}_0\sin(\mathbf{k}_0\mathbf{r}_0 - \omega t)(\mathbf{k}\cdot\mathbf{r} - \mathbf{k}_0\mathbf{r}_0) + \cdots \tag{2.20}$$

$$= \mathbf{A}^{\mathrm{d}}(\mathbf{r}_0,t) + \mathbf{A}^{\mathrm{q}}(\mathbf{r},t) + \cdots . \tag{2.21}$$

Hence $\mathbf{A}^{\mathrm{dipole}}(\mathbf{r}_0,t)$ is independent of position, $\mathbf{r}$, and the corresponding electric field

$$\mathbf{E}^{\mathrm{d}}(\mathbf{r},t) = \mathbf{E}(t) = -\frac{1}{c}\frac{\partial}{\partial t}\mathbf{A}^{\mathrm{d}}(t) \tag{2.22}$$

is also independent of position [33]. Within the dipole approximation the interaction Hamiltonian, $\hat{H}_{\mathrm{int}}$ in velocity gauge is given by

$$\hat{H}^V_{\mathrm{int}} = \frac{1}{2}\left[\frac{1}{c}\mathbf{A}(t).\hat{\mathbf{p}} + \frac{1}{c}\hat{\mathbf{p}}.\mathbf{A}(t)\right] + \frac{1}{2c^2}\mathbf{A}(t)^2 = \frac{1}{c}\hat{\mathbf{p}}.\mathbf{A}(t) + \frac{1}{2c^2}\mathbf{A}(t)^2 \tag{2.23}$$

To study magnetic field effects in quantum dynamics, the easiest way is to include quadrupole and higher order terms of Eq. (2.21) into the interaction Hamiltonian.

There is an alternative gauge which is easier to implement numerically is called length gauge. While in quantum mechanics the observables and wavefunction are invariant under gauge transformation, one can write

$$\Psi^L(\mathbf{r},t) = \exp(-\frac{i}{c}\mathbf{A}(t)\cdot\mathbf{r})\Psi^V(\mathbf{r},t) \tag{2.24}$$

which is equivalent to a gauge transformation of the interaction Hamiltonian of Eq. (2.23). By inserting the transformed wavefunction $\Psi^L(r,t)$ in Eq. (2.13) with the dipole approximation one gets

$$i\frac{\partial}{\partial t}\Psi^L(\mathbf{r},t) = \left(\frac{1}{2}\hat{\mathbf{p}}^2 + \mathbf{r}\cdot\mathbf{E}(t) + V(\mathbf{r})\right)\Psi^L(\mathbf{r},t) \tag{2.25}$$

Thus the interaction Hamiltonian in length gauge is defined by

$$\hat{H}^{\mathrm{L}}_{\mathrm{int}} = \mathbf{r}\cdot\mathbf{E}(t), \tag{2.26}$$

which is valid only with the dipole approximation [33]. However, one can use the length gauge and include the magnetic interaction to the time-dependent Hamiltonian of the system by a Taylor expansion of the vector potential in respect to the position.

Intense field parameters

Since strong-field physics of atoms and molecules began with development of the intense lasers, the dynamics of the electrons in external lasers can be characterized with two parameters.

A direct ionization of electron form atomic or molecular potential can be identified by Keldysh parameter [35]. Keldysh described an adiabaticity parameter, which is known as the Keldysh parameter γ. It shows the validity of the tunneling model of the ionization and can be defined as a ratio of tunneling time of a bound electron in a combined external field and core potential to the period of the laser field,

$$\gamma = \frac{\omega_{\text{laser}}}{\omega_{\text{tunnel}}} = \frac{\omega_{\text{laser}}\sqrt{2I_p}}{E_0} = \sqrt{\frac{I_p}{2U_P}} \tag{2.27}$$

where I_p is the ionization potential of a Coulomb field, E_0 is the electric field amplitude. The last term in Eq.(2.27) indicates γ in terms of I_P and the ponderomotive potential of the field. For low frequency lasers when $\gamma << 1$, ionization happens via tunneling, while the multiphoton ionization happens for $\gamma >> 1$. For a low intensity and high frequency laser fields where $\gamma > 1$, multiphoton ionization dominates, while for a high intensity where $\gamma < 1$, tunneling ionization or over-the-barrier ionization will be significant. The Keldysh parameter indicates the weak field regime where $\gamma >> 1$ and strong-field regime where $\gamma << 1$. The ionization dynamics with $\gamma = 1$ can be a mixture of MPI and tunneling type. Near-perturbative and intense field effects are briefly explained in the next paragraphs.

Second intense field parameter is ponderomotive energy, U_P, which leads to the effective ionization potential in intense laser field, $I_P + U_P$, and it identifies the classical signatures of motion in a laser field like maximum energy cutoff of ATI and HHG spectra.

2.3 Low intensity regime

Now we consider the effect of a light field on an atom, specifically the response of the atomic energy levels when they are perturbed by an external laser field [36].

Near-linear response

As we mentioned above, in near-linear response regime Keldysh parameter is much larger than unity, $\gamma >> 1$. The well-known effects of linear response of the electronic structure of atoms and molecules are the direct photoionization and the resonant excitations by absorption of photons. The main part of the studies in linear response regime is to identify spectral properties of the sample. For intensities in the linear response regime the electron can absorb photons and oscillates between the bound states. If the photon energy is larger than the ionization potential, $\omega >> I_P$, the electron can be also ionized as the photoelectric effect. Near-linear response effects happen in the intensity region up to $I < 10^{13}\,\text{Wcm}^{-2}$ for a typical 800 nm wavelength and the energy levels of the atomic system are no longer static. A detailed of the interaction of light with atoms in near perturbation regime can be found in an early review by Mainfray *et al.* [38].

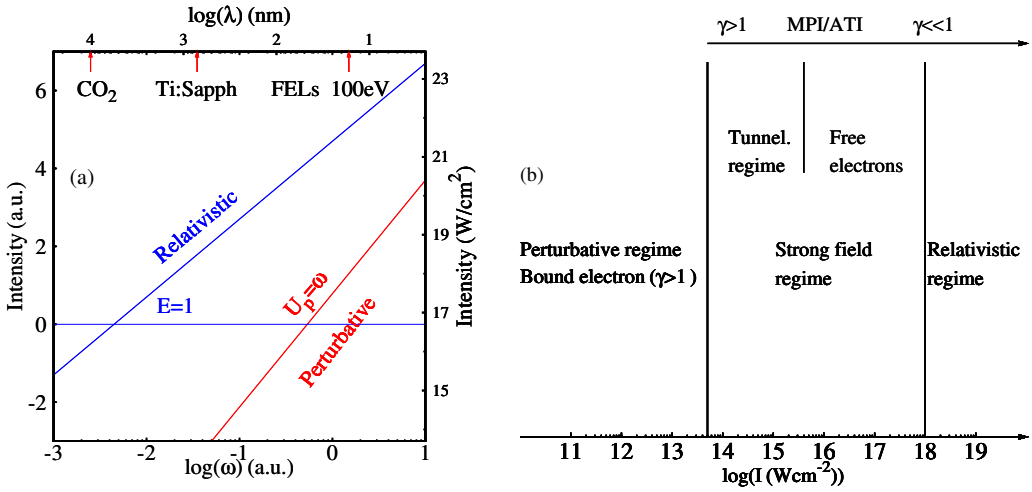

Figure 2.1: Schematic diagram showing different intensity regimes with respect to the intensity parameters: (a) U_P (adapted from Fig.(1) in ref. [37]). (b) γ for 800 nm Ti:Sapphire laser (adapted from Fig.(2.1) in ref. [29]).

AC-stark shift

The Stark shift is one of the most and interesting effects of the light field on the atomic structure. Although, this effect is an old topic of the light-matter interaction [39], it has influence on the ionization dynamics and dynamic resonances in laser-atom interaction [40]. The interaction Hamiltonian based on the vector potential associated with a monochromatic laser field with the dipole approximation is given by Eq. (2.23). With monochromatic approximation for the laser field $\mathbf{E}(t) = -c\partial_t \mathbf{A}(t)$, the matrix element of the interaction Hamiltonian in the basis of field-free states can be calculated via perturbation theory. The result up to the second order perturbation theory [39, 41] for the linear polarized light field along the x axis takes the form

$$\delta E_n = \frac{E_0}{4\omega_l^2} - \frac{E_0}{4\omega_l^2}\left[\sum_{n\neq m} 2|\langle\psi_n|x|\psi_m\rangle|^2 \frac{\omega_{mn}^2}{\omega_{mn}^2 - \omega_l^2}\right]. \tag{2.28}$$

In the above expression, the sum in the second term has infinite terms which should be used with a finite number in practice, ω_{mn} is the energy gap of field-free states and $2\omega_{mn}|\langle\psi_n|x|\psi_m\rangle|^2$ is the oscillator strength. The first term is ponderomotive potential which results from the zeroth order term of the perturbation method and the second term is the second-order correction. The atomic polarizability due to the interaction with an external field, can be calculated from the similar expression.

For weakly bound states or Rydberg states, $\omega_{mn} << \omega$, the Ac-Stark shift is equal to the ponderomotive energy [41, 42].

For deeply bound states (for example the ground state) the energy-gap of the atomic levels is much larger than the laser frequency (here $\lambda = 800\,\text{nm}$), $\omega_{mn} >> \omega$, thus the

sum is dominated by oscillator strengths. In this case the Ac-stark shift is canceled by the ponderomotive energy.

With this condition, in case of low intensity and small frequency lasers, $\omega_l << \Delta E_{nm}$,

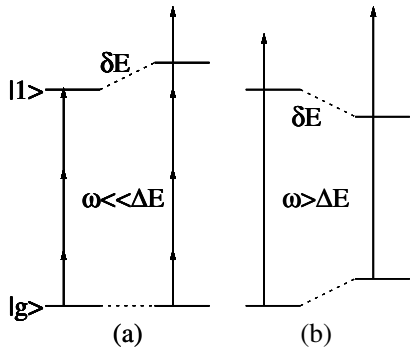

Figure 2.2: Schematic diagram of Ac-Stark shift for the two lowest bound states. The laser frequency is much smaller than energy gap in (a) and is larger than energy gap in (b).

the energy of the ground state changes slightly due to the Ac-Stark shift. The weakly bound states and the continuum stats are shifted by ponderomotive potential. This leads to an effective ionization potential increasing by U_P (Fig. 2.2(a)). The direction (sign) of the Ac-stark shift depends on the frequency of the laser field. For frequencies larger than the energy gap of the field-free states, the energy of the lowest state increases and the energy of the upper state decreases (Fig. 2.2(b)). For the high frequency lasers, $\omega_l > I_P$, the energy of the first dressed state increases and the energy of the other dressed states decreases with respect to the intensity of the laser pulse.

In the stabilization regime, the atomic potential completely is deformed by laser field and the large Stark shift can be considered in the framework of Kramers-Henneberger states which will be explained later.

By going to higher intensities some other processes occur, so called strong-field effects. In the following sections, some of strong-field processes in atoms and molecules at moderate intensities ($10^{12} \simeq 10^{14}\,\mathrm{Wcm}^{-2}$) are summarized.

2.4 High intensity regime

The production of intense laser pulses has been advanced by chirped pulse amplification technique. The term 'intense' is used for the intensities greater than $10^{13}\,\mathrm{Wcm}^{-2}$ but nowadays the intensities of about $10^{22}\,\mathrm{Wcm}^{-2}$ [43] in a wide variety of frequencies are available. It is also important that the pulse duration for intense lasers reaches in a femtosecond or attosecond domain. The intensity I, and the electric field E, of a laser

pulse are related to each other by

$$I = \frac{1}{2}\epsilon_0 c E^2 \tag{2.29}$$

where ϵ_0 is the permittivity of vacuum and c the speed of light. For example, the Coulomb electric field in a hydrogen atom is about $5.0 \times 10^9\,\mathrm{V/cm}$ corresponding to an equivalent intensity of $3.51 \times 10^{16}\,\mathrm{Wcm^{-2}}$ [30].

If the ionization rate or ionization probability of the dynamics being studied, at such high intense laser pulses, during the raising edge of the pulse all atoms will ionize. Then the population of atoms in the original field-free states become zero when the maximum of the pulse arrives. Intense lasers drive many simple and correlated nonlinear processes that compete with weak-field processes. The ponderomotive force, that is negligible in the linear regime, becomes significant. Moreover, the Ac-Stark shift and ponderomotive energy have different impact in the energy shift of the levels and effective ionization potential. As a result, it is necessary to develop theoretical models and techniques beyond the limits of conventional perturbation theory. Several theoretical methods are nowadays used to investigate the interaction of matter with intense laser fields. However, in quantum mechanical approaches most of the methods are based on single active electron approximation and recently these methods are developed for few photon ionization of two active electron systems. The theoretical models and calculations suggest new experiments and new experiments require new analytical or numerical techniques. The most of the new experiments in this area cannot be considered in theory without approximations.

One area of strong-field physics which has been extensively studied, is multiphoton ionization (MPI) meaning that an atom or molecule ionized by the absorption of several photons with the frequency much smaller than the ionization potential. The first order perturbation theory cannot provide a reliable rate for MPI, but higher order terms in the perturbation expansion are able to describe the MPI process at the moderate intensities [38]. The MPI rate could be measured by counting either the ions or the electrons with time-off flight experiments. The energy distribution of the ionized electrons in intense field regime shows that some of electrons have absorbed more than the minimum number of photons necessary to reach the continuum. This high energy electrons was related to a phenomenon was called above threshold ionization (ATI) [9].

From history of physics, the absorption and emission spectra of atoms and molecules led gradually to the confirmation of stationary quantum theory. In strong-field regime these processes helped the understanding of the atomic and molecular processes within the short time scales. The following sections focus on the fundamentals of the ionization dynamics in intense laser fields and gives an overview of the knowledge in this topic in the well studied low frequency regime. The presented overview is partly discussed in some references of multiphoton processes in intense laser fields [30, 44, 45].

2.4.1 Multiphoton ionization

Since 1960, multiphoton processes including ionization and excitation were intensively studied. Early MPI investigations have been done by Delone *et al.* [46] theoretically and studied later by Mainfray *et al.* [38]. Multiphoton ionization is an extension of a single photon ionization known from the photoelectric effect. The ionization potentials (I_P) of many atoms and molecules is larger than a few electron-volts. Thus, a single photon ionization requires visible light or shorter wavelengths (see Fig. 1.1) which results in the electron kinetic energy of $E_k = \omega - I_P$.

Atoms or molecules can also be ionized in a radiation field with frequencies smaller than the ionization potential, by absorbing multiple photons as predicted by Göppert-Mayer [8]. In intense field regime, in the absence of resonances of the laser frequency with dressed states, absorption of multiple photons proceeds through the virtual states, with an infinitely small lifetime which specified by the uncertainty principle. Multiphoton ionization occurs via absorption of a large number of photons which indicates the requirement of high intensity laser or high photon flux, I/ω. The resulting electron kinetic energy in the continuum after MPI is given by

$$E_k = m\omega - I_P(I). \tag{2.30}$$

where m is the minimum number of photons needed for ionization. The ionization potential I_P now depends on the intensity, because the AC-Stark shift and ponderomotive potential cannot be neglected at high intensities. The intensity dependent ionization potential can be approximated by $I_P(I) = I_P(I = 0) + U_P$. The MPI results in $E_m \leq \omega$. This implies that the MPI in the photoelectron spectra show a red shift with increasing of the intensity. However, in high frequency lasers in the stabilization regime due to the larger Ac-Stark shift respect to the U_P the MPI shows a blue shift. The MPI probability can be approximately explained by LOPT, in which the m-photon ionization rate is given by $T_m = \sigma_m I^m$, where I is the laser intensity and σ_m is the absorption cross section of MPI or one can call it generalized absorption cross section. From the history of quantum mechanics, according to Bohr theory the electron oscillates between the two orbits if there would be an additional light wave with the frequency equal to the energy gap between the two states. This effect is called static resonance without Stark shift and the other dynamical effects. In modern quantum mechanics, however, the Bohr theory is no longer valid. Therefore, strong-field dynamics needs to take in to account non-stationary effects which are absent in the Bohr theory. The MPI in intense field regime was first described theoretically by Keldysh [35] beyond the perturbation theory for short-range potential in circularly polarized light.

One of the weak-field processes which can compete with MPI is resonance excitation. If the final state $|\phi_f\rangle$ is not a continuum state and is a bound states with an energy level which fulfills the resonance condition

$$E_f - E_0 = n_{\text{res.}}\omega \tag{2.31}$$

the multiphoton excitation is possible. Eq. (2.31) is a generalization of static Bohr theory of multiphoton transition, which is not a static resonance in intense field regime and mainly is a dynamical process [40, 47]. Now the electron can ionize with single photon or MPI from the excited state. This process has been studied in literature and will be briefly reviewed latter. However, electron can be stabilized via Rabi oscillation which is not yet well understood. The excited electron, however can emit photon and relax to the ground state.

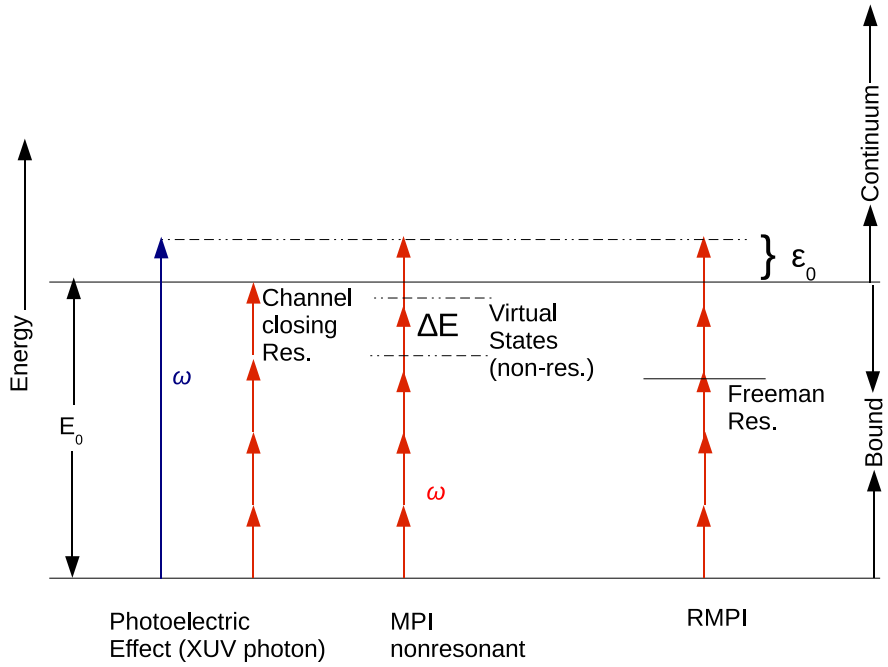

Figure 2.3: Schematic illustration of multiphoton ionization processes, from an initial quantum state with binding energy E_0 in a static representation. Each process results in a free electron with kinetic energy ϵ_0. The photoelectric effect requires a single (typically UV) photon. The MPI process can occur with multiple lower energy photons. A dynamic resonant multiphoton ionization (RMPI) which can have either higher probability because of the lifetime of the bound states or lower probability because of Rabi coupling (adapted from Fig.(2.1) in ref. [12]).

Above-threshold ionization

MPI itself, however, exist only for low intensities near to the linear response limit. In high intensity lasers, photonelectrons can be observed at photon numbers higher than the minimum number of photons for the MPI. These higher order photoelectrons are called above-threshold ionization (Fig. 2.1). The ATI is an important intense field effect which has been observed for the first time in 1979 by Agostini [9]. A series of photoelectron peaks appears in the photoelectron spectra. One has to add n extra photons to the equation

Eq. (2.30) to calculate the position of the ATI peaks

$$E_k = (n+m)\omega - I_P - U_P \tag{2.32}$$

where n is called the number of extra or above-threshold photons absorbed by the electron [48]. Lowest order perturbation theory cannot be used anymore for the ATI for laser intensities above $10^{13}\,\mathrm{Wcm}^{-2}$. This is due to the fact that the higher-order terms in the frame work of perturbation theory become significant but it makes the calculation more difficult with a little improving of the results. The methods beyond the perturbation were needed to take into account all strong-field effects such as Stark shift and resonance effects. In intense pulsed lasers, the bound states show a time-dependent Stark shift which induces a broadening in the ATI peaks. Moreover, due to the Stark shift the new field induced resonances appear between the dressed states. It was assumed that if the initial state is n-photon resonant with an excited state of the system, the ionization rate will be much larger than for non-resonant ionization. The ionization rate, however can be smaller than the non-resonant state due to the Rabi oscillation between the states [49]. It is noted that these processes are mostly valid for the low frequency regime where $\omega < I_P$. At higher frequencies when the electron ionizes with two or three photons, the Rabi oscillation and Raman type coupling play an important role in the ionization dynamics. The structure of the ATI spectrum is strongly related to the resonances between the dressed states which are briefly explained in the following.

Freeman resonances

The ATI is one of the strong-field effects which can be used as an experimental tools to study the internal dynamics of the atom during the interaction with a laser pulse. The first type of resonances was experimentally observed by Freeman *et al.* [48] in the ATI spectra of xenon atom. The lowest atomic dressed states due to the AC-Stark shift come in to a resonance and the ionization rate shows a resonant enhancement. The effect of the Freeman resonance, however, depends on the intensity and the length of the laser pulse in addition to the coupling strength of the resonant states. The original experiment considered the ATI processes using the dye laser pulses in the picosecond domain. As explained in previous section, the ATI spectra consist of a series of peaks with spacing of photon energy. In longer laser pulses, the peaks were narrower which is related to the photoelectric effect of a photon with infinite duration. Due to the spatial dependence of the intensity, the ATI peaks showed no red shift. In fact, the ponderomotive energy resulting from the long laser pulse can be converted to the kinetic energy. This process compensate the red-shift of ATI peaks. Electrons in a long laser pulse have enough time to response the spatial gradient of the laser pulse and the average energy due to the gradient of the laser pulse and Stark-shift will be canceled.

The situation is slightly different for shorter pulse. A series of less narrow ATI peaks were observed as in a longer pulse. In short pulse, the ATI peaks consist of some sub-peaks due to the light-induced resonance of dressed states. In a laser pulse, the dressed states show an intensity dependent energies resulting from the Stark-shift, $E_{i_{\mathrm{res.}}} = E_i + U_P$, [48]

leading to

$$E_{k\text{res.}} = E_i + n\omega - I_p - U_P \tag{2.33}$$
$$= E_i(I=0) + U_P + n\omega - I_p - U_P \tag{2.34}$$
$$= n\omega - (I_p - E_i(I=0)). \tag{2.35}$$

The above equation shows that in resonance multiphoton ionization (RMPI) with an intensity dependent of energy levels, the final kinetic energy of the ionized electron is independent of the intensity and is related to the field-free binding energy of the initial state. By increasing of the intensity, some of the dressed states come to a n-photon resonance as it was observed in that experiment. We note that at VUV frequencies which is the subject of this work, the Freeman resonances play a more important role in the ionization dynamics and compete with other processes like Raman and Rabi couplings.

Channel closing resonances

Another resonance effect which has been theoretically and experimentally studied so called Channel closing resonance [50]. Channel closing resonance is related to the n-photon threshold ionization. By increasing of the laser intensity the ponderomotive energy will increase. As the effective ionization potential in a laser pulse is given by $I_P(I) + U_P$, the minimum number of photons to ionize electron exceed from n to $n+1$ with respect to the intensity. Channel closing resonance depends only to the ground states energy and lowest continuum states, this implies that this resonances can be considered well within the strong-field approximation.

Resonances with Rydberg states

Resonance process between the ground state and Rydberg states was first studied by means of the ATI spectra calculated by Muller [51]. The ground state is in resonance with Rydberg states via tunneling excitation and the average ionization probability increases. This resonance is similar to the one in the case of channel closing. The effect of the Rydberg levels on the rescattering part of the ATI spectra is reviewed later.

2.4.2 Tunneling ionization

When the laser intensity becomes very strong ($I > 10^{14}$ and $\lambda = 800\,\text{nm}$), the atomic potential is strongly deformed by the external laser field and the potential barrier shows a maximum that is called saddle point (see Fig.2.4(b)). One can consider the effect of the static field on the Coulomb potential in intense field ionization at low frequency regime as a good approximation, and calculate the ionization rate, the rate at which bound electrons can tunnel through the barrier. A comprehensive description of quantum tunneling can be found in the book by Razavi [52]. In the tunneling model of strong-field ionization, the laser field is treated classically in contrast to MPI, and the characteristic parameter is γ (I_P and U_P). There are two main approaches for the analytic calculation of ionization

rates, the Keldysh theory [35,53,54] and the Ammosov, Delone, and Krainov (ADK) theory [14]. All tunneled electrons are born with zero velocity at the moment of ionization. Based on ADK theory, the ionization rate is exponentially related to the field strength. Therefore, the most of electrons are produced at the peak of the laser field. The ionization probability is defined by first step and the evolution of ionized electron in the combined laser and Coulomb field determines the final kinetic energy of electrons. Due to the maximum tunneling probability at the peak of the field, the most of ionized electrons are not able to gain momentum from the field due to the fact that the electron has zero velocity. Thus the photoelectron spectrum shows an exponential decay with respect to the kinetic energy of electron.

Recently, it has been shown by Reiss [37] that the ideal tunneling regime $\gamma \to 0$, cannot be achieved due to the relativistic criterion and magnetic field effect, and tunneling process plays still an important role in the ionization dynamics in the transient regime $\gamma > 1$.

2.4.3 Over the barrier ionization

At certain intensity the initial bound state is not bound anymore. This is called over-the-barrier ionization (OTBI), Fig. 2.4(c), which is the extreme case of tunneling ionization. This occurs at a critical field value, F_c, given by

$$F_C = \pi\epsilon_0 \frac{I_P^2}{Z} \tag{2.36}$$

in the case of a pure Coulomb potential with nuclear charge Z and a bound state of energy E_b [55]. The corresponding intensity is given by

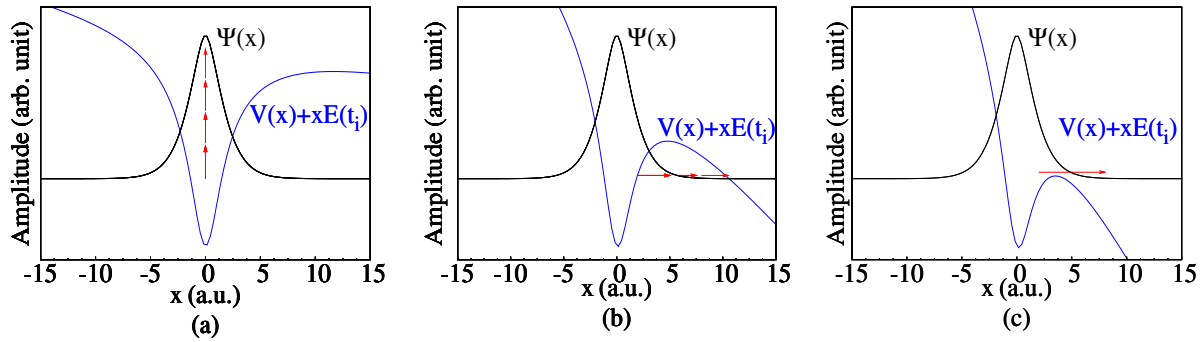

Figure 2.4: Schematic diagram for different photoionization mechanisms. The sum of atomic potential and the maximum electric field of the laser pulse. The dominant ionization process evolves from (a) multiphoton ionization at low intensity to (b) tunneling ionization at moderate intensity, and (c) Over-the-barrier ionization at higher intensity (adapted from Fig.(8) in ref. [30]).

$$I_{OTBI}[W/cm^2] = 4 \times 10^9 \frac{(I_P[eV])^4}{Z^2}. \tag{2.37}$$

For example, the critical intensity for the ground state of the hydrogen atom is $1.4 \times 10^{14}\,\mathrm{Wcm}^{-2}$ [55, 56]. The atoms can be ionized completely before the laser pulse reaches to its peak at low frequency regime. This is called saturation of the ionization, where the corresponding intensity can be smaller than the critical intensity. For Xenon atoms the saturation intensity is about $2.5 \times 10^{13}\,\mathrm{Wcm}^{-2}$, lower than the critical intensity $8.6 \times 10^{13}\,\mathrm{Wcm}^{-2}$ [57], which means that Xenon atoms ionize completely before I_{OTBI}. Thus the ionization of the Xenon atoms will be via MPI or tunneling rather than OTBI.

In intense laser fields in the low frequency regime ($\omega << I_P$), the electrons are ionized within each optical cycle around the peaks of the laser field in a short time scale in the attosecond domain. Therefore, with attosecond spectroscopy, one would be able to observe fundamental particles.

2.4.4 Atomic stabilization in a super strong laser field

Stabilization of atoms and molecules against of the ionization is one of the old and interesting features in quantum dynamics requiring ultra high intensity and high frequency lasers for the initially in the ground state of the bound electrons. Atomic stabilization at high frequency laser field was predicted theoretically by Gavrila [15, 18]. Nowadays, the experimental test of high frequency stabilization can be done with the new free-electron facilities in high frequency regime. The two main mechanisms of the atomic stabilization, are the Kramers-Henneberger (KH) or adiabatic stabilization [18] and interference stabilization (IS) of Rydberg atoms [19,20]. The stabilization of Rydberg atom was observed in experiments in 1992 [20,21]. The adiabatic (KH) stabilization can be treated by two forms theoretically, quasienergy stabilization (QS) [18] and dynamic stabilization (DS) [22]. As the aim of this work is the investigation of the ionization dynamics in high frequency intense laser fields, the mechanisms of the atomic stabilization are briefly discussed in the following.

Quasienergy stabilization in super strong laser field

Quasistationary stabilization can be formulated with the assumption of monochromatic and infinite duration of the laser field. The ionization rates of the dressed states which can be calculated from Floquet theory and its high frequency version, decrease with respect to the intensity in the super strong limits. There are different formulation of Floquet theory. High frequency and R-matrix Floquet theory have been intensively used in atomic physics in strong laser pulses [18].
This method, however, is limited to the monochromatic assumption of the laser field. The evolution from the field free-states to the monochromatic light induced state in a pulsed laser is a big question within this formalism.

Dynamic stabilization in super strong laser field

In dynamic stabilization, the electronic wavefunctions calculated in the KH potential,

$$V_{\mathrm{KH}}(\mathbf{r}+\alpha_0) = \int_0^{2\pi} \frac{dt}{|\mathbf{r} - x\alpha_0 \cos\omega t|}, \tag{2.38}$$

which depends only on the average electron displacement in an intense laser field, α_0, are well defined states for the quantum mechanical discussion of the stabilization. However, the higher order terms of the Fourier components of the KH potential involve in the time evolution of the quantum system which induces a fine structure in the photoelectron spectra (see chapter 5). In fully time-dependent simulations, the wavefunction in the high frequency laser field illustrates distorted and quasi-symmetrically dichotomy structure of the potential for the stabilized atom [25]. The KH potential and the corresponding electronic ground state wavefunction at two different α_0 are shown in Fig. 2.5. This figure show that the dichotomy of the wavefunction is well established at larger α_0. The ionization probability at the end of a laser pulse with an arbitrary shape and duration does not approach unity as the peak intensity is increased but either starts to decrease with the intensity or remains constant. The stabilization dynamics of the one-dimensional model atoms was investigated since 1990 by Su *et al.* [22] which provided valuable insights into this phenomenon. Later Geltman, one of the pioneers in the area of theoretical quantum dynamics investigated stabilization of one dimensional model atoms to clarify previous results [27]. Two and three dimensional models were also considered [25, 26]. However, more research is desirable to solve interesting open problems for high frequency light sources, such as XUV-FELs or attosecond pulses from high-harmonic generation.

In the next chapters we will show that the significant part of the ionization dynamics occurs via KH states at high frequency laser pulse in the stabilization regime. But due to the higher order terms of the Fourier components of the time-dependent potential, additional coherent coupling between the induced KH states exists which results in a destructive interference from a low-lying coupled KH states.

Interference stabilization of Rydberg atoms

A simple description of the interference stabilization is illustrated in Fig. 2.6. One can assumes that an atom is first excited to a certain high energy bound state (Rydberg state), ψ_n with energy $E_n = -1/(2n^2)$ where $n >> 1$. If a light with frequency $\omega > |E_n|$ interacts with this Rydberg atom, it can ionize the atom via one photon transition to the continuum. The ionization rate Γ_0 given approximately by a formula derived from the first order perturbation theory (Fermi's golden rule)

$$\Gamma_0 = 2\pi |V_{nE}|^2 = 2\pi | < \psi_n | \hat{H}_{\mathrm{int}} | \psi(E) > |^2 \tag{2.39}$$

where $\psi(E)$ and $E = E_n + \omega$ are the wavefunction and the energy of a photoelectron in the continuum [19]. The interaction Hamiltonian is given by $\hat{H}_{\mathrm{int}} = -\mathbf{d}\cdot\mathbf{E}$ where $\mathbf{d}$ is the dipole moment of an atom and $\mathbf{E}$ is the electric field amplitude of the laser. The ionization

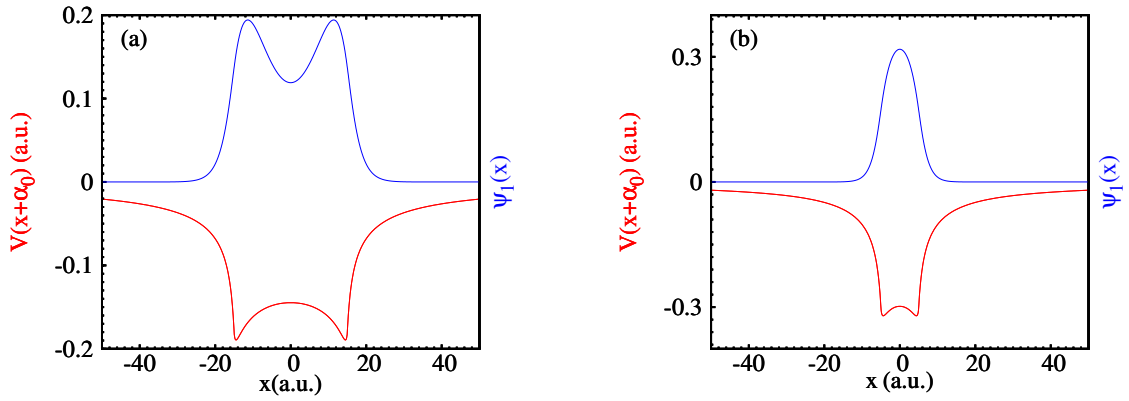

Figure 2.5: (red) the KH potential defined in Eq. (2.38) of a 1D model hydrogen atom irradiated by a high frequency laser pulse. (blue) Ground state electronic wavefunction in KH potential. (a) $\alpha_0 = 15$, (b) $\alpha_0 = 5$.

rate given by the above formula, depends linearly on the intensity, $I = E_0^2$. The width of the atomic level with energy E_n now is given by Γ_0. The validity of the perturbation theory is for small Γ_0 where the width of the states is smaller than the level spacing of Rydberg atom, i.e. ($\Gamma_0 \ll E_{n+1} - E_n \simeq 1/n^3$). In stronger fields, perturbation theory is not invalid when $\Gamma_0 \gg 1/n^3$. Another interpretation of above condition is that the ionization time $t_{ion.} = 1/\Gamma_0$ of an atom should be much longer than the classical Kepler period $t_{Kep.} = 2\pi n^3$. From classical mechanics [58], the motion of a charged particle of energy E_n in the Coulomb field is indicated in general by an elliptical orbit. The motion of the electron in Rydberg states can be also treated as a Kepler orbit. Therefore, in addition to the direct transitions to the continuum, one can expect also Raman-type transitions (see Fig. 2.6) resulting in a population transfer between the adjacent or a group of Rydberg levels [19]. The resultant coherent populations transfer of Rydberg levels are locked in phase. Thus, the subsequent transitions from these levels to the continuum interfere destructively and stabilize the atom against the ionization. The interference stabilization was observed in experiment by Noordam [20]. This type of interference was intensively studied theoretically by Fedorov and a comprehensive description can be found in Ref. [19].

2.5 Rescattering and recombination of electron in a laser field

The response of the atoms and molecules to such intense laser pulses were investigated via the ionization and dissociation dynamics of the electronic and nuclear motions. The frequency of the driving laser pulses were in the near-infrared regime. Therefore, the response of the atoms and molecules were similar to the single electron atoms in an intense

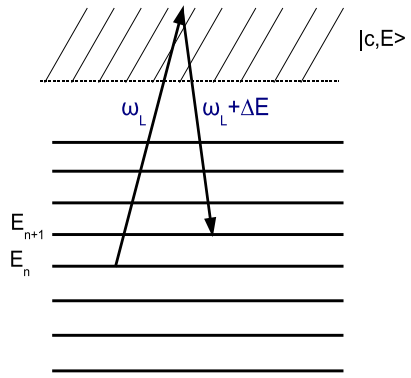

Figure 2.6: λ-type Raman transitions between the Rydberg levels of an atom leads to a coherent coupling among a group of Rydberg states (adapted from Fig.(1) in ref. [19]).

laser field. The low-frequency intense field dynamics can be grouped in three different phenomena.

Once electron is ionized by tunneling or OTBI, the freed electron moves classically in the laser field. First the electron accelerated by laser field and then after approximately one half of an optical cycle it returns back to the core when the laser field changes its sign. If this accelerated electron now returns to the core, three phenomena can occur. It can recombine to the ground state or another excited state and emit its energy as a high energy photon which is called high-harmonic generation (HHG) [59]. The electrons can also be elastically scattered from the parent ion, by absorbing extra photons form the laser pulse (high-energy ATI). The returning freed electrons can also be scattered inelastically by transferring part of their energy to another electron, in multi-electron atoms or molecules and release the second electron to the continuum Fig. 2.7 (NSDI). This simple three-step model, developed by Corkum [60] and Kulander *et al.* [61] based on an earlier simple-man's theory by Muller and van Linden van den Heuvell [32], illustrates these three important phenomena in one framework.

In the following the post processes after the ionization in the ATI and HHG are briefly reviewed as the high intensity observables for the understanding of strong-field processes.

2.5.1 Rescattering of above-threshold ionization

The general structure of ATI spectra in strong laser field is indicated in Fig. 2.8(a). This figure shows two different plateaus. The first one is connected to the direct photoelectron and second one is due to the rescattering of the ionized electronic wavepacket. As an important fundamental process of atomic physics in intense laser field, ATI has been

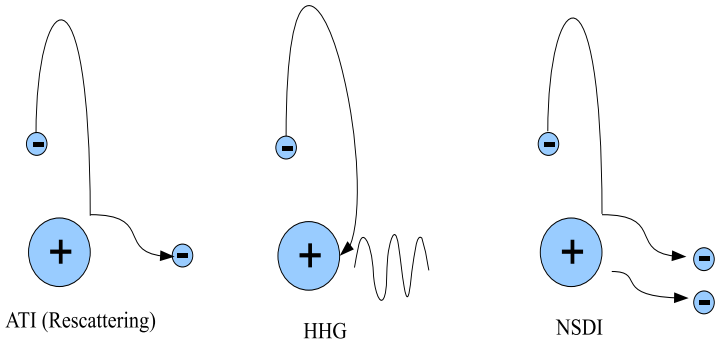

Figure 2.7: Schematic diagram for rescattering in above-threshold ionization (ATI), high-order harmonic generation (HHG) and non-sequential double ionization (NSDI), (adapted from Fig.(1.2) in ref. [28]).

intensively studied after its observation by Agostini [9]. If the ponderomotive energy becomes larger than the photon energy, the first ATI peak disappear from the spectrum due to a red shift [48]. The red-shift of the ATI peaks with respect to the intensity defines the channel closing resonance. A semi-classical model [60] indicates that the maximum energy that the electrons can gain from the laser field is $2U_P$.

The next features of ATI experiments observed by Paulus *et al.* [62] in the high kinetic energy electrons in the ATI spectrum. The ATI plateau and scattering rings of its angular distribution are explained in the framework of the three-step model [63, 64]. Van Woerkom *et al.* [65] and Muller *et al.* [66] both observed a resonant-like enhancement of rescattering and substructure in the plateau region of the ATI spectra. This process was explained by Muller *et al.* [51, 67–69] that the resonances to the Rydberg states above the saddle point of potential barrier increase the rescattering probability. The enhancement of the rescattering probabilities of the ionized electron in the plateau region via resonance to the Rydberg levels was shown theoretically by Maquet *et al.* [70].

In part II of this thesis, the above-threshold ionization of a model atom is considered theoretically for the XUV frequency fields. This investigation will help to achieve a deep understanding of the atomic photoionization process and rescattering in the strong attosecond XUV lasers. The ATI spectra in high frequencies show complex structure due to the different mechanisms of interference and coherent coupling of the dressed states.

2.5.2 High harmonic generation

HHG by atoms and molecules in intense laser fields is another interesting phenomenon. The electron in a laser field can return to the core and recombine to the ground or excited states by releasing a high energy photons with a non-linear response [60]. According to

the parity of the atomic wavefunction in the ground state, odd or even harmonics are emitted. Different atoms feel different intensities and phases with respect to the time and spatial variation of the laser pulse. The phase-matching condition ensures that only the harmonics with constructive interference survive. Generally, the power spectrum of HHG falls off in the first few orders, then a plateau of constant amplitude follows, and finally a sharp cut-off appears (see Fig. 2.8(b)). Semi-classical calculations based on simple

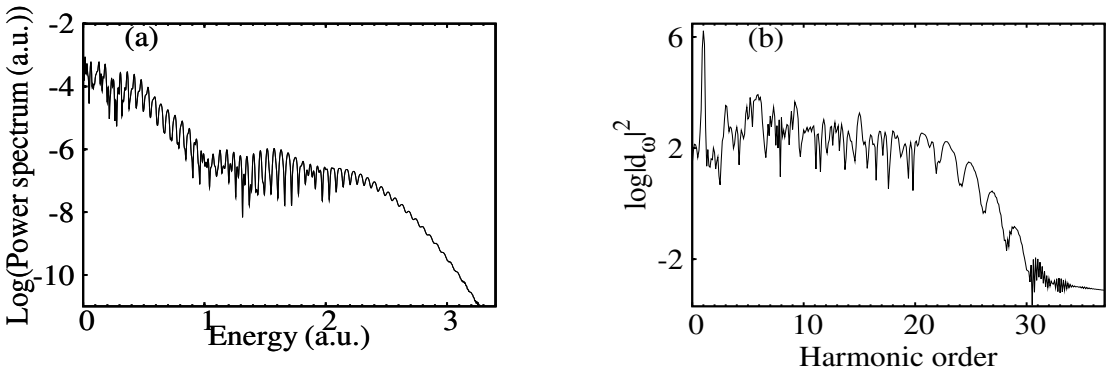

Figure 2.8: (a) The ATI spectra of an atom irradiated by an intense laser field of $\omega = 0.057$a.u. and $E = 0.054$ a.u. ($U_P = 0.22$ a.u.). (b) High harmonic spectrum generated by recombination of ionized electron wavepacket.

man's model and strong-field approximation give a maximum kinetic energy $3.17U_P$ for the emitted harmonics. This maximum energy related to the electrons that are ionized at certain phases with respect to the maximum of the laser field. Thus, the highest energy which can be observed as a harmonic is I_p+$3.17U_P$ where I_P is the ionization potential. In high frequency lasers where $\gamma > 1$, the harmonics can be observed higher than the classical cut-off prediction.

The HHG and ATI studies were started with 800 nm lasers but these studies were extended in long wavelength regime [71, 72]. As the ponderomotive energy decrease with the inverse of the square of the photon frequency the HHG cut-off was extended to the higher order in the long wavelength regime [73, 74].

There are many applications of HHG in studies of ultrafast dynamics in solid state devices and surfaces science similar to traditional spectroscopical method in linear response regime. Nowadays, ultrafast X-ray imaging is applied by X-ray sources from the free electron facilities in real applications in biology, which cannot be studied fully quantum mechanically.

The HHG of an atom in XUV-frequency will help to achieve a deep understanding of the role of the atomic potential on the electron dynamics and photoemission of the ionized

electron at XUV lasers.

The generation of attosecond laser pulses is another application of HHG. By combining a set of plateau harmonics or selecting of cut-ff harmonics sub-femtosecond or attosecond pulses can be generated. This allows one to study electron dynamics in attosecond time scale. As the main results of this work are based on the interaction of atom with XUV pulses in the sub-femtosecond and attosecond domain, the attosecond pulses are briefly reviewed in the following. The team around Muller [75] applied different streaking techniques (energy streaking and angular streaking) in pump-probe experiments in attosecond domain to study the fundamental dynamics with attosecond resolution. In chapter 4 we show a method to consider the time-profile of ionization which can be efficiently used in the theoretical study of pump-probe experiments.

2.6 Attosecond pulses

Time-resolved spectroscopy of atomic and molecular processes with femtosecond resolution by femtosecond laser pulses provided a huge wealth of understanding in physics and chemistry. Ahmed Zewail was one of the pioneer in time-resolved spectroscopy and he was awarded Nobel prize in 1999 for his contributions to femtochemistry. However, the electron dynamics in atomic ionization and bond formation occurs on a sub-femtosecond or attosecond time scale. Time-resolved spectroscopy with attosecond precision needs new light sources and the suitable time-resolved techniques.

The shortest laser pulse which was generated in a Ti:Sapphire laser was about 3.8 fs [76], which is very close to a single optical cycle (2.7 fs) at 800 nm. On the other hand, propagation of the electromagnetic pulse in an atomic or molecular medium needs at least one cycle. Therefore, it is not possible to make shorter the pulse durations at IR (800 nm) and smaller frequencies. In order to have a laser pulse with many cycles in attosecond domain, it is necessary to move to higher frequencies.

Nuclear motion in molecules are on a femtosecond time-scale. It can be assumed that at attosecond time scales nuclear motions are frozen. This allows one to probe the evolution of electronic wavepacket in matter. The short pulses in attosecond domain will increase the understanding in atomic and molecular physics, chemistry and material science. With such short pulses many processes such as, the evolution of wave packet (see chapter 4), electron transfer in the condensed matter and chemical reaction at surface can be studied. HHG is one of the common methods to generate short and train of laser pulses in the attosecond and sub-femtosecond domain. However, the new free-electron laser facilities such as LCLS, DESY and SCSS [6] are able to generate short laser pulses in attosecond domain with a wide variety of frequencies. Note, that this subsection is particularly close to ref. [28].

Generation

The most important technique for the generation of short pulses is mode-locking. A single short laser pulse can be produced by superimposing a broad band of frequencies via Fourier synthesis Fig. 2.9(a,b). The pulse duration is proportional to the inverse of the frequency bandwidth (see Fig. 2.9 for a schematic illustration). This method was first

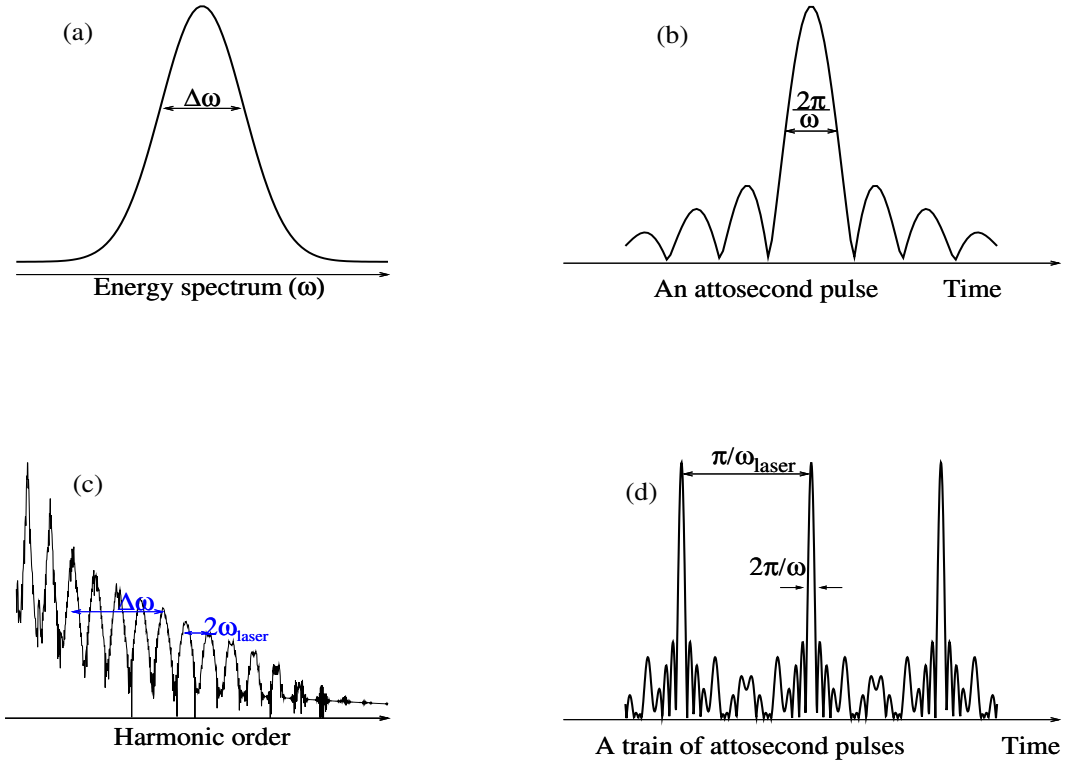

Figure 2.9: Schematic diagram of attosecond pulse generation (adapted from Fig.(1.5) in ref. [28]). (a,b) Generation of single attosecond laser pulses. (c,d) Generation of a train of attosecond laser pulses from a series of plateau harmonics. In (d) the two pulses are generated in a half of period of the driving laser pulse. (c) Is the HHG resulting from the three-dimensional TDSE code developed in this work.

proposed by Farkas *et al.* [77] and Harris *et al.* [78] based on HHG by an intense IR laser.

A train of attosecond pulses can be produced by superimposing a broad band of harmonics from the plateau region due to the fact that all harmonics in the plateau region have approximately equal amplitude Fig. 2.9(c). It has been shown by Antoine *et al.* [79] that the phase of harmonics in the plateau region are locked. Therefore, a single atom emits a train of ultrashort pulses Fig. 2.9(d). The harmonic emission occurs twice per half cycle corresponding to the long and short trajectories. A large number of theoretical calculations and experiments [80–83] have shown that the short and long trajectories correspond to the different ionization and return times. This means that the attosecond emissions

happen at two different field amplitudes corresponding to the short or long trajectories. Thus the HHG from the two trajectories have a different intensity dependent phase allowing to separate the two contributions via phase-matching. Due to the two trajectories, the time profile of the attosecond pulse is strongly related to this phase variation. Separation of single and long trajectories can be used to overcome this problem [79] and results in a better phase-matching.

Single attosecond pulses are necessary for pump-prob experiments. As HHG can only occur for linear polarization providing an electron-ion re-collision, Ivanov *et al.* [84] proposed an appropriate method to generate single attosecond pulses. In this method two driving laser fields of circular polarization are used with an opposite ellipticity. A linear polarized pulse is produced at a certain short time interval around the field's maximum with superimposing of two lasers and controlling of their ellipticity. This provides a scheme that the harmonic generation occurs only within one half-cycle of the laser pulse generating a single attosecond pulse. This approach called polarization gating technique and provides a clever way of producing single attosecond pulses from a long driving laser pulse [85–90].

Another approach for generating a single attosecond pulse is using only the cut-off harmonics from a few cycle driving laser pulses [91, 92]. The harmonics in cut-off region contain the highest photon energies which can be only emitted within half cycle close to the pulse maximum. By spectral filtering a single attosecond pulses can be obtained. Generation of single attosecond pulses by selecting the cut-off harmonics from few cycle driving laser pulse can be found in Refs. [93, 94]. As mentioned above, for the reliable single attosecond pulse generation, a few-cycle driving pulse is more convenient [95].

Characterization

Due to the short wavelength and small duration of attosecond pulses, their experimental characterization is a big challenge. Attosecond metrology is an active research topic in laser laboratories to construct the suitable schemes and optical devices in the XUV regime. The most common characterization techniques are based on correlation of the attosecond pulse and the driving laser field which can be done by pump-probe experiments. Most of these pump-probe experiments can be easily studied in theory by the single active electron approximation. These techniques are based on the generation of the electron wave-packet in the continuum from the photoionization of atoms by a XUV laser pulses.

The first technique of attosecond metrology for a train of pulses, is explained in Ref. [96] by Muller *et al.* which is called RABBITT "Reconstruction of attosecond harmonic Beating By Interference of Two-photon Transitions". The photoelectron spectrum of an atom contains a series of peaks corresponding to the harmonics (XUV) frequency and sidebands resulting from the absorption of additional infrared photons. The time delay between the XUV (harmonic) pulse and the driving infrared is a key parameter in this method. However, this technique is convenient for a train of attosecond pulses.

In fact, due to a very broad bandwidth of single attosecond pulse the sidebands cannot be distinguished from harmonic peaks. This technique have been used in Ref. [97] to measure the kinetic energy and the angular distributions of the resulting photoelectrons. The characterization of single attosecond pulses would require more techniques and efforts.

2.7 Theoretical methods in quantum dynamics

As there is no exact analytical solution of the TDSE for an arbitrary time-dependent Hamiltonian, many theoretical tools have been proposed to solve the TDSE with different approximations. Time-dependent perturbation theory [98] which is the most familiar method from traditional quantum mechanics in linear response regime, is no longer valid in strong-field regime.
Therefore, other methods are necessary for the theorists to study experimental investigations or predict new phenomena for experimentalists. In addition to the direct numerical integration of TDSE, other methods were developed in strong-field dynamics. The strong-field approximation which is valid for the low frequency regime, can be efficiently applied for single active electron systems. Floquet theory and its high frequency version are powerful methods to study the ionization rate of single electron atoms and molecules in an external monochromatic field. In the following, these methods are briefly discussed.

Strong-field approximation

The strong-field approximation beyond the perturbation theory was described first by Keldysh [35] which gives the ionization rates in a closed form and demonstrates the ionization dynamics in the tunneling and multiphoton regime for a short range potential without intermediate states and internal dynamics effects.

According to S-matrix formalism, the transition probability amplitude of a system from the initial state $|\phi_i\rangle$ to a final state $|\phi_f\rangle$ is given by

$$p_{i\to f} = -i\int_{-\infty}^{\infty} dt \langle\phi_f(t)|\hat{H}_{\rm int}(t)|\phi_i(t)\rangle, \tag{2.40}$$

which is similar to the time-dependent perturbation theory. The Volkov states are the best choice as a final state solution of TDSE and the initial state is chosen from the bound field-free states. The Volkov states are the wave function of a free electron in a time dependent electromagnetic field:

$$\phi_f(\mathbf{k},\mathbf{r},t) = \frac{1}{(2\pi)^{3/2}}\exp\Big(i\mathbf{k}.\mathbf{r}\Big)\exp(-i\frac{|k|^2}{2}t)\exp[iS(\mathbf{k},\mathbf{r},t)], \tag{2.41}$$

where $S(\mathbf{k},\mathbf{r},t)$ is the Volkov phase

$$S(\mathbf{k},\mathbf{r},t) = \mathbf{A}(t).\mathbf{r} - \mathbf{k}.\int_{\infty}^{t} dt'\mathbf{A}(t') - \frac{1}{2}\int_{\infty}^{t} dt'[\mathbf{A}(t')/c]^2. \tag{2.42}$$

With the help of Bessel functions, an exact expression can be derived for the ionization spectra [99]. Further approximation which is called saddle point approximation, is routinely used to calculate the resulting integrals in SFA [100]. The Volkov states, however, cannot accurately describe the ionization rates for the long-range potentials like Coulomb one due to the fact that the Volkov states have properties of a plane-wave. The effect of range of potential is recently considered in the same framework [101–103]. Eq.(2.40) explains a direct ionization from the initial bound states to the continuum. In order to calculate rescattering probability of the ionized electron from the core potential, additional time-integral is necessary. The SFA was used in this work to test the validity of the results in the low frequency regime. However, due to the fact that SFA breaks down in high frequency limit the main results of the next chapters are based on the numerical solution of the TDSE. Strong-field approximation can be found in details in Refs. [50,100].

Floquet theory

Floquet theory is a widely used and a powerful approach in atomic physics, but its applications in strong laser fields is limited to the monochromatic laser fields with infinite duration and one-single active electron. The efficiency of this method is low for the two electron system due to the structure of equations which have to be solved numerically. This method is used in other branches of atomic and molecular spectroscopy [104].

For a monochromatic external field with frequency ω, the Hamilton operator possesses a periodic time dependence with the period $T = 2\pi/\omega$. Thus, the solution of the TDSE has the periodic form

$$\Psi(t) = \exp(iEt)\Phi_E(t) \quad \text{with} \quad \Phi_E(t+T) = \Phi_E(t), \tag{2.43}$$

and obeys the same periodicity of Hamiltonian. By inserting above solution into the TDSE one obtains

$$(\hat{H} - i\frac{\partial}{\partial t})\Phi_E(r,t) = E\Phi_E(r,t) \tag{2.44}$$

which is an eigenvalue problem for the non-Hermitian operator $\hat{H} - i\partial/\partial t$. Floquet theory allows one to evaluate the ionization rate of the dressed states in intense laser fields. The method have been frequently used by Gavrila to study the stabilization dynamics in the high-frequency lasers [18]. With Floquet theory [105] one can calculate quasistationary solutions of TDSE including an interaction Hamiltonian containing a monochromatic light field. The solution takes the form

$$\Phi^m(\mathbf{r},t) = e^{-iE_m t}\sum_n \phi_n^{(m)}(\mathbf{r})e^{-in\omega t}, \tag{2.45}$$

where E_m is the quasienergy. The Floquet components $\phi_n^{(m)}$ have to satisfy an infinite set of time-independent coupled differential equations with the same boundary conditions needed for the full time-dependent wavefunction. In practice one needs an appropriate basis set which are mostly chosen Sturmian basis set in radial coordinate. The resulting

equation leads to an generalized eigenvalue problem and a set of complex eigenvalues $\{E_m,\ m = 1 \cdots \infty,\ E_m = \varepsilon_m - (i/2)\Gamma_m\}$ [105]. The state m is an ionization channel of the atom, ε_m is the energy in the corresponding channel in laser field and Γ is its ionization rate. At zero field amplitude, E_0^{laser}, the Floquet system reduces to the unperturbed time-independent Schrödinger equation. In each Floquet block, only one of the components of $\phi^{(m)}$ survives and the system of equation becomes an unperturbed eigenvalue equation with eigenfunction ϕ_m and corresponding field-free eigenvalue $E_m = \varepsilon_m(I = 0)$. More applications and detailed calculations of ionization rates can be found in the Refs. [106, 107].

2.7.1 Numerical integration of the TDSE

Here the direct numerical integration of the one-particle TDSE will be discussed which is mostly used in this thesis. The numerical solution of the TDSE based on the standard Crank-Nicolson procedure is discussed and in the following the most common methods are briefly explained to prepare the initial state. Different techniques, like imaginary time propagation, direct diagonalization and spectral method are explained. As the focus of this thesis lies on high-frequency laser-atom interaction, the transformation of the TDSE to the KH frame is also discussed. The last paragraphs of this chapter demonstrate the computation of observables and energy spectra.

In spatial coordinate representation, the Schödinger equation for a single particle reads

$$i\frac{\partial}{\partial t}\Psi(\mathbf{r},t) = \hat{H}\Psi(\mathbf{r},t), \tag{2.46}$$

where $\hat{H}$ is the Hamilton operator which is given by:

$$\hat{H} = -\frac{1}{2}\nabla^2 + V(\mathbf{r},t), \tag{2.47}$$

where $V(\mathbf{r},t)$ denotes the potential energy which includes all time-dependent external fields. The numerical solution of the TDSE is a widely studied topic for the one particle problems and recently for the two active electron systems. There exist different approaches. For a hydrogen like atom in intense laser fields with linear polarization the Hamiltonian of the system obeys a cylindrical symmetry which can be written as

$$\hat{H}(r,\theta,\phi,t) = -\frac{1}{2}\left[\frac{\partial^2}{\partial r^2} - \frac{\hat{L}^2}{r^2}\right] + V(r) + \hat{H}_{\text{int}}(r,\theta,\phi,t) \tag{2.48}$$

in spherical coordinates or

$$\hat{H}(\rho,z,\phi,t) = -\frac{1}{2}\left[\frac{1}{\rho}\frac{\partial}{\partial\rho}\rho\frac{\partial}{\partial\rho} + \frac{\partial^2}{\partial z^2} + \frac{\partial^2}{\rho^2\partial\phi^2}\right] + V(\rho,z) + \hat{H}_{\text{int}}(\rho,z,\phi,t) \tag{2.49}$$

in cylindrical coordinates. With the dipole approximation the ϕ-dependence can be eliminated and the equation can be considered in a two dimensional picture. In spherical

coordinates, Muller [108] derived an efficient algorithm to find the time-dependent wavefunction $\psi(r)Y(\theta,\phi)$ and later the algorithm was used by Bauer [109]. However, one has to choose a suitable coordinate system and procedure according to the system of investigation. Each computational technique has its own range of applicability and difficulty. The

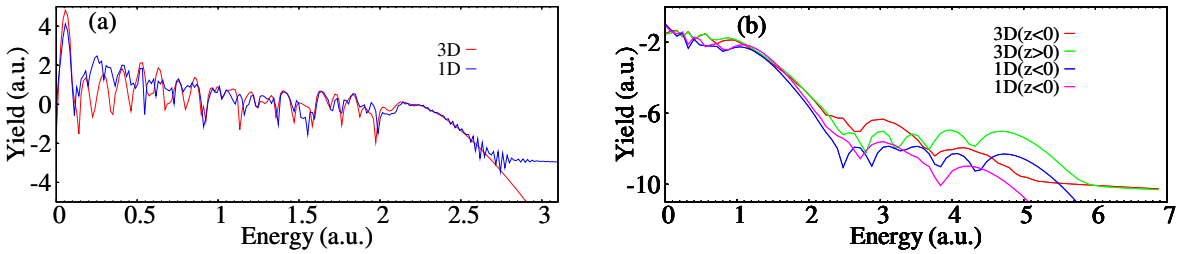

Figure 2.10: (a) HHG and (b) ATI spectra of the 1D and 3D model atom irradiated by a 4-cycle $\sin^2$ laser pulse of $\lambda = 800\,\text{nm}$ and $I = 2.4 \times 10^{14}\,\text{Wcm}^{-2}$.

central systems investigated throughout this work are ionization and rescattering in one dimension which the results agree qualitatively with two or three dimensional model in dipole approximation as indicated in Fig. 2.10. The results of ATI and HHG in Fig. 2.10 are obtained with our 3D and 1D simulation with the same lattice and time-step parameters. Cartesian coordinates is the best for the representation of the TDSE in one and two dimensional problems. In two dimensional problems, however, one can use polar coordinate with a combination of the closed coupling approach. The numerical schemes which are suitable for these types of systems are grid methods based on finite differences. The algorithm can be used in higher dimensions with increasing of the number of operations. In the following section, the common numerical scheme for the solution of TDSE is illustrated.

Crank-Nicholson method

The accuracy of the results in quantum dynamics including wavefunction and observables, require a reliable numerical representation of the propagator. In order to have a stable and unitary propagator, the optimal choice is Crank-Nicholson scheme which preserve the unitarity of the wave function with high numerical stability compared to explicit method.

The one-dimensional version of Eq. (2.46) reads

$$j\frac{\partial}{\partial t}\Psi(x,t) = -\frac{1}{2}\frac{d^2}{dx^2}\Psi(x,t) + V(x)\Psi(x,t), \tag{2.50}$$

which has a general solution

$$\Psi(x,t) = e^{-j\hat{H}t}\Psi_0(x), \tag{2.51}$$

where $\Psi_0(x)$ represents the initial wave function at $t = 0$. The Hamiltonian, $\hat{H}$, in general is time-dependent and there is no exact solution of Eq. (2.51) for an arbitrary time-dependent Hamiltonian. However, when the time evolution of the wavefunction is

achieved by applying of exponential operator within a set of short time steps Δt one can assume that the total Hamiltonian is nearly constant in each time step. Then the Crank-Nicolson procedure [110] which is based on Cayleys form of the operator $e^{-j\hat{H}t}$ takes the form:

$$e^{-j\hat{H}t} \simeq \frac{1 - \frac{1}{2}j\hat{H}\Delta t}{1 + \frac{1}{2}j\hat{H}\Delta t} \tag{2.52}$$

Which implies a unitary time evolution, hence the norm of the time-dependent wave function is conserved. Using Eq. (2.52), one obtains the wave function at any time step $\Psi(x, t + \Delta t) \equiv \Psi_i^{n+1}$ from the wave function at previous time step $\Psi(x, t) \equiv \Psi_i^n$

$$(1 + \frac{1}{2}j\hat{H}\Delta t)\Psi_i^{n+1} = (1 - \frac{1}{2}j\hat{H}\Delta t)\Psi_i^n \tag{2.53}$$

where the index i indicates the spatial lattice points with the step size Δx and the superscript n denotes discretization in time with time step Δt. Now, the kinetic energy operator of Hamiltonian $\hat{H}$ is replaced by a finite difference approximation. Throughout this work a second-order expression for the derivatives is used:

$$\partial_x^2 \Psi_i^n \equiv \frac{d^2}{dx^2}\Psi(x, t) \simeq \frac{\Psi_{i+1}^n - 2\Psi_i^n + \Psi_{i-1}^n}{(\Delta x)^2}. \tag{2.54}$$

Higher order finite difference approximation can be also used but the efficiency of the method decreases compare with increasing of the accuracy. Combining Eq. (2.53) and Eq. (2.54) with the notations

$$\alpha = \frac{1}{4}j\frac{\Delta t}{(\Delta x)^2} \tag{2.55}$$

and

$$c_i = -\alpha = e_i, \quad d_i = 1 + 2\alpha + \frac{1}{2}j\Delta t V_i^{n+1}, \quad i = 1 \cdots N \tag{2.56}$$

yields for the left hand side of Eq. (2.53):

$$(1 + \frac{1}{2}j\Delta t\hat{H}_i)\Psi_i^{n+1} = c_i\Psi_{i-1}^{n+1} + d_i\Psi_i^{n+1} + e_i\Psi_{i+1}^{n+1}. \tag{2.57}$$

Analogously the right hand side of Eq. (2.53) converts into

$$(1 - \frac{1}{2}j\Delta t\hat{H}_i)\Psi_i^{n+1} = (1 - 2\alpha - \frac{1}{2}j\Delta t V_i^n)\Psi_i^n + \alpha\Psi_{i-1}^n + \alpha\Psi_{i+1}^n \equiv r_i^n, \quad i = 1 \cdots N. \tag{2.58}$$

Combining Eq. (2.57) and Eq. (2.58) one obtains a set of linear equations for the unknown variable Ψ_i^{n+1} which in matrix form reads

$$\begin{pmatrix} d_1 & e_1 & 0 & 0 \\ c_2 & d_2 & e_2 & 0 \\ . & . & . & . \\ 0 & 0 & c_N & d_N \end{pmatrix} . \begin{pmatrix} \Psi_1^{n+1} \\ \Psi_2^{n+1} \\ . \\ \Psi_N^{n+1} \end{pmatrix} = \begin{pmatrix} r_1^n \\ r_2^n \\ . \\ r_N^n \end{pmatrix} . \tag{2.59}$$

In above equations, j is $\sqrt{-1}$. The boundary conditions indicate the elements of the first and last rows of the matrix. The usual boundary conditions in quantum dynamics is an absorbing boundary, which is used throughout the present calculations. Eq. (2.59) can be solved efficiently to find the time-dependent wave function within the finite difference approximation. By small modification of Eq. (2.53) the right hand side can be simplified to reduce the number of computational operations.

2.7.2 Initial state

The final and time-dependent wavefunction and consequently observables are strongly depend on the initial state. For atoms and molecules one needs well defined bound state as an initial state. A Gaussian wavepacket, however, can be used for the special problems like scattering of the wavepacket from the ionic target. There are several methods to calculate stationary solution of the time-independent Schrödinger equation as an initial state. In the following different methods are discussed to find the eigenstates of the system: The solution of the TDSE by a spectral and imaginary time methods. The first one is very convenient for relativistic Hamiltonian, while the latter can be applied only on non-relativistic problems. Each method has its advantages and difficulties.

Spectral method

The eigenstates ψ_n of a 1D system with the potential $V(x)$ are given by the stationary Schrödinger equation

$$\left(-\frac{1}{2}\frac{d^2}{dx^2} + V(x) \right)\psi_n(x) = E_n\psi_n(x) \tag{2.60}$$

where $\{E_n\}$ are the corresponding energy eigenvalues. The spectral method which was introduced by Feit *et al.* [111], can be used to calculate the eigenvalues and eigenfunctions of a time-independent Hamiltonian. In this method an arbitrary initial wavepacket containing all states of Hamiltonian, is propagated in real time with a propagator containing of field-free Hamiltonian. The Fourier transform of autocorrolation function, $\langle\psi(x,0)|\psi(x,t)\rangle$ gives the spectral power of the Hamiltonian

$$F(\omega) = \int_0^\infty \langle\psi(x,0)|\psi(x,t)\rangle e^{\omega t} dt. \tag{2.61}$$

As it is indicated in above equation, the true spectrum is obtained by a time propagation to infinity. In practice, one uses a finite time interval for the propagation. Thus the efficiency of this method is related to the time interval of the propagation. For the one dimensional problems with soft-Coulomb potentials the method is convenient and fast while there is no degeneracy. Once the energy spectrum was obtained, the corresponding eigenfunction is calculated by

$$\psi_n(x,t) = \int_0^\infty W(t)\langle\psi(x,0)|\psi(x,t)\rangle e^{E_n t} dt. \tag{2.62}$$

where $W(t)$ is a window function. A Gaussian and $\sin^2(t)$ window functions are well known from Fourier analysis. The propagation method which explained in previous section based on Crank-Nicholson algorithm, can be easily implemented in this method. The efficiency, however, decreased by increasing of the dimensional of the system.

Imaginary time propagation

The real-time propagation scheme can easily be used to calculate stationary states by replacing the time step Δt with an imaginary time $i\Delta t$. An arbitrary initial state can be

written as a superposition of eigenstates

$$|\Psi(t)\rangle = \sum_n c_n \exp(-iE_n)|\psi_n\rangle, \tag{2.63}$$

where $|\psi_n\rangle$ describe the stationary states. In the imaginary time, one obtains

$$|\Psi(t)\rangle = \sum_n \langle\psi_n|\Psi(t)\rangle \exp(E_n t)|\psi_n\rangle \tag{2.64}$$

in which all states apart from the ground state decay exponentially. If the Hamiltonian is bound from below, then only the ground state survives because it decays less faster than the other states. Within this scheme the normalization of the wavefunction is not conserved thus the wave function has to be normalized at each time step. This process is also applicable to find the excited states by Gram-Schmidt orthogonalization. The efficiency of the method is low for calculation of many bound states with imaginary time Gram-Schmidt orthogonalization. The advantage of this method is that it can be applied in higher dimensions although becoming computationally expensive. The method cannot be used in relativistic equations, because the relativistic Hamiltonians are not bound from the below.

There are other methods to find the static solution of the Hamiltonian on the grid. The shooting method, direct diagonalization of the Hamiltonian in one dimensional problems or radial Schrödinger equation are other alternatives to calculate the stationary states. These methods, however, limited only in one-dimensional problems. The damped-relaxation technique is a powerful and general method for finding the static solution of the relativistic and non-relativistic equations [112]. This method can be consider as a generalized imaginary-time scheme.

2.7.3 Kramers-Henneberger frame

As we will show in the next chapters, it is convenient sometimes to describe processes in laser fields in an accelerated frame, which is called Kramers-Henneberger (KH) frame. The Schrödinger equation in the laboratory frame reads in minimal coupling:

$$\frac{1}{2}\left[\frac{1}{i}\nabla - \frac{1}{c}\mathbf{A}(t)\right]^2 \Psi^{\text{lab}}(\mathbf{r},t) + V(r)\Psi^{\text{lab}}(\mathbf{r},t) = i\frac{\partial}{\partial t}\Psi^{\text{lab}}(\mathbf{r},t). \tag{2.65}$$

One can introduce a new wave function $\Psi^{KH}(\mathbf{r},t) = \hat{U}\Psi^{\text{lab}}(\mathbf{r},t)$ which is generated by the unitary transformation

$$\hat{U} = \exp\left[i\int_{-\infty}^{t} \hat{H}_{\text{int}}(\tau)d\tau\right] = \exp\left\{i\int_{-\infty}^{t}\left[\frac{i}{c}\mathbf{A}(\tau).\nabla + \frac{1}{2c^2}\mathbf{A}^2(\tau)\right]d\tau\right\}. \tag{2.66}$$

As the dipole approximation is used ($\mathbf{A}$ is independent of the position) the transformation operator can be written as

$$\hat{U} = \hat{U}^1\hat{U}^2 = \exp\left[-\int_{-\infty}^{t}\frac{1}{c}\mathbf{A}(\tau).\nabla d\tau\right].\exp\left[\frac{i}{2c^2}\int_{-\infty}^{t}\mathbf{A}^2(\tau)d\tau\right], \tag{2.67}$$

where the operator $\hat{U}^1$ is a translation operator consisting of momentum operator as a generator of translation and $\hat{U}^2$ induces a phase on the wavefunction [16,17]. The translation operator on an arbitrary function changes the position by free electron displacement in an oscillatory field

$$\hat{U}^1 f(\mathbf{r}) = f\Big[\mathbf{r} - \alpha(t)\Big]. \tag{2.68}$$

The transformed wave function $\Psi^{KH}(\mathbf{r}, t)$ satisfies the time-dependent Schrödinger equation in the KH frame

$$\Big[-\frac{1}{2}\nabla^2 + V(\mathbf{r} + \alpha(t))\Big]\Psi^{KH}(\mathbf{r}, t) = i\frac{\partial}{\partial t}\Psi^{KH}(\mathbf{r}, t), \tag{2.69}$$

in which $\alpha = -\int_{-\infty}^{t} \frac{1}{c} A(\tau) d\tau$.

Another advantage of the KH frame which recently was intensively used by Tolstikhin [113, 114] is the possibility of the expansion of the time-dependent wave function in Siegert-scattering states in the range of the free electron displacement. This approach allows one to calculate photoelectron spectra efficiently. However the time behavior of the ionization dynamics which is the object of this work was not reported by this approach.

It is noted that the observables in the KH and the lab frames are not the same. In this thesis most of the calculations have been done in the lab frame but in order to consider strong-field effects at XUV lasers the wavefunction is transformed to the KH frame and back to the lab frame.

By averaging $V(x + \alpha_t)$ over one optical cycle one arrives at a time-independent problem and corresponding KH wave functions, $\Psi(x)_{KH}$,

$$\Big[\frac{1}{2}\hat{p}_x^2 + V(x + \alpha_0)\Big]\Psi(x)_{KH} = E_{KH}\Psi(x)_{KH}. \tag{2.70}$$

The KH frame is convenient to represent the dynamics in intense high frequency lasers in the stabilization regime. This potential is a zero order component of the Fourier expansion of the time-dependent potential at high frequencies according to

$$V(x + \alpha_0 cos\omega t) = \sum_{n=-\infty}^{+\infty} V_n(x) e^{in\omega t}. \tag{2.71}$$

One can approximately describe the atomic system in an intense high frequency laser field in terms of the KH states Eq. (2.70). However, our results show that the laser field still is involved in the interaction with an atom in the average KH potential. This indicates a complex dynamics. It is shown in chapter 3 that the phase-space representation of the ATI spectra shows the classical cutoff ($10U_P$) for the rescattered photoelectrons. The position of the peaks, however corresponds to the absorption of the multiphotons from the KH states.

2.8 Observables

Most of the physical observables can be calculated from the wave function $\Psi(t)$ during the propagation except a true ATI spectrum. In the following, 1D calculations are shown. The same methods can be applied to higher dimensions if the additional integration for the other directions are included. In the three-dimensional models based on radial and spherical harmonics, one can use Legendre polynomial properties to simplify the three-dimensional integrations. To obtain HHG and true ATI, one needs additional post-calculations on the observables and final wavefunction.

The simplest observables are diagonal operators. The surviving probability of the wavepacket is calculated via

$$N(t) = \int_{-\infty}^{\infty} |\Psi(x,t)|^2 dx \simeq \int_{-x_{min}}^{x_{max}} |\Psi(x,t)|^2 dx \simeq \sum_{i=1}^{N} |\Psi_i(t)|^2 . \Delta x, \tag{2.72}$$

which can be used to define the unitarity of the time propagator. The average potential energy $\langle V \rangle(t)$ with respect to the ionic potential is calculated by

$$\langle V \rangle(t) = \int_{-\infty}^{\infty} |\Psi(x,t)|^2 V(x) dx \simeq \int_{-x_{min}}^{x_{max}} |\Psi(x,t)|^2 V(x) dx \simeq \sum_{i=1}^{N} |\Psi_i(t)|^2 V(x_i) . \Delta x. \tag{2.73}$$

The expectation value of the induced dipole is calculated by

$$\langle d_x \rangle(t) = \int_{-\infty}^{\infty} |\Psi(x,t)|^2 x dx \simeq \int_{-x_{min}}^{x_{max}} |\Psi(x,t)|^2 x dx \simeq \sum_{i=1}^{N} |\Psi_i(t)|^2 x_i . \Delta x \tag{2.74}$$

in the length form and

$$\langle d_a \rangle(t) = \int_{-\infty}^{\infty} |\Psi(x,t)|^2 \frac{\partial V}{\partial x} dx \simeq \int_{-x_{min}}^{x_{max}} |\Psi(x,t)|^2 \frac{\partial V}{\partial x} dx \simeq \sum_{i=1}^{N} |\Psi_i(t)|^2 \frac{\partial V}{\partial x}(x_i) . \Delta x \tag{2.75}$$

in the acceleration form. HHG can be calculated by a post-processing via Fourier transform of the induced dipole in the system. The calculation of the expectation value of non-diagonal operators like kinetic energy operator and momentum operator requires more computational effort. For example the kinetic energy can be calculated by

$$E_{kin}(t) = \langle -\frac{1}{2} \frac{d^2}{dx^2} \rangle = -\frac{1}{2} \langle \Psi(x,t) | \Psi''(x,t) \rangle \tag{2.76}$$

where Ψ'' is evaluated by a finite difference scheme or in Fourier space with an extra Fourier transform of the wavefunction. The current density can be calculated from imaginary part of $\Psi^* \nabla \Psi$

$$j_x(t) = Im \langle -i \frac{d}{dx} \rangle = Im(i \langle \Psi(x,t) | \Psi'(x,t) \rangle). \tag{2.77}$$

2.9 Energy spectra

The ATI spectra can be calculated by applying the window operator $\hat{W}(\varepsilon, n, \sigma)$ to the final wavefunction $|\Psi_f\rangle$:

$$\hat{W}(\varepsilon, n, \sigma) = \frac{\sigma^{2^n}}{(\hat{H}_0 - \varepsilon)^{2^n} + \sigma^{2^n}}, \tag{2.78}$$

where $\hat{H}_0$ is the field free Hamiltonian, ε the energy of the extracted wavefunction, 2σ the energy bandwidth and the parameter n defines the sharpness of the energy window [115]. The probability that the electron after the interaction has an energy ε within a bandwidth of 2σ is given by

$$\rho_\sigma(\varepsilon) = \langle \Psi_f | \hat{W}^2(\varepsilon, n, \sigma) | \Psi_f \rangle = \int dx\, \rho_\sigma(\varepsilon, x). \tag{2.79}$$

We interpret the distribution function $\rho_\sigma(\varepsilon, x)$ as a quantum phase space distribution (in energy and position space) following [109]. It is similar to the Wigner phase space distribution but has an advantage in resolution.

We derive a time-profile of the ionization for the analysis of details of the phase space distribution by cutting across the phase space distribution at a certain energy with an energy bandwidth of 2σ. Later, by applying an appropriate coordinate-to-time mapping $t = x/\sqrt{2\varepsilon}$, it provides the time-profile of the ionization WP at a given electron energy.

2.10 Phase-space distribution based on simple man's model

From the solution of the classical Newton equation of motion, the final position and the energy of the direct photoelectron ionized at time t_0 are given by

$$x^d(t_f) = \int_{t_0}^{t_f} dt' A(t') - A(t_0)(t_f - t_0) \tag{2.80}$$

and

$$E^d_{kin}(t_f) = \frac{1}{2}[A(t_f) - A(t_0)]^2, \tag{2.81}$$

respectively. If the electron is driven back to the nucleus it may rescatter at later time t_r. The final position and the energy of the rescattered photoelectron is given by

$$x^{res.}(t_f) = \int_{t_0}^{t_f} dt' A(t') + A(t_0)[t_f + t_0 - 2t_r] - 2A(t_r)(t_f - t_r) \tag{2.82}$$

and

$$E^{res.}_{kin}(t_f) = \frac{1}{2}[A(t_f) + A(t_0) - 2A(t_r)]^2 \tag{2.83}$$

respectively [109].

Chapter 3

Above-threshold ionization with XUV laser pulses

In strong field physics irrespective of the frequency of the laser pulse above threshold ionization is one of the most important phenomena to generate photoelectron spectra. These spectra can then be used to explain the electronic properties of the atom and ionization dynamics in intense laser pulses and has been investigated intensively, both theoretically and experimentally at low frequencies [50, 51, 62]. The aim of this chapter is to investigate the details of above-threshold ionization in a strong XUV laser fields. While in the low frequency regime the well-known simple man's model [60] provides an adequate intuitive explanation of the dynamics, there is no such transparent intuitive understanding in the XUV regime. To gain an insight, we investigate the electron distribution in the quantum phase space after the interaction. The phase space analysis allows us to uncover the damped contribution of the rescattered electrons in the stabilization regime which is usually hidden in the background of the ATI spectra. In particular, we want to clarify to what extent the classical description of the electron dynamics in the stabilization regime is adequate and what are the specific quantum signatures. In fact, in the stabilization regime the characteristic electron energy U_P is much larger than the photon energy: $U_P/\omega \gg 1$, which indicates a possible classical character of the electron dynamics.

3.1 The model system

We describe the electron dynamics in a strong XUV laser field by the Schrödinger equation in the dipole approximation. Relativistic effects are known to be negligible when $\lambda\xi^2/2 < a_\perp$ [116], for laser wavelength λ, relativistic laser intensity parameter $\xi = E_0/(c\omega)$, electron wave packet size in the laser propagation direction $a_\perp$, and speed of light c. For example, this condition is fulfilled at $\omega = 3\,\text{a.u.}$ for laser field strengths up to $E_0 = 35\,\text{a.u.}$. The time-dependent Schrödinger equation is used as equation of motion:

$$i\frac{\partial}{\partial t}\Psi(x,t) = \left\{\left[\frac{\hat{p}_x}{2} - \frac{1}{c}A_x(t)\right]^2 + V(x)\right\}\Psi(x,t) \tag{3.1}$$

where $V(x) = -Ze^{-(x/R)^2}/\sqrt{(a/Z)^2 + x^2}$ is the potential of a 1D model atom with a soft-core parameter $a = 1.4$ chosen to fit the ionization potential of a hydrogen atom with Z the nuclear charge and $E(t) = E_0 f(t)\cos\omega t$ the laser pulse. The range of the potential is defined by R which is ∞ for a soft-Coulomb potential. The laser pulse envelope $f(t)$ is trapezoidal with an overall t_d duration:

$$f(t) = \begin{cases} \sin^2(\pi t/2t_{\rm on}) & 0 < t < t_{\rm on} \\ 1 & t_{\rm on} < t < t_{\rm off} \\ \sin^2(\pi(t_{\rm d} - t)/2t_{\rm on}) & t_{\rm off} < t < t_{\rm d} \end{cases} \tag{3.2}$$

In order to avoid reflection of the wave packet at the boundaries, a negative imaginary potential is used. Eq. (3.1) is solved numerically with a Crank-Nicholson finite-difference scheme. We study the ionization dynamics in two regimes: low frequency ($\omega < I_p$) and high frequency ($\omega > I_p$). Furthermore, the ATI spectra and its phase-space distribution are calculated by applying the window operator $\hat{W}(\varepsilon, n, \sigma)$ to the final wavefunction $|\Psi_f\rangle$:

$$\hat{W}(\varepsilon, n, \sigma) = \frac{\sigma^{2^n}}{(\hat{H}_0 - \varepsilon)^{2^n} + \sigma^{2^n}}, \tag{3.3}$$

where $\hat{H}_0$ is the field free Hamiltonian, ε the energy of the extracted wavefunction, 2σ the energy bandwidth of the extraction and the parameter n defines the sharpness of the energy window [115]. The probability that after the interaction the electron has an energy ε within a bin of 2σ is given by:

$$\rho_\sigma(\varepsilon) = \langle\Psi_f|\hat{W}^2(\varepsilon, n, \sigma)|\Psi_f\rangle = \int dx\, \rho_\sigma(\varepsilon, x). \tag{3.4}$$

Following [109], we interpret the distribution function $\rho_\sigma(\varepsilon, x)$ as a quantum phase space distribution (in energy and position space). It is similar to the Husimi or Wigner phase space distribution but has an advantage in resolution. To visualize the classical orbits of the ionized electron, a rather small energy bandwidth σ of the distribution function should be applied. The ATI spectra and its phase-space representation of a model atom is reviewed in the next section at IR frequency and then the characteristic of the ATI spectra with XUV lasers is considered.

3.2 Above-threshold ionization at IR frequencies

We consider a short-pulse Ti:Sapphire (800 nm) laser with an intensity suitable for generating tunneling and over the barrier ionization. From three step rescattering model in tunneling ionization, above-threshold ionization spectra must be included of a two plateau. The first plateau one is related to direct ionization, taking the value $2U_P$, while the second one is due to rescattering of ionized electron from the parent ion, taking the value $10U_P$. However, the probability of rescattering is some order of magnitude smaller than for the production of direct photoelectrons. Figs. 3.1(c,d) show the envelope of the calculated photoelectron spectra after propagating the TDSE for a 4-cycle laser pulse.

The spectra for lower intensity ($E_0 = 0.1$) consists of two clear plateaus for direct and rescattered photoelectrons. However, at higher intensity ($E_0 = 0.2$) the second plateau shows a sub-plateau and steplike structure. This structure is due to the few cycle pulse being in the clear over the barrier regime in the low frequency limit, a most of the electron wavepacket ionizes at the edge of the pulse and a small part remains to ionize and rescatter at the peak of the pulse. In a few cycle laser and over the barrier intensity, each cycle has its own cutoff. In this figure the semi-classical energy cutoff ($10U_P$) is fullfiled which is more clearly seen at lower intensity ($E_0 = 0.1$) because the ionization is less during the edge of the pulse. An alternative powerful tool for the investigation and ob-

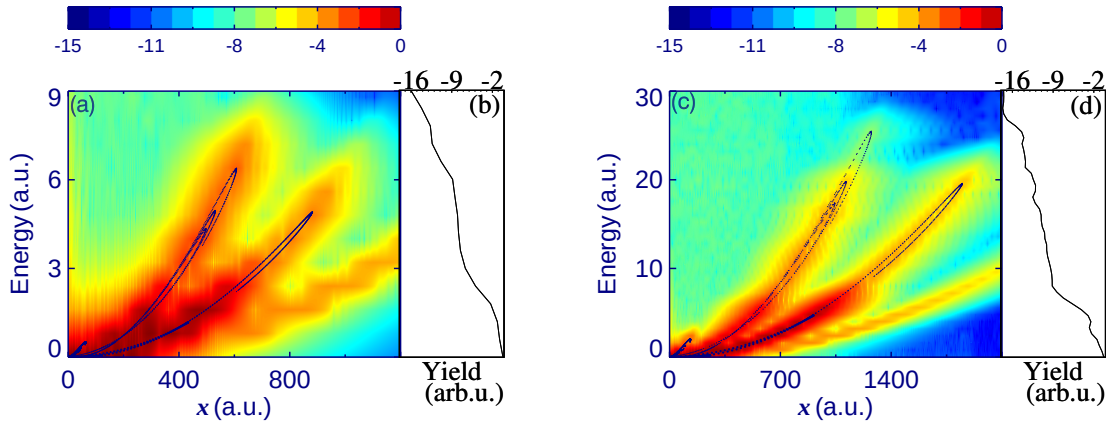

Figure 3.1: The ATI spectra of a 1D model atom irradiated by a laser pulse of $\omega = 0.056$ a.u. including 4 cycles with zero flat part. (b) $E_0 = 0.1$ ($U_P = 0.8$), (d) $E_0 = 0.2$ ($U_P = 3.2$). (a,c) The phase space representation of the ATI. The SM model results are indicated with dots.

servation of ionization and rescattering processes is the phase-space representation. With phase-space representation, one can investigate classical orbits in quantum mechanical calculations. Moreover, the energy cutoff and probability of ionization and rescattering can be extracted better than the integrated ATI spectra. The phase-space distribution of the ionized WP of the same ATI spectra of Fig. 3.1(b,d) are calculated and shown in Fig. 3.1(a,c). Moreover, the final energy-position of the trajectories is calculated with the SM's model and is indicated with dots in the figure to compare with quantum trajectories. This figure shows in two intensities very clear trajectories for each optical cycle. At lower intensity, the probability of the trajectories (indicated by color) for each cycle are the same, on the other hand at higher intensity the probability of the earlier ionized WP is more than the later one which corresponds to the ionization within the rising ramp of the pulse. In the following, the signature of the ionization is explained in XUV lasers.

3.3 Above-threshold ionization at XUV frequencies

Now we want to show the difference and similarity of the ionization dynamics at XUV frequencies and low (IR) frequency limit. Because the integrated ATI spectra are not

adequate at high frequencies, we also use phase-space representation.

The phase-space distribution of the ionized WP and corresponding ATI spectra are calculated at the end of a 16-cycle pulse with 4 cycle ramp and is shown in Fig. 3.2. The frequency of the pulse is $\omega = 0.3$ which is still smaller than I_p but in the VUV regime. With increasing angular frequency the ionization of the atom decreases and one can use longer pulses including more optical cycles. However, some non-adiabatic effects (shaking) come from the short ramp but with 4-cycle ramp, one is able to explore trajectories in the phase space within the flat part of the pulse. There are few differences in the envelope of the ATI spectra compared to the low frequency case. First, although the spectra show a plateau structure at lower intensity ($E_0 = 0.6$, Fig. 3.2(b)), the double plateau for direct and rescattered parts of the spectrum is completely absent at higher intensity (($E = 2$), Fig. 3.2(d)). Second, the yield of the photoelectrons falls very fast such that most of the ionization happens near the threshold. We notice that these properties are characteristic of the ionization in the XUV regime. The third difference is that the classical energy cutoff in ATI spectra disappears especially for higher intensity. The origin of the first and second difference is stabilization at higher frequencies, while in the latter the tail of the potential also has an influence. Now the phase space distribution of the ionized

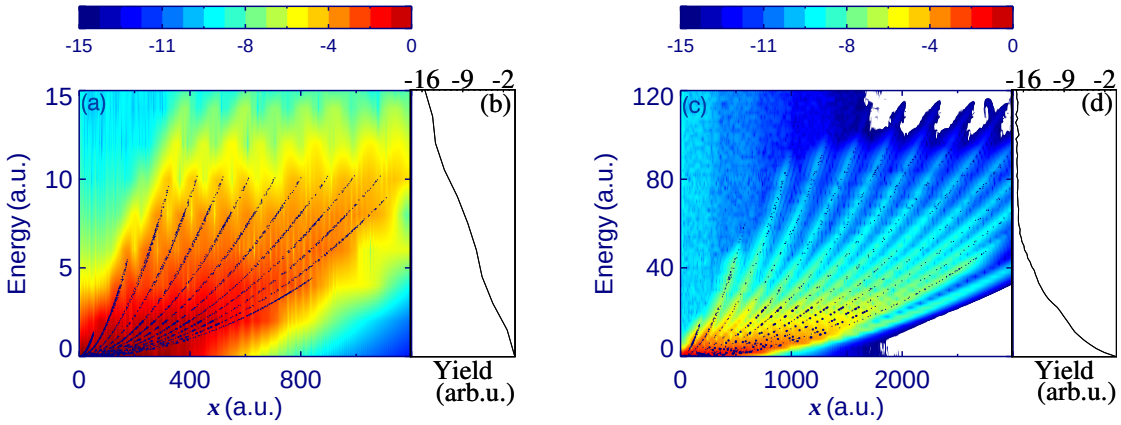

Figure 3.2: The ATI spectra of a 1D model atom irradiated by a 16-cycle laser pulse with frequency $\omega = 0.3$ a.u. including a 4-cycle ramp, (b) $E_0 = 0.6$ ($U_P = 1.0$); (d) $E_0 = 2.0$ ($U_P = 11.0$). The corresponding phase space distributions are shown in (a,c).

WP complements the comparison of the ionization at different frequencies. This figure clearly shows trajectories for each optical cycle at higher intensity (Fig. 3.2(c)) which is similar to low the frequency case in which for each optical cycle there is ionization with maximum probability corresponding to the SM model paths. However, from the phase space representation an important signature of the ATI spectra can be seen, where the energy of the rescattered electron can be as large as the classical cutoff $10U_P$ although, in the ATI spectra the rescattered probability is at the level of the background and the plateau is not observable.

Now we extend our investigation to the higher frequencies i.e. $\omega > I_P$. Fig. 3.3 shows the envelope of the calculated photoelectron spectra and its phase-space representation at the end of the pulse. The frequency of the pulse is $\omega = 3.0$ which is larger than I_p. A laser pulse with 20 cycles including a 5-cycle ramp is used in this simulation. The laser pulse must have a 5-cycle ramp at this frequency to avoid large nonadiabaticity (shaking) effects and population transfer to excited states during the short ramp. With increasing angular frequency, the ionization of the atom decreases more and shows very clear stabilization (chapter 4). One can see that the differences with respect to the low frequency (800 nm) are more pronounced in the envelope of the ATI spectra. In addition, the ATI spectra shows that the probability of the photoelectron spectra decreases exponentially with increasing frequency of the laser pulse. The difference of the ionization mechanism between high and low frequencies increases with the frequency of the laser pulse. For each optical cycle there is ionization with maximum probability correspond-

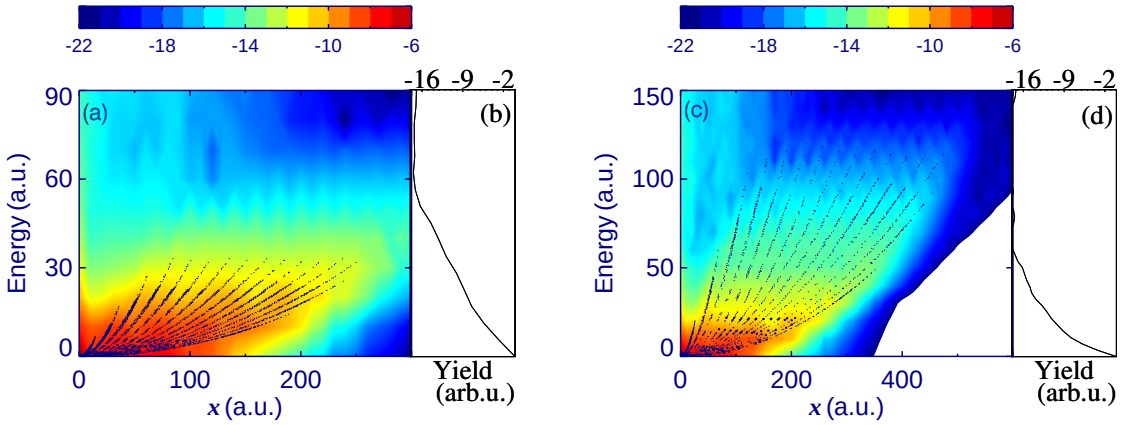

Figure 3.3: The ATI spectra (b,d) and its phase-space distribution (a,c) of a 1D model atom irradiated by a laser pulse with frequency $\omega = 3.0$ a.u., and a pulse length of 20 optical cycle including a 5-cycle ramp. The peak electric field is set (a,b) $E_0 = 10$ ($U_P = 2.8$); (c,d) $E_0 = 20$ ($U_P = 11.0$).

ing to the SM model path. However, from the phase space representation an important signature of the ATI can be seen, where the energy of the rescattered electron can be as large as the classical cutoff 10 U_P although, there are no rescattered photoelectrons in the ATI spectra. In fact, the probability of the rescattered photoelectrons is very small and abscured in the background of the ATI spectra.

Now the necessary condition for the energy-position resolution is explained. Due to a finite energy bandwidth, the electron momentum p has an uncertainty $\delta p \sim 2\sigma/p$ which brings an uncertainty for the coordinate during the time Δt: $\delta x \sim \delta p \Delta t \sim \sigma x/\varepsilon$. Any structure in the phase space with a characteristic size $(\Delta x, \Delta p)$ will be visible if $\delta x \ll \Delta x$ and $\delta p \ll \Delta p$. In particular, the characteristic distance between electron trajectories which emerge at adjacent laser cycles is $\Delta x \sim 2\pi p/\omega$. Then the requirement for the electron trajectory to be visible, is

$$\sigma \ll \frac{2\pi\varepsilon p}{x\omega}. \tag{3.5}$$

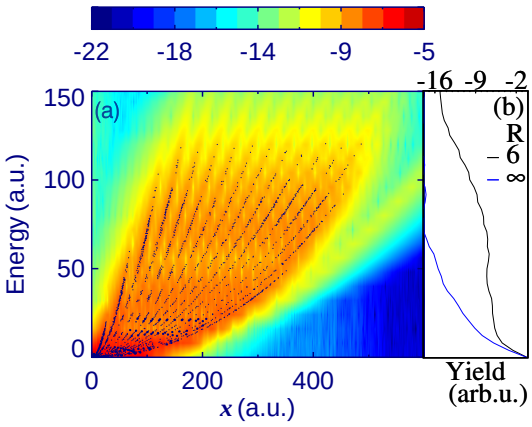

Figure 3.4: (a) Phase space distribution of the ionized WP of a 1D model atom with short range potential with 4 field-free bound states. (b) The envelope of the ATI spectra compared with a 1D soft-Coulomb potential. The laser parameter is the same as Fig. 3.3(c,d).

If the laser pulse consists of N cycles ($x = 2\pi Np/\omega$) then from the condition Eq.(3.5), the electron orbits will be distinguishable when $\varepsilon \ll N\sigma$. Note also that the uncertainty requirement $1/\delta p \ll \Delta x$ imposes another condition $\sigma \ll \omega$.

It is shown in the next chapters that the ionization in the stabilization regime happens by multiphoton absorption from the KH states, and one can see the classical cutoff ($10U_P$) for the rescattered photoelectrons is fulfilled from KH states.

In order to estimate the effect of the the Coulomb tail on the rescattering events, the energy-position phase space distribution of the ionized WP of a 1D model atom with a Yukawa soft-Coulomb potential interacting with a laser pulse of $\omega = 3.0$ is calculated, with the corresponding ATI spectra shown in Fig. 3.4. It can be seen from the energy-position distribution, that the probability of the whole of the trajectories up to $10U_P$ is higher than the background which is distinguishable from Fig. 3.4(b). Furthermore, the large difference in the amplitude of the photoelectron in the rescattering region of the ATI spectra between the short and long range potentials, shows that the tail of the potential on the rescattering dynamics. Although, the tail of the potential influences the ionization probability, which corresponds to the direct photoelectrons, damps the rescattering probability exponentially. In next chapter the time-analysis of the ionized WP indicates the characteristic ionization at high frequencies.

3.4 Classical trajectory Monte-Carlo

We have also carried out classical trajectory Monte-Carlo (CTMC) simulations and derived classical phase space distribution to compare with its quantum counterpart.

The classical trajectory Monte Carlo (CTMC) method, proposed by Abrines and Percival [117], has proved remarkably successful for ion-atom collisions. Moreover, this method has been widely used to calculate ionization dynamics of atoms and molecules in intense laser fields. Although, some features of the intense field dynamics are deduced from the CTMC calculation, it is related strongly to the wavelength and the intensity of the laser pulse. For example in the tunneling regime, one needs to manipulate the equation of motion to include the tunneling condition of the ionization. On the other hand, in the over-the barrier intensity regime, the ionization dynamics and intense field features are related to the frequency of the laser pulse. In addition to the laser parameters, the dimension of the model system changes the CTMC results dramatically where as in the quantum case, the results are qualitatively the same in different dimensions.

In this section, the corresponding results of the CTMC for our model atom are compared to the quantum calculations to explore the classical signature. In the CTMC method, exact classical dynamics is performed on trajectories whose initial conditions are chosen from the classical ensemble. The only quantum-mechanical information used in the method originally put forth, is the initial energy of the model atom, e.g. $E_0 = -0.5$ a.u. for the hydrogen atom. It is assumed that the initial coordinates and momenta are uniformly distributed in the phase space on this energy shell, i.e. the microcanonical distribution. In this work, the microcanonical distribution of the ground state of the 1D model atom is used as an initial condition.

Phase-space distribution of CTMC propagation

The energy-position phase space distribution is calculated with CTMC method and the results for the $\omega = 1.0$ at two different intensities are shown in Fig. 3.5(a,b). This figure shows in the stabilization regime Fig. 3.5(b) the maximum energy of the ionized electron is much smaller than the classical prediction ($2U_P$) with the SM model. As it was observed from the quantum calculation above, the probability of photoelectron emission falls significantly within a few atomic units which means in the classical calculation, ionized electrons gain only a small amount of energy and one cannot see true SM cutoff for direct ionization. Due to the multicycle ionization, which is also the origin of the stabilization at higher frequency, the electron trajectories see more optical cycles of the external field in addition to the Coulomb potential. However, one can see the energy of the ionized electron ends up closer to the cutoff energy at low intensity Fig. 3.5(a) where the model atom shows no stabilization but still multicycle ionization prohibits any rescattering effects. We show later that for IR frequency and OBI regime in the 1D CTMC calculation there is no efficient rescattering like in the quantum case, although there exists traces of rescattering from Coulomb potential. In order to complete our description of the photoelectron emission at high frequency, the energy-position phase space distribution for the near-IR frequency, $\omega = 0.056$, at two different intensities are shown in Figs. 3.5(c,d). As this figure shows, the energy of the ionized trajectories is larger than the cutoff energy of the direct trajectories from the SM's model which means the electron can still gain extra energy from laser field as the rescattering conditions happens. We mention that there is

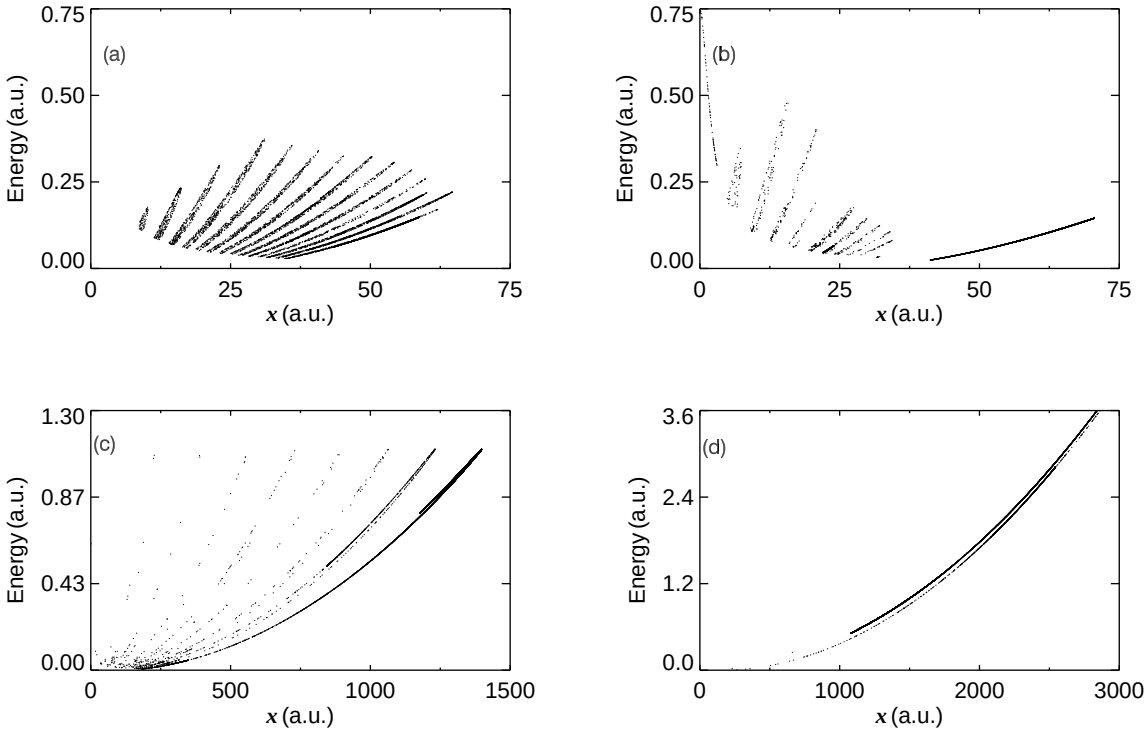

Figure 3.5: The final energy-position distribution of the ionized trajectories calculated with CTMC of a 1D model atom irradiated by a laser pulse with frequency $\omega = 1.0$ a.u. and a pulse length of 40 optical cycle including a 5-cycle ramp. The peak electric field is set (a) $E_0 = 1.0$ and (b) $E_0 = 4.0$. In (c) and (d) a laser pulse of $\omega = 0.056$ a.u. and a pulse length of 10 optical cycles including a 1-cycle ramp is used. A peak electric field is set (c) $E_0 = 0.07$ and (d) $E_0 = 0.2$.

no report on the existence of the rescattering of the CTMC trajectories in one dimensional calculation. Here the phase-space representation shows the trace of the rescattering in low frequencies in one dimension.

The classical motion of the particles in the combined laser-Coulomb fields becomes chaotic if the number of cycle of the laser pulse increases. However, the chaotic behavior is related to the energy of the particles and is pronounced when the energy of the trajectories is close to the threshold energy. With increasing velocity of the particle at ionization time, the chaotic behavior decreases. At higher frequencies the electron moves closer to the nuclei and the bound electron sees more optical cycles before the ionization, consequently the chaotic behavior increases and the final energy of the trajectories become smaller than the cutoff.

3.5 Summary

The ionization dynamics and the photoelectron spectra of a model atom by a laser pulses of various frequencies at different intensities are studied. This was carried out in terms of a solution of the time-dependent Schrödinger equation. An adequately large box-size and fine grid was taken to ensure good accuracy in the resulting ionization probabilities and paths. The classical $10U_P$ cutoff in the ATI spectra is reached for different frequencies which proves that the rescattering is independent of the frequency and has a classical origin and for soft-Coulomb potential is observed in the phase-space representation. The frequency of the laser pulse has an influence on the probability of ionization. It has been shown that the ionization happens at any optical cycle regardless of the frequency and the ionization is not a multicycle process at high frequencies. The large decreasing of the amplitude of the photoelectron spectra in TDSE calculations comes from the range of the potential and the stabilization at high frequencies. The CTMC simulation showed that the rescattering at low frequency increases the final energy of the ionized trajectories at low intensity while at high frequency the many cycle dynamics before the ionization and chaotic behavior smears the rescattering energy of the electron.

Chapter 4

Time analysis of above-threshold ionization at XUV lasers

The response of atoms and molecules in strong laser fields depends essentially on the frequency and the amplitude peak of the applied electric field. It is well known that in the high frequency limit when $\omega \gtrsim I_p$, where ω is the laser frequency and I_p the atomic ionization potential, stabilization of atoms against ionization can happen in a rather intense laser field [18]. A formalism of the high-frequency Floquet theory (HFFT) has been developed to explain this phenomenon in a monochromatic laser field (quasistationary stabilization) [118], according to which the stabilization is due to the formation of electron quasi-stationary states in the atomic potential averaged over the fast electron oscillations in the laser field (Kramers-Henneberger potential [16, 17]).

On the other hand, direct integration of the time-dependent Schrödinger equation has been used to study nonadiabatic effects for the stabilization in a pulsed laser field (dynamic stabilization). Though the stabilization phenomenon has been discovered and explained about 20 years ago, the interest to this regime has been renewed recently. A recent study of Gavrila [107] within HFFT indicates that the atomic stabilization can be established even at laser frequencies lower than the atomic frequency when a condition fulfilled $\omega\alpha^{2/3} >> 1$, where $\alpha = E_0/\omega^2$ is the classical excursion amplitude of the electron in the laser field and E_0 the amplitude of the laser field. A unified view of low and high frequency regimes has been proposed in [119]. In this chapter the time analysis of the ionization at laser fields is derived and it is used as a stabilization evidence in a laser field with an arbitrary frequency.

4.1 The model system

From a solution of the TDSE

$$i\frac{\partial}{\partial t}\Psi(x,t) = \left\{\frac{1}{2}[\hat{p}_x - \frac{1}{c}A_x(t)]^2 + V(x)\right\}\Psi(x,t), \tag{4.1}$$

under a soft-core scalar potential in the x axis

$$V(x) = -\frac{Z}{\sqrt{(a/Z)^2 + x^2}}\exp(-(x/R)^2), \tag{4.2}$$

and the laser pulse

$$E(t) = E_0 f(t)\cos(\omega t), \tag{4.3}$$

the wavefunction at the end of a pulse is used to analyze the dynamics during the interaction with the laser pulse. In order to study the ionization dynamics at high frequency with time and trace it to the lower frequencies, Eq. (4.1) is solved for two different regions of the carrier frequency of the laser pulse: *i*) frequencies smaller than the ionization potential (i.e. $\omega < I_P$), and *ii*) higher frequencies (i.e. $\omega > I_P$). To this end, the ionization probability as a function of the intensity for each frequency is calculated to extract the suppression ionization region. The above-threshold ionization spectra and its time-profile in different regions are calculated and compared. The ATI spectra and the time-dependent analysis are deduced by applying the window operator

$$\hat{W}(E_k, n, \sigma) = \frac{\sigma^{2^n}}{(\hat{H}_0 - E_k)^{2^n} - \sigma^{2^n}} \tag{4.4}$$

which is explained in chapter 2. By cutting the phase space distribution at a certain energy and by an appropriate coordinate-to-time mapping $t = x/\sqrt{2E_k}$, we drive the time-profile of the ionization wave packet (WP) at a given electron energy. Having presented the general theory, we are now ready to look at the results of the time analysis of ATI.

In this part we present the ionization probabilities as a function of intensity and frequency. We are interested in finding the stabilization intensity for each frequency. To this end, ionization probability of the electron WP of a 1D model hydrogen atom is calculated at different frequencies $\omega = 3.0$ and $\omega = 0.4$ as a function of the intensity by projection on the bound state at the end of the pulse and the results are displayed in Fig. 4.1. The number of optical cycles of the laser pulse is set to 20 for $\omega > I_P$ and 10 for $\omega < I_P$. To avoid large nonadiabaticity effects a $\sin^2$ pulse with zero flat duration are used , i.e. $t_{\text{on}} = t_{\text{off}}$. This Figure shows that under the laser field, ionization probability at high intensities (i.e. $\alpha = E/\omega^2 > 1.0$) in the case of high frequency decreases and remains constant for low frequencies. The oscillation is due to the resonances between the dressed states, which is the character of the one dimensional model atom and in a three dimensional model atom diminishes in virtue of many angular ionization paths and spreading. Now we consider the ionized part of the wavepacket within the dynamic stabilization framework which can be described with dichotomy. To have KH condition one needs a laser pulse with a flat part. The bound states at the end of the pulse are projected out and the result for the laser pulse with 10 cycle flat part are shown in Fig. 4.2. The laser frequency and the intensity are $\omega = 3.0$ and $E_0 = 25$ respectively. After the ionization of the WP in raising ramp of a laser pulse the ionized part moves with the velocity at ionization time. The main part of the ionization occurs at the raising and falling ramp of the laser pulse which

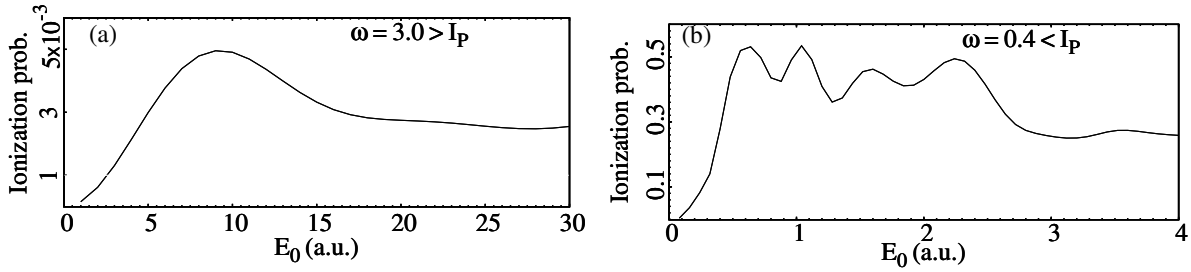

Figure 4.1: Ionization probability of a 1D model atom is calculated as a function of the electric field of the laser pulse by the projection of the final WP on the total bound states.

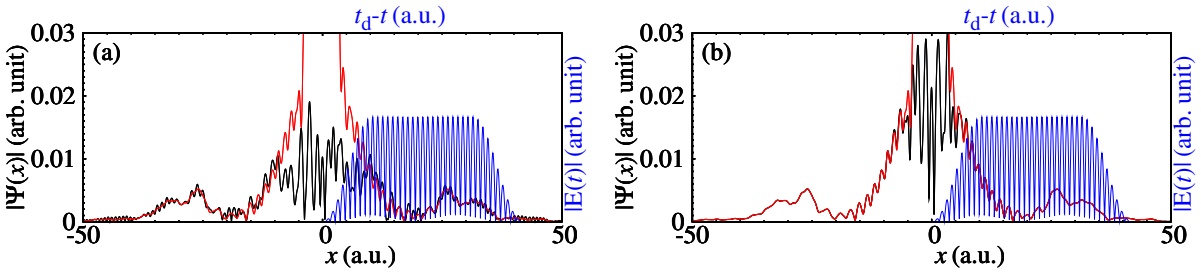

Figure 4.2: (a) red, The total WP; Black, ionized WP at the end of the pulse of frequency of $\omega = 3.0$ a.u. and electric field of $E_0 = 25$ a.u.;(b) The same as (a) in which 4 bound states are projected out. The pulse shape is indicated with blue.

have different travel distances. The bound WP is distributed mostly in few low lying bound states. Due to the superposition of the ionized continuum states in the final WP, the ionization dynamics is not clearly resloved in time. Although the dichotomy structure of the WP and time-dependent potential during the pulse at high frequency is another evidence for the stabilization, is not clear in low frequency (i.e $\omega < I_p$). In the following we show that the time analysis of the ionization can be used to explore the stabilization evidence at frequencies smaller than the ionization potential.

4.2 Time analysis of the ionization

Since 1970, when the ATI spectra were discovered, there is no clear time analysis of the ionization in a laser field. In this section we show the time behavior of the ATI which gives more information about the dynamics.

The ATI spectra and the time-analysis of the ionization is used to explain the stabilization during the laser pulse. To visualize the evidence of the stabilization from the ionization one has to analyze the time of the ionization of the WP, which is done and shown in this section by monitoring of the continuum states in the discretized representation with an

appropriate width including the desirable information.

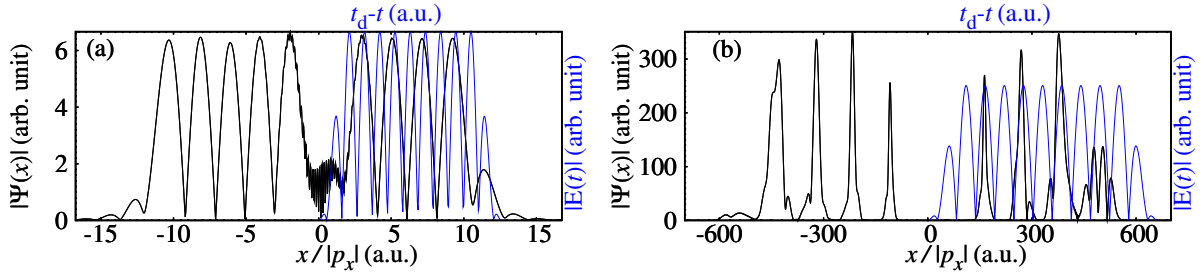

Figure 4.3: (a) The time profile of the ionized electron WP with energy $E_k = 6.0$ correspond to $N = 2$ in Eq. (4.5). The peak electric field and frequency of the laser pulse are set to $E_0 = 5$ and $\omega = 3.0$ respectively. The pulse length is 6 cycles including one cycle ramp on and off which is pointed out with the blue line; (b) The energy of the continuum is chosen $E_k = 5.0$ correspond to $N = 80$ in Eq. (4.5) for the same pulse shape of $E_0 = 0.095$ and $\omega = 0.057$.

One can extract the time analysis in quantum dynamics, according to the approximation:

$$E_k = N\omega + N_0\omega - (U_P + I_P) \tag{4.5}$$

where, the parameter N we have used to define energy of the continuum states in our calculation is varied with frequency. N_0 is the minimum number of photon to ionize the electron. On the other hand, the energy of the continuum states is low enough to have maximum ionization probability and less overlap with the bound states according to the energy bin (σ) in Eq. (4.4). Here the width of the continuum states 2σ is less than one photon. To show the ionization in the domain of one optical cycle, the time profile of the continuum states centered around the fixed energy in the rescattering region for the two frequency $\omega = 3.0$ and $\omega = 0.057$ are calculated and shown if Fig. 4.3. The width of the window operator (σ) is chosen 4 and 0.2 for $\omega = 3.0$ and $\omega = 0.057$ respectively. The intensity and the length of the pulse in the high frequency is low enough to avoid the stabilization effects. Fig. 4.3(a) shows the phase of the ionized WP in the energy larger than $2U_P$ is shifted with respect to the phase of the vector potential of the pulse, which is in agreement with the result of the simple man's model (SM) presented in the next paragraph. Moreover, in the high frequency case from Fig. 4.3(a) one can observe the envelope of the ionization follows the envelope of the pulse.

Time-energy and time-final position of the ionized electron with SM model are analyzed and shown in Fig. 4.4. According to SM model which is independent of the frequency and intensity of the laser pulse, the energy of the direct ionized electron at the end of the pulse is given by $E_k(t) = [A(t_d) - A(t)]^2/2$ where t is the ionization time. Fig. 4.3(a) shows that the final position of the direct electron (black) is in phase with the vector potential (red) of the pulse therefore ionization probability is in phase with the vector potential. The final energy of the direct and rescattered electron in Fig. 4.3(b) indicates that the rescattered electron (blue) shifts almost $\pi/2$ respect to the vector potential, which is in agreement with Fig. 4.3. We note that the final position of the electron with respect to the origin depends on the sign of the momentum of the pulse at the ionization

and rescattering moments and is consequently related to the vector potential of the laser pulse at the corresponding time. Moreover, Fig. 4.4(b) shows the ionization with a fixed energy is related to the vector potential of the laser pulse at certain time.

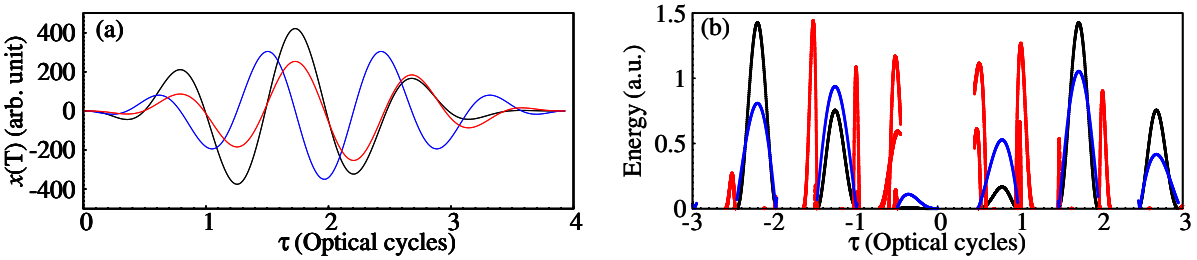

Figure 4.4: (a) Black: the final position of the electron trajectories ionized according to the SM's model without rescattering. Red: vector potential of the laser pulse. Blue: electric field of the laser pulse. (b) Time-energy analysis of the ionized electron trajectories according to the SM's model. Black: vector potential. Blue: direct ionized trajectories. Red: rescattered trajectories. The pulse length is 4 cycles with $\sin^2$ envelope and $U_P = 0.14$.

Stabilization evidence

In this section we apply our approach to consider the time analysis of the ionization in high frequency laser field in the stabilization regime. The ionized electron WP of the model atom at high frequency in the two regimes of the intensity are shown in Fig. 4.5. In fact we use a cross-section of the phase space distribution (see chapter 3) at a certain energy with an energy bandwidth of σ and an appropriate coordinate-to-time mapping $t = x/\sqrt{2E_k}$ to provide the time-profile of the ionization WP at a given electron energy. Below the stabilization regime $E_0 = 4.0$ the ionization WP follows the envelope of the laser pulse which indicates the prevailing of one photon process, i.e. the instantaneous ionization probability is proportional to the laser intensity. At high intensities, the two peak structure is indicative for the stabilization regime. The ionization probability is suppressed at the pulse maximum due to the stabilization and the ionization is enhanced only at the raising and the falling edge of the laser pulse. We observe also intermediate peaks between the major ionization bursts which arising during the flat part of the laser pulse or in the case of a rather long laser pulse which we will look more closely further. In Fig. 4.6 the electron WP in continuum states with $N = 5$ in Eq. (4.5) is shown for the different intensities selected from Fig. 4.1(b) where $\omega < I_P$. The width of the continuum states is set $2\sigma = 0.6$. In Fig. 4.6(a) shows at the low intensity the time profile pursues the envelope of the laser pulse conversely, at high intensity in Fig. 4.6(f) the two main ionization probability is obvious. There is two differences from the corresponding dynamics in high frequency, one is left-right asymmetry which is due to the electron drift on the raising ramp of the laser pulse during which the ionization probability in one side (e.g. Fig. 4.6(c) raising ramp right) of the oscillation length is higher and the bound WP has disposable drift in the same direction, alternatively, throughout the lowering ramp of the laser pulse the coulomb force accelerates the WP and induces more ionization probability to the opposite direction (e.g. Fig. 4.6(c) lowering ramp left). The second is some other

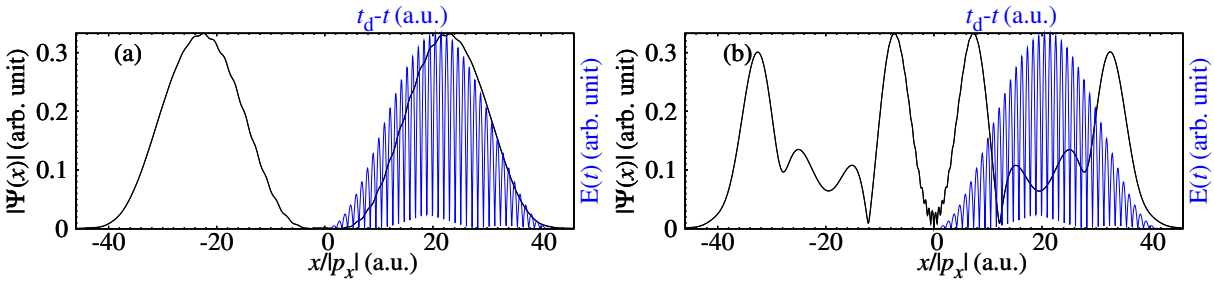

Figure 4.5: Time-analysis of the ionization of the electron WP of a 1D model atom with $N = 1$ in Eq. (4.5) and $\sigma = 1.0$. The peak electric field is (a) $E_0 = 4.0$ and (b) $E_0 = 25.0$. The blue curve indicates the pulse shape with $\sin^2$ envelope including 20 optical cycles.

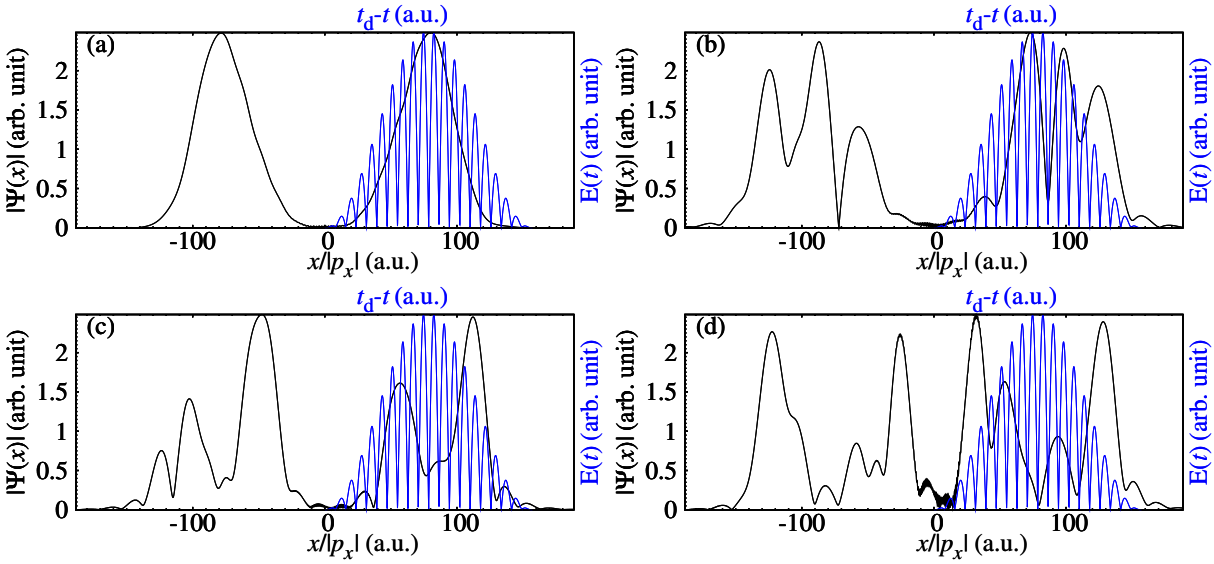

Figure 4.6: Time-profile of the ionization probability of the electron WP with $\varepsilon = 2$ and $\sigma = 0.3$. The peak electric field is (a) $E_0 = 0.16$, (b) $E_0 = 0.64$, (c) $E_0 = 1.28$ and (d) $E_0 = 2.88$. The laser pulse of 10 optical cycles and frequency $\omega = 0.4$ is used and shown with blue.

peaks between the two main ionization probability for which the physical origin can not be distinguished because of the repopulation of the exited states due to resonances or short pulses in the intermediate frequencies (i.e.$\omega << I_P$).

Now we consider time profile of the ionization in a laser field with a flat part (i.e. $t_{\text{off}} >>_{\text{on}}$) where we can use efficiently the KH frame to analyze the dynamics. The time-dependent Schrödinger equation in KH frame reads

$$-i\partial_t \Psi_{KH} = \left\{ \frac{1}{2}\hat{p}_x^2 + V(x+\alpha_t) \right\} \Psi(x)_{KH} \tag{4.6}$$

where $\alpha_t = \int_0^t A(\tau)d\tau$ is a classical trajectory of the moving particle in an oscillating field and $A(t)$ is the vector potential of the laser field. By averaging of $V(x+\alpha_t)$ in one optical cycle one arrives at a time-independent problem and corresponding KH wave functions,

$\Psi(x)_{KH}$.

$$\left\{\frac{1}{2}\hat{p}_x^2 + V(x+\alpha_0)\right\}\Psi(x)_{KH} = E_{KH}\Psi(x)_{KH} \tag{4.7}$$

KH frame is convenient to represent the dynamics of an electron in an intense high frequency lasers field. One can describe the system in terms of the KH states and the laser field. It has been shown in chapter 3 that the phase-space representation of the ATI spectra shows the classical cutoff ($10U_P$) for the rescattered photoelectrons. The position of the peaks however corresponds to the absorption of the multiphoton from the KH states. This means that the electron dynamics is in the KH states and small part feels the coulomb field like low frequency. The higher order terms of the potential have to be included in addition to the KH potential. The time-profile of the photoelectron WP with

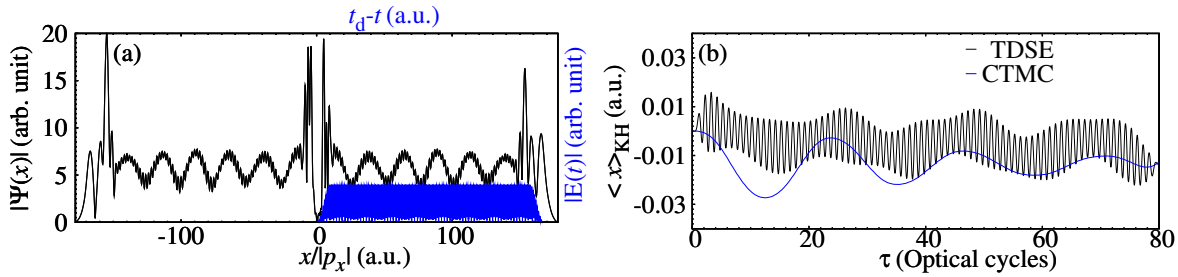

Figure 4.7: (a) Time profile of the ionized WP with energy $E_k = 10\omega$ under the interaction of 80 cycle laser pulse including 5 cycle ramp with $\omega = 3.0$, $E_0 = 25$. (b) Expectation value of the electron displacement (black) TDSE, (blue) CTMC.

a certain energy in a 80 cycle laser pulse with 70 cycle constant amplitude is shown in Fig. 4.7(a). The characteristic time scale of the periodic enhancement of the ionization yield during the interaction is much larger than the laser period (the corresponding energy scale is much smaller than the photon energy). This hints to the possible connection of the ionization enhancement with the slow drift of the electron classical trajectory in the KH potential. It is known that in a laser field an electron drifts with a uniform velocity, along with oscillations at the laser frequency. At high laser frequencies the drift is not uniform but the direction of the drift changes to the opposite when the electron oscillation turning point approaches the nucleus [120]. At this closest point of the electron WP to the nucleus the ionization probability can be enhanced because the nucleus can provide more effectively the necessary momentum for transition to the continuum. To check this hypothesis we have to analyze the electron trajectories and observables during the pulse in the KH frame.

The single trajectory of the electron in a field of Coulomb and intense laser field in KH frame within the framework of the CTMC method in the stabilization regime is calculated and for the two different pulse length is shown in Fig. 4.8. This figure as explained in Ref. [120] shows different dynamics such as drift and wiggling in KH frame. As can be seen from this figure, the trajectory remains bound at the end of the pulse. However, as an electron meets the position of the nuclei in the KH frame it changes its momentum. This

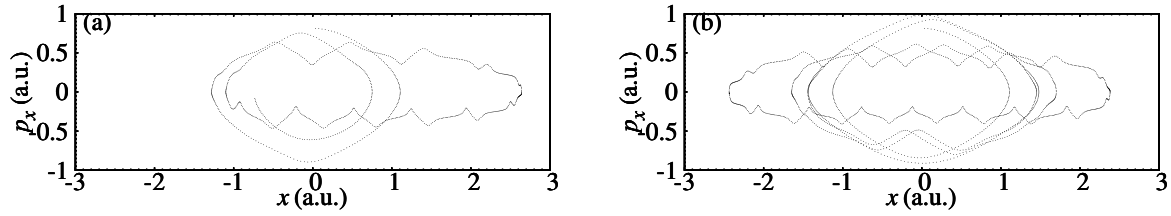

Figure 4.8: Single trajectory of the electron moving under the combined one dimensional soft-Coulomb potential and a laser pulse in the KH frame is calculated in the frame work of the CTMC. The laser pulse of $\omega = 3.0$ and $E_0 = 25$ is used which involve (a) 20 and (b) 40 cycles including 5 cycles ramp on and off.

process repeats during the interaction with the laser pulse if the electron gains enough momentum it can ionize classically. The nonionizing trajectories show the maximum number of drifts in the KH frame through the interaction with the laser field and increase with increasing pulse length Fig. 4.8(b). However, in quantum mechanical calculation within the change of the momentum one expects to see a change in the ionization probability. This process in quantum mechanical simulation is accompanied with the coupling of the field dressed states (the KH states). As can be seen from Fig. 4.5(b), the peaks inside the two bump of the ionization during the ramp are the evidence of the classical signature which has been explained by another approach in Ref. [113]. One has to notice that the single classical trajectory is not enough to describe completely the oscillation in the time profile of the ionized WP in certain energy. To check this hypothesis, we have calculated the quantum expectation value of the electron coordinate via TDSE solution as well as the average coordinate according to the CTMC simulation, see Fig. 4.7(b). The average value of the electron displacement from the CTMC and TDSE calculations are qualitatively consistent. Moreover, the maxima of oscillations in the time-profile of the ionized WP corresponds to the maxima and minima of the electron displacement $\langle x \rangle$.

The integrated spectrum of the ionized WP with one and four photon absorption for the system of Fig. 4.7 is indicated in Fig. 4.9. The two peaks in the spectral line result from the

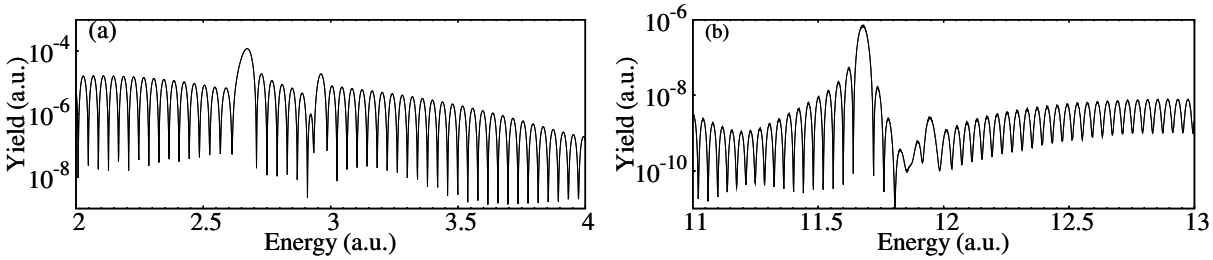

Figure 4.9: The first and forth peaks of the ATI spectra for the same system of Fig. 4.7(a). A short range potential with the same $I_P = 0.5$ is used.

photoionization of the ground and the second excited KH light induced states, while the deep position corresponds to the absorption of four photon from the second KH state. One

can see a good correlation between the time-profile of the ionized WP in Fig. 4.7(a) and the electron spectrum in Fig. 4.9. According to the spectrum, the ionized WP of a certain energy ε (with a bandwidth $\sigma = 1$) is formed from the contributions which originate either from the ground state or from the second excited state: $\psi_\varepsilon = a_1 \exp(ip_1 x - i\varepsilon_1 t) + a_2 \exp(ip_2 x - i\varepsilon_2 t)$, where $\varepsilon = n\omega$, $\varepsilon_{1,2} = \varepsilon_{g,e2} + n\omega$, $p_{1,2} = \sqrt{2\varepsilon_{1,2}}$ and $\varepsilon_{g,e2}$ are the energy of the ground and the second excited state, respectively. Consequently, the density of the ionized WP at the energy ε is modulated by a frequency corresponding to the energy difference $\varepsilon_{e2} - \varepsilon_g$:

$$|\psi_\varepsilon|^2 = |a_1|^2 + |a_2|^2 + 2|a_1||a_2| \cos(\Delta p x - \Delta\varepsilon t + \Delta\varphi), \tag{4.8}$$

where $\Delta\varphi = \arg\{a_1^* a_2\}$. The modulation length is $\Delta x = 2\pi/\Delta p = 2\pi p/\Delta\varepsilon$ which, scaled in the number of laser cycles, reads $\Delta N = \Delta x/Tp = \omega/\Delta\varepsilon$, where $T = 2\pi/\omega$. From the spectrum of Fig. 4.9 $\omega/\Delta\varepsilon \approx 10.6$ which approximately corresponds to the modulation duration in Fig. 4.7(a) $\Delta N \approx 11.3$. The period of the slow oscillations of the average electron displacement $\langle x \rangle_{KH}$ is approximately two times larger than the modulation period of the ionization. This is because $\langle x \rangle \equiv \langle \psi | x | \psi \rangle \approx \langle g | x | e1 \rangle \sim c_g^*(t) c_{e_1}(t) \exp(i(\varepsilon_g - \varepsilon_{e1}))$ and the modulation period of $\langle x \rangle$ is determined by the energy difference $\varepsilon_{e1} - \varepsilon_g$ which is almost two times smaller than $\varepsilon_{e2} - \varepsilon_g$ and the fast oscillation is due to $c_g^*(t) c_{e_1}(t)$.

A question arise why the peak corresponding to the ionization from the first excited state is absent. Is this bound KH state not populated during the ramp of the laser pulse? To answer this question, we investigate the population dynamics of the bound states in the laser field, see Fig. 4.10. The non-vanishing oscillatory population dynamics however, shows that the peak from the second KH state should exist in the ATI spectra but due to a destructive interference is absent (see chapter 5). The oscillations on the envelope

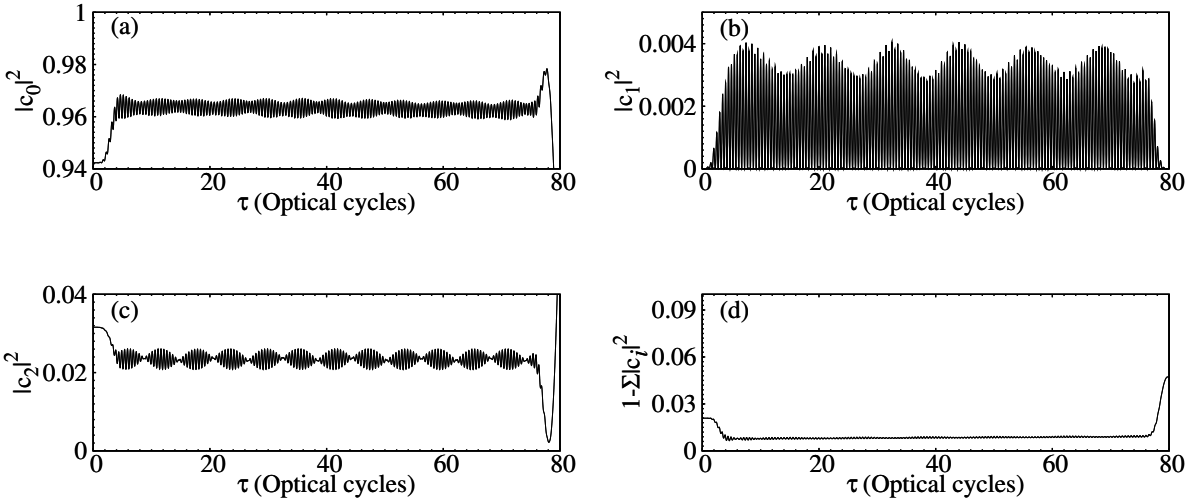

Figure 4.10: (a-c) Time profile of the population dynamics of the bound KH states of our model atom under the interaction of 80 cycle laser pulse including 5 cycle ramp with $\omega = 3.0$, $E_0 = 25$; (d) Population dynamics of the continuum states. A short range potential with 5 KH states is used.

of the population dynamics indicates the drift population transfer which agree with the oscillation of the envelope of $\langle x \rangle_{KH}$ for odd states. First of all, we see that the population of the first excited state does not vanish and in principle could have produced an ionization peak in the ATI spectrum. We see also that the drift of bound electron WP induces also oscillation of the population of bound states. The population in the odd KH state shows six oscillations on the envelope during the constant part of the pulse which corresponds to the number of extrema of the envelope of $\langle x \rangle_{KH}$ (three maxima and three minima). With increasing of the laser intensity, the field dressed states evolve from the field free states to the bound and continuum light-induced states. During the fast ramp of the laser pulse the states with the same parity as the initial states are populated without photon absorption. Later, during the flat part of the laser pulse, the dressed bound states couple to each other via continuum due to photon absorption. In this way, the states with different parity from the initial one can be populated during the interaction with the laser pulse, for example, population of the first and third excited state in Fig. 4.10. We see that this type of the population transfer is correlated with the electron drift motion. The population of the odd KH state is larg when the drift distance of the bound WP is large corresponding to the amplitude of the excursion confirmed by the expectation value of electron displacement. The population transfer from the first KH state to the second one due to the drift can be related to the fact that at the turning points of the drift motion the bound WP becomes very asymmetric and requires contribution from the negative parity bound state for its formation. One can deduce from the latter that the Coulomb disturbance during the drift of the bound wave packet causes transitions between the ground and the first excited states.

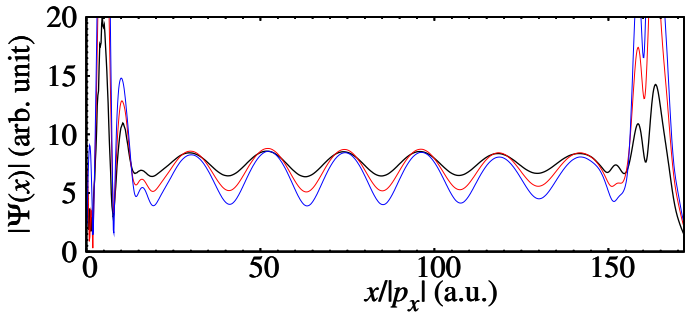

Figure 4.11: The time-profile of the ionization probability of the electron WP of a 1D model atom with $\sigma = 1.0$. (black) $\varepsilon = 4\omega$, (red) $\varepsilon = 5\omega$, (blue) $\varepsilon = 6\omega$. The peak electric field of the laser pulse is $E_0 = 25.0$ and the laser frequency is $\omega = 3.0$ a.u.

The time-profile of the ionization probability of the electron WP of a 1D model atom at three consecutive photon number (4, 5, 6) is calculated and shown in Fig. 4.11. This figure shows the same modulation on the envelope of the ionization due to the fact that the total ionization probability has the same time profile.

4.3 Rescattering of multiple returns

The response of the atoms and molecules in strong laser fields depends essentially on the frequency and the amplitude of the applied electric field. In the low frequency limit the tunneling and quasi-static over the barrier ionization is applicable [50]. On the other hand in the high frequency limit i.e. $\omega >> I_P$ the multiphoton and over the barrier stabilization ionization occurs [121].

The atomic behavior at low frequency and tunneling regime can be qualitatively described within the strong-field approximation (SFA) or classical simple man's model. According to SM model electron ionizes directly at any time of the interaction with the laser pulse with equal probability where its energy proportional to the vector potential of the field at the time of the ionization. In order to extract the rescattering electron within this model it needs to manipulate the equation of motion. Due to the absence of the Coulomb potential one needs to estimate the rescattering time and the momentum manually to generate the rescattering photoelectrons and plateau. When the electron ionizes at time t_0, it generally rescatters not only within the next half cycle but it can be crossed over the core to another side without interaction and rescatters in the next cycle which can be considered until the end of the pulse. SM model promises to separate the rescattering in the next cycles from those in the first cycle of the ionization time. But in a real quantum mechanical system this is impossible. The purpose of this section is to consider rescattering at $\omega \gg I_p$ quantum mechanically and compare with SM model to show how important the rescattering in the next cycles after the ionization (multiple returns) is. At low frequency, ionization happens at each optical cycle with the same probability in the multiphoton and tunneling ionization regime and it is not possible to explore the differences in the probability of the photoelectrons in the rescattering plateau ($E_k > 2U_P$) and direct plateau ($E_k < 2U_P$) region. Moreover, at high intensities due to the barrier suppression, ionization saturates on the rising ramp of the laser pulse at low frequency. Therefore, at high frequency laser pulse in the stabilization regime one can use the time-profile of the ionization to consider higher order return in high frequency laser pulses.

In Fig. 4.12 the time behavior of the ionization at certain energy in low (MPI) and high (high OTBI) intensity regime for two different frequencies are compared. In MPI regime, Fig. 4.12(a,b) irrespective to frequency the majority of the ionization corresponds to the peak of the pulse and in high frequency case regularly follows the shape of the pulse. At high intensities a huge difference appears between the time profile of the ionization in two frequencies. Although the pulse at $\omega = 3.0$ has a flat part with ramp, shows left-right regular symmetric behavior with two major of the ionization during the ramps instead at low frequency the ionization is completed within the rising ramp of the pulse with completely asymmetric structure. We note that at high frequency ionization is less than 0.2 persent. With this properties of the envelop of the ionization probability we are able to trace the rescattering process with time and energy.

The time-energy profile for $\omega = 3.0$ in the stabilization regime is calculated and indicated in Fig. 4.13. This figure shows the two bump ionization probability within the ramp and

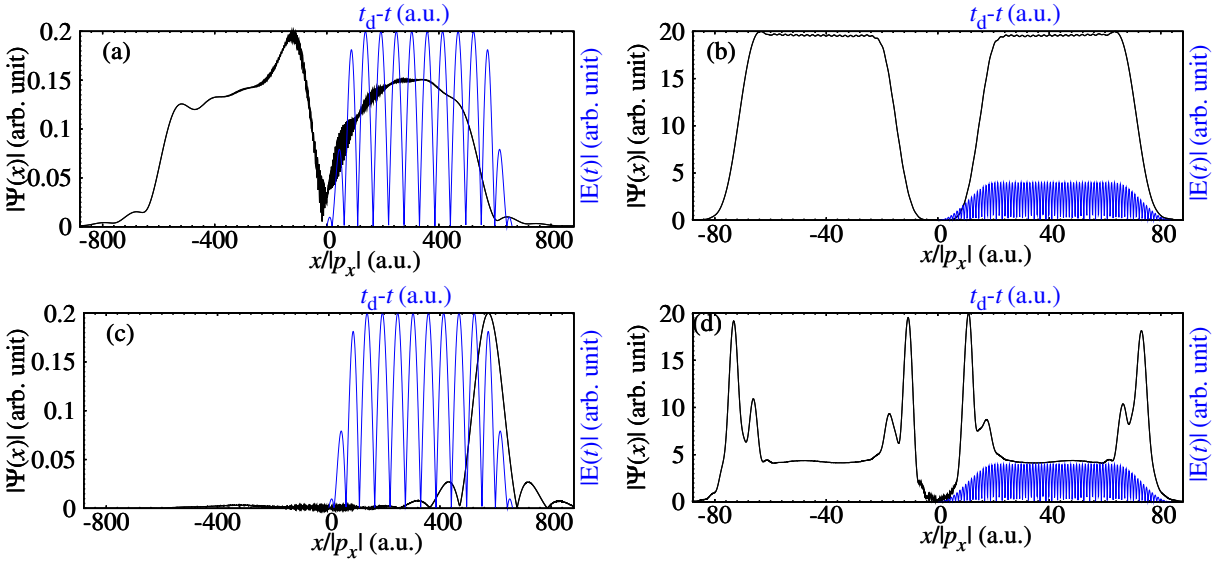

Figure 4.12: (a,c) The time profile of the ionized electron WP with energy $E_k = 15.0\omega$. A laser pulse of $\omega = 0.057$ is used. The peak electric field is set to 0.05 in (a) and 0.35 in (c). (b,d) The energy of the continuum is $E_k = 2\omega$ for a laser pulse of $\omega = 3.0$ and peak electric field 5 in (b) and 25 in (d). The laser pulse envelope is indicated with blue.

stays constant between the ramp on and off. According to SM model which is independent

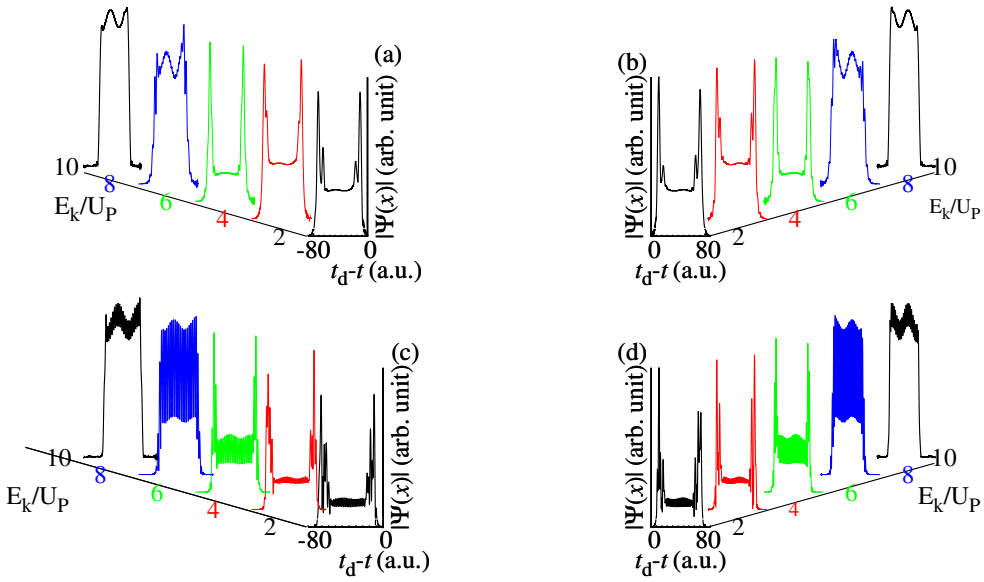

Figure 4.13: The time-energy analysis of the ionization of the electron WP of a 1D model atom (a,b) $\sigma = 1.0$ and (c,d) $\sigma = 2.0$. A 80 cycles pulse with 5 cycles ramp of $E_0 = 25.0$ and $\omega = 3.0$ is used. (a) and (c) indicate the ionization to the left. (b) and (d) indicate the ionization to the right.

of the frequency and intensity, the energy of the direct ionized electron at the end of the pulse is given by $E_k(t) = [A(t_d) - A(t)]^2/2$ where t is the ionization time. The final energy of rescattered ionized electron moving with SM model in the laser pulse respect to the ionization and rescattering time are shown in Fig. 4.14. To separate the rescattering

in the same or the next optical cycle of the ionization time, the ionization is restricted to one half cycle (3,3.5) and the rescattered trajectories in the first return (red) or next returns (blue) are indicated separately. The dependence on the ionization or rescattered

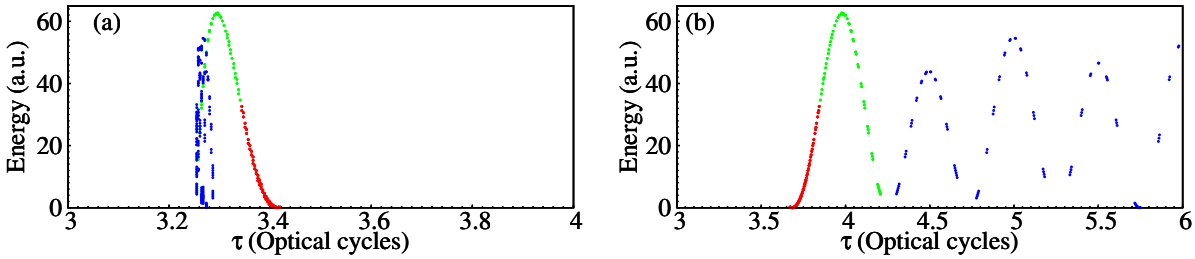

Figure 4.14: The time-energy analysis of SM model ionization of point charge in one dimension with $U_P = 6.5$.

time are shown in Fig. 4.14(a) and Fig. 4.14(b) respectively. One can see the well known results in this figure that the trajectories rescatter with the ionization time in the second quarter. Moreover this figure indicates that the energy of the next returned electron ends up to $9U_P$. With comparison of the SM model and the quantum results in Fig. 4.13 it can be understood that the probability of the rescattering of the next returns are negligible while in the quantum mechanical calculation there is no effect of the bump ionization in the next cycle as a function of energy. To trace the rescattering at next returns of the ionized electron WP, after the first major of the ionization and establishing of the KH states the bound KH states are projected out and the time-energy profile is indicated in Fig. 4.15. The absence of the major of the ionization within the falling ramp confirms the validity of the KH states, moreover there is no ionization or remarkable rescattering at higher return.

4.4 Summary

In this chapter the time-analysis of the ionization is derived and the ionization of a model atom is explained in time at different frequencies. The time domain can be deduced with an appropriate coordinate-to-time mapping. The time-analysis is carried out by applying of the projection operator at a certain energy of a continuum states with an appropriate width on the final wavepacket. The stabilization dynamics have been proved by a time-analysis at XUV lasers with an arbitrary frequency.

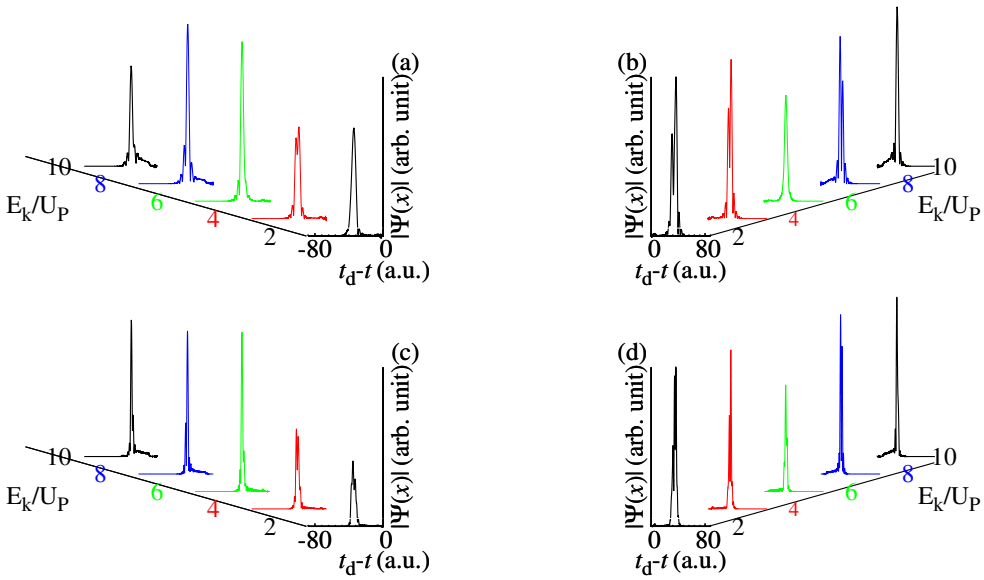

Figure 4.15: The time-energy analysis of the ionization of the electron WP of a 1D model atom (a,b) $\sigma = 1.0$ and (c,d) $\sigma = 2.0$. A 80 cycles pulse with 5 cycles ramp of $E_0 = 25.0$ and $\omega = 3.0$ is used. (a) and (c) indicate the ionization to the left. (b) and (d) indicate the ionization to the right. The first KH state is projected out after the raising ramp of the laser pulse.

Chapter 5

Interferences of photoelectrons at XUV lasers

Short laser pulses allow for studying the ionization process in detail and the interference effect which has intensively studied at IR frequencies for tightly bound states and microwave frequencies for Rydberg states. The response of atomic systems in intense high frequency laser fields (i.e. $\omega >> I_P$) has recently been studied theoretically. Fine structures in HHG spectra in the stabilization regime due to hyper-Raman transitions have been shown in [122]. Other interesting developments concerning dynamic stabilization are reported in Ref. [113, 114]. The first effect connecting the fine structure of the ATI spectral line which is due to the interference of ionization waves emitted at the rising and falling edges of the laser pulse. The second effect is the emission of slow electrons due to an adiabatic variation of the envelope of the laser pulse.

There are two different processes to suppress ionization in an intense laser field. The quantum interference from the coupled Rydberg states is studied in so called Rydberg interference stabilization. On the other hand high frequency stabilization via KH states is predicted at high frequency lasers where $\omega > I_P$. In this chapter the different types of the interferences at XUV lasers are shown. In addition it will be shown that the quantum interference occurs from the coupled KH states at high frequency XUV lasers.

5.1 Ramsey-type interference

In Fig. 5.1 the ATI spectra for two selected intensities (multiphoton and stabilization regimes) are shown. By comparing of the spectra at low (black) and high (red) intensities, we note that, when the intensity is high enough to stabilize the atom in addition to the broadening of the peaks, each peak has a sub structure which is expanded in Fig. 5.1(b). The ATI spectra shows two types of fine structure, one occurs on the background of the spectrum and the other is the splitting of the main peaks. The former is due to the background ionization of the short pulse which depends on the length of the pulses

and the latter is the interference of the ionized electron at the raising and lowering edge of the laser pulse [113]. Since the rising and the lowering part of the ionization do not repeat coherently and are not multiphoton processes, they have the strongest intensity in the first few peaks. Another effect in the stabilization regime is the ionization of the electron WP with low energy near the threshold [114]. In this figure one can see a slow electron peaks which represents the nonadiabatic ionization of the electron WP during the ramp of the pulse.

One observes that the classical cut-off energy ($10U_P$) is not fullfield in the ATI spectra which is due to the stabilization and ionization at the level of the numerical background but it is found, that the energy of the scattered WP ends at the classical cut-off and is confirmed via phase-space representation (see chapter 3).

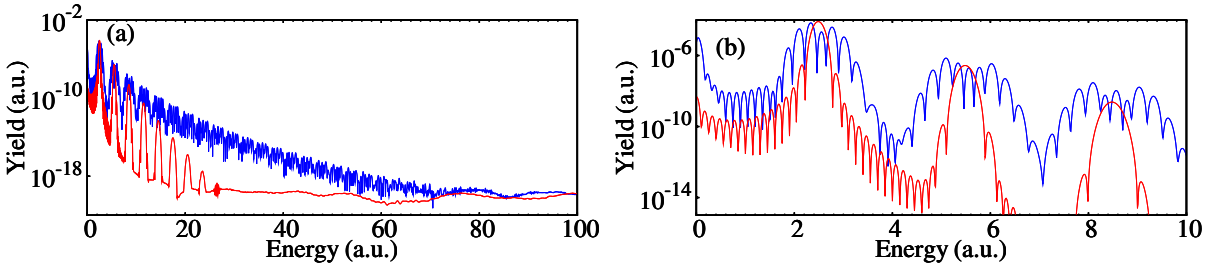

Figure 5.1: (a) The energy spectra of a 1D model atom irradiated by a laser pulse with frequency $\omega = 3.0$ a.u., and a pulse length of 20 optical cycle. The peak electric fields are set to $E_0 = 4.0$ (red) and $E_0 = 25.0$ (blue). (b) The enlarged detail of the first peaks.

5.2 Interference of Kramers-Henneberger states

Now let us go back to the intermediate structures which arise during the flat part of the pulse and the connection to the interference of the ionization which was shown in Fig. 4.7 and explained in the previous chapter. On the other hand, this intermediate structures are due to the coupling between the KH states which results also an interference in the ionization spectra. To clarify the type of the interference and its origin, we consider the ATI spectra of a model atom with short range potential because one needs finite bound states to simplify the spectrum. The spectrum of the ionized WP with four photon absorption for our model atom with four field free states is shown in Fig. 5.2 (blue line). Due to the coupling of the bound KH-states via continuum, there can be additional quantum paths for ionization besides the direct ionization path creating interference effects in the ATI spectrum. Let us investigate the possibility for interference of different quantum paths to the continuum originating from different bound states. We have calculated the ATI spectrum by projecting out the population of either the ground KH-state Fig. 5.2(a, black line) or the first excited one Fig. 5.2(b, black line) after the raising ramp of the laser pulse. In the first case, when the ground state population is projected out, the ionization path starting from this state is cancelled (the peak corresponding to the ionization from the

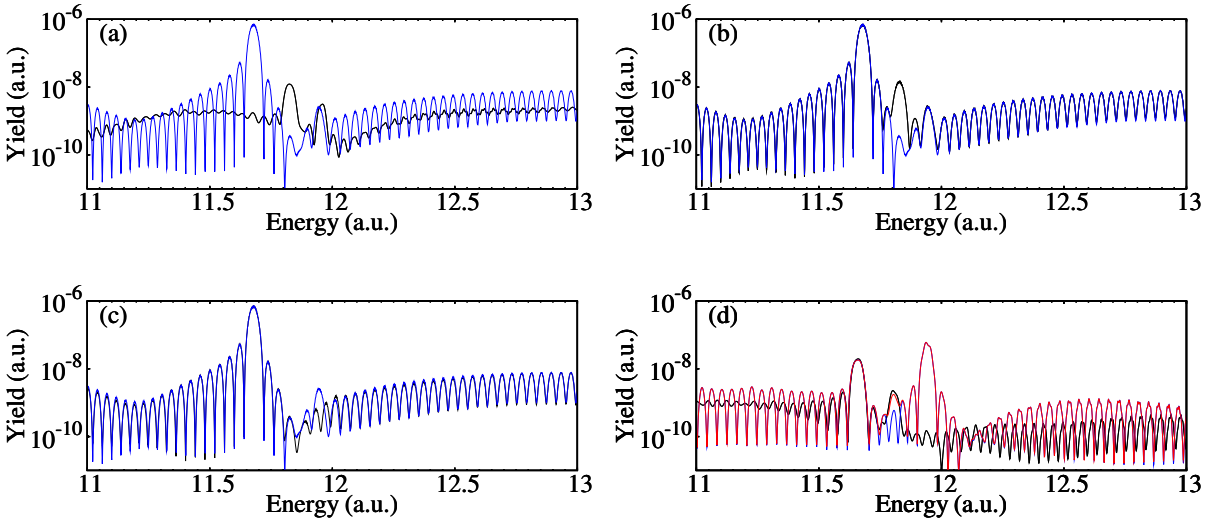

Figure 5.2: The forth peak of the ATI spectra of a model atom irradiated with a laser pulse of $\omega = 3.0$ and a peak electric field of $E_0 = 25$. (a) the first (b) the second and (c) the third light-induced state after the raising ramp are projected out. The reference peak is indicated with blue. (d) initially in the second excited state; (black) the third KH state after the ramp is projected out; (red) the second KH state after the ramp is projected out and (blue) indicates the reference spectrum.

ground state disappears) as one expects. At the same time, it is remarkable that the peak related to the first excited KH-state appears in this case. This indicates the existence of the direct ionization path from the first excited KH-state to the continuum, see path 1 in Fig. 5.3(b). However, there is another ionization path originating from the first excited state due to Raman stimulated coupling of the ground to the first excited states, shown in Fig. 5.3(a,b) by blue (gray) arrows. It proceeds to the continuum via the ground state, see the path 2 in Fig. 5.3(b).

In the second case, see Fig. 5.2(b), there is no initial population in the first excited KH-state. However, surprisingly, the peak corresponding to the ionization from this first excited state still persists, along with the expected peak from the ground state. This is due to no stimulated population transfer from the ground state to the first excited one (only an upward blue (gray) arrow in Fig. 5.3(b). One can conclude from these results that an additional path exists to the continuum which originates from the first excited state proceeding to the ground state and further to the continuum. Thus, there are two interfering paths ending up at the same continuum state: 1) direct transition from the first excited KH-state to the continuum and 2) transition from the first excited KH-state to the ground state and further to the continuum, see Fig. 5.3. The interference between the mentioned two paths to the continuum is destructive as it suppresses the ionization peak corresponding to the ionization from the second KH-state, see Fig. 5.2(a,b). Note that this interference is different from the one in the regime of the interference stabilization of Rydberg atoms [19]. In the interference stabilization regime, the different paths to the continuum from the different closely situated Rydberg states interfere because the

bandwidth of the energy levels exceeds the level spacing resulting in the suppression of ionization. While in the considered case, the levels are well separated and the interference arises due to the drift-induced transition which suppresses only the ionization from the specific KH-state. In the interference stabilization regime, the interference is the origin of the stabilization, while in the considered case the stabilization is a precondition to observe the interference effect in ATI spectra. In order to clarify the other possible couplings between bound dressed states, the third KH-state is projected out after the raising ramp and the ATI spectra at the end of the pulse is calculated and compared with the complete spectrum in Fig. 5.2(c). This figure shows no other interference signature with this initial condition.

However, the ATI spectra after the laser pulse for the 4^{th} photon absorption of a model atom initially in the second excited state is calculated and shown in Fig. 5.2(b). This figure shows that the peak from the second KH state appears by projecting out the third KH states after the ramp of the pulse. With this initial condition the main coupling is between n_2 and n_3 which induces interfering paths from these states.

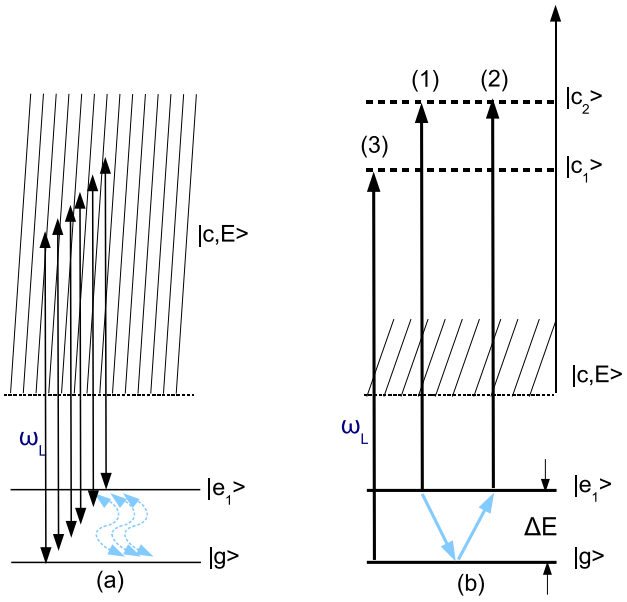

Figure 5.3: (a) Schematic energy-level diagram: two adjacent light induced bound states $|g\rangle, |e_1\rangle$ are coupled to a common continuum $|c, E\rangle$ which results in the Raman transitions and coherent population transfer between the bound dressed states. (b) Schematic for interfering ionization paths (1) and (2). The pathway (2) is mediated via Raman coupling as indicated in subfigure (a) (blue/gray arrows). Comparing with ATI spectra of Fig. 4.9, the first peak corresponds to the path (3), direct ionization from the ground state, and the second peak corresponds to the transition from the third bound state to the continuum which is not shown in (b).

In the last part of this section, we discuss how the changes of the fine structure of the spectral line, when some bound states are projected out after the ramp of the laser pulse (see Fig. 5.2), can be explained using the details of the modified drift motion and the

bound state population dynamics. Removing the population of one of the coupled bound states after the ramp of the laser field changes the time-profile of ionization. The time profile of the ionized WP with energy 4ω corresponding to the same peak in Fig. 5.2(a) for the case that the ground state is projected out, is shown in Fig. 5.4(a,b) and compared with the time profile of the population in the second KH-states. The ionization in the negative direction of the box is shown in (a) and in the positive direction in (b). One can see that the number of oscillations within the envelope of the time profile of the WP is half of that of Fig. 4.7, while the oscillation of the population of the first excited state is the same with a different amplitude and form. The phase of modulation of the ionization WP moving left are shifted by π with respect to that of right, in contrast to the case when all dressed bound states are contributing, see Fig. 4.7. Moreover, we observe the

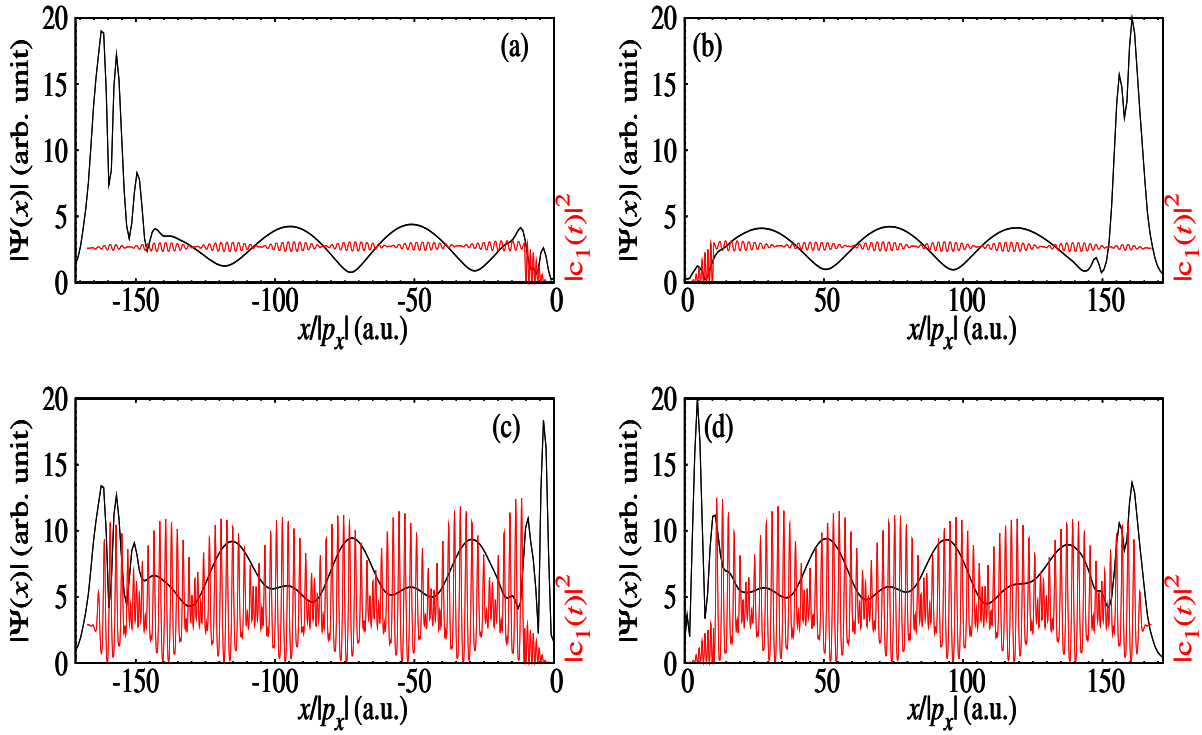

Figure 5.4: (black) the time-profile of the ionization probability of the electron WP of a 1D model atom $\varepsilon = 5\omega$ and $\sigma = 1.0$ for the system from which the first KH state after the ramp is projected out. The peak electric field is $E_0 = 25.0$ and the laser frequency is $\omega = 3.0$. (red) The time variation of the population of the second KH state. (a) positive and (b) negative direction. (c) and (d) are for the system from which the second KH state after the ramp is projected out.

following correlation between the drift motion and the enhancement of the ionization in the case when projecting out some of the bound states. When the WP drifts to one side, the ionization in the same side is larger than the one in the opposite side at the same moment. This can be explained inspecting the variation of the expectation value of the electron displacement, see Fig. 5.5. While the displacement is small at the turning points when no states are projected out ($\langle x \rangle \approx 0.01$), it is rather large when some states are projected out ($\langle x \rangle \approx 2$ in (b) or 0.2 in (c)). This can be the reason which creates the left-right asymmetry of the ionization WP in Fig. 5.4. However, the population transfer

between the bound states happens with the same probability irrespective of the drift direction. Consequently, the number of oscillations of the envelope of the ionization WP on each side is half of the oscillation of the population of the bound state. At last, the fast oscillation in Fig. 5.5(a,d) which is mainly due to the coupling of the first two KH-states with different parity vanishes in (b) and (c) by projecting out one of them. This figure shows that projecting out the population of one of the KH states, first KH state in (b), second KH state in (c) and third KH state in (d), after the ramp changes the time-profile of $< x >_{KH}$ which are more similar to the CTMC results (b-d blue line). However, the fast oscillation in Fig. 5.5(a,d) which is mainly due to the coupling of the first two KH states with different parity, is vanishes in (b) and (c) by projecting out one of them.

The time profile of the ionized WP with energy 4ω corresponding to the same peak in Fig. 5.2(b) for the case that the second KH-state is projected out, is shown in Fig. 5.4(c,d) and compared with the time profile of the population of the second KH-state. The relation between the number of the oscillations of the envelope of the time profile of the WP and oscillations of the population of the second light-induced state is similar to Fig. 5.4(a).

The couplings which are locked with the laser field are changed by projecting out one of the coupled states, afterwards the remaining electron WP oscillates in the box in bound states without compensation of the population transfer to the opposite direction of the box from the part of the WP which is projected out. Therefore, the population transfers between the states in one direction of the box and consequently, the time profile of the ionization and observables such as $< x >_{KH}$ show the same behavior. The population can be transferred between the two states in one direction of the box or in both directions. The latter occurs in the presence of the stimulated coupling locked with the laser pulse. The time profile of the ionization at $\varepsilon = 4\omega$ is compared in Fig. 5.6 with the expectation value of the electron displacement in the KH frame of a model atom irradiated by a laser pulse of frequency $\omega = 3$ and electric field $E = 25$. This figure shows that the time of the enhancement of the ionization corresponds to the turning point of the electron trajectory. The correspondence, however, is increased by projecting out one of the coupled states. In fact the ionization probability in each direction of the interaction region is proportional to the probability of the bound KH states in the same direction. The coupling of the KH states with $c_i \neq 0$ $(i > 0)$ or projecting out of one of the KH states after the ramp breaks the left-right symmetry of the distribution of the bound KH states. The ATI spectra after the laser pulse for the 4^{th} photon absorption of a model atom initially in a superposition of the ground and first excited states with $|c_{e_1}|^2$ equal to, red 0.002, green 0.004, blue 0.006, violet 0.008, light green 0.01, yellow 0.05, black 0.2 and brown 0.25 is shown in Fig. 5.7. The idea is to find a condition with zero population of the second KH state. The population dynamics of the second KH state shows fast oscillation of $2\omega_l$ if $c_1(0) = 0$ and ω if $c_1(0) \neq 0$. This oscillation can be derived approximately from a two level system representation. The solution of a two level system for the population with neglecting of the transition frequency compared to the present laser frequency $\omega << \omega_l$ reads

$$c_i = \alpha e^{iA(t)} + \beta e^{-iA(t)}, \tag{5.1}$$

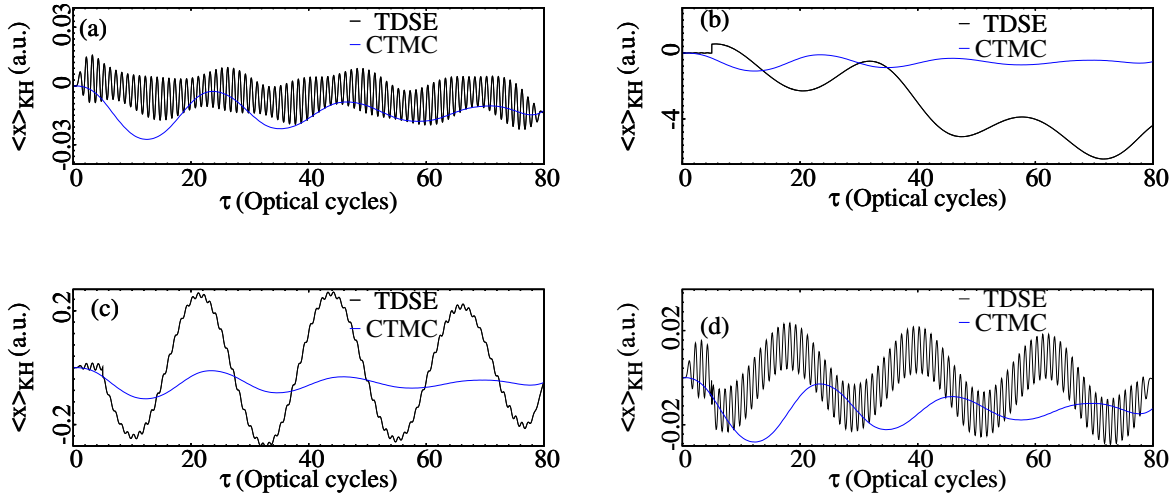

Figure 5.5: The expectation value of the electron displacement of a model atom irradiated by a laser pulse of frequency $\omega = 3.0$ a.u. and electric field $E = 25$ a.u. in the KH frame; (black) TDSE, (blue) CTMC; (a) no state is projected out, (b) first KH state (c) second KH state and (d) fourth KH state are projected out after the raising ramp of the laser pulse.

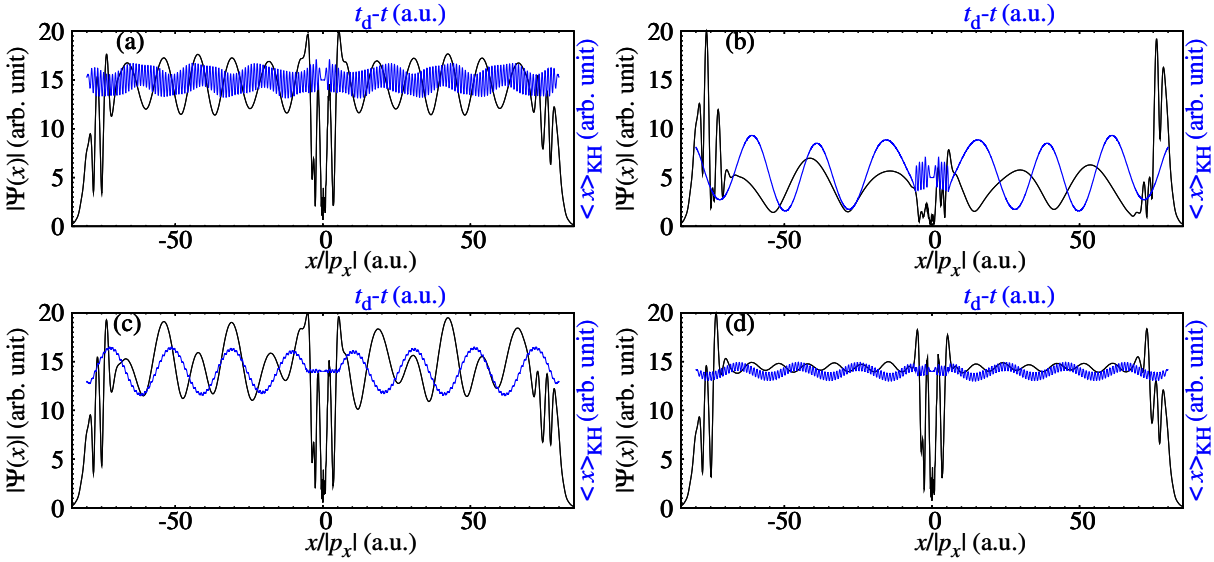

Figure 5.6: Time profile of the ionization at $\varepsilon = 4\omega$ (black) is compared with the scaled expectation value (blue) of the electron displacement of a model atom irradiated by a laser pulse of frequency $\omega = 3$ and electric field $E = 25$ in KH frame; (a) no state is projected out, (b) first KH-state (c) second KH-state and (d) third KH-state are projected out. The time is reversed for the negative direction. $< x >_{KH}$ is calculated with the bound part of WP.

which explains the fast oscillation of $|c_2(t)|^2$ i.e $2\omega_l$, but can not explain the fast oscillation of ω_l in the case of $c_2(0) \neq 0$ or $c_2(t_0) \neq 0$ where t_0 is the time after the ramp. However, a

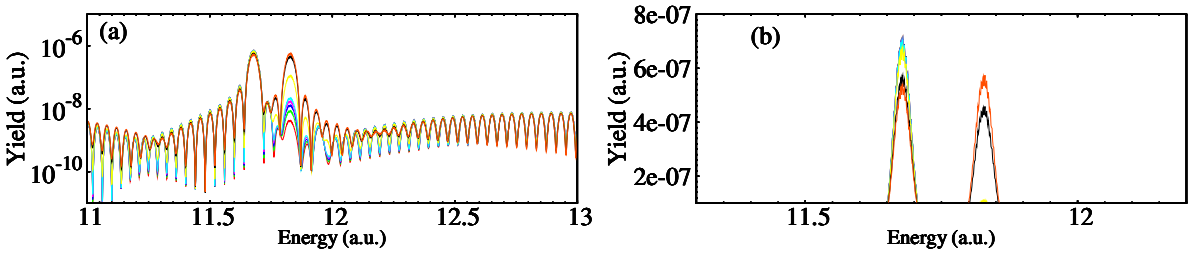

Figure 5.7: ATI spectra after the laser pulse for the 4^{th} photon absorption of a model atom initially in a superposition of the ground and first excited states. $|c_{e_1}|^2$ is set in red 0.002, green 0.004, blue 0.006, violet 0.008, light green 0.01 and yellow 0.05, black 0.2 and brown 0.25 with ($|c_g|^2 = 1 - |c_{e_1}|^2$).

solution of a two level system by a successive approximation up to the second order reads

$$\begin{aligned} c_1 &= c_1(0)e^{i\varphi}\cos(A(t)) - ic_2(0)e^{-i\varphi}\sin(A(t)) \\ c_2 &= c_2(0)e^{-i\varphi}\cos(A(t)) - ic_1(0)e^{i\varphi}\sin(A(t)), \end{aligned} \tag{5.2}$$

Where $A(t)$ is the vector potential of the laser field and φ is the phase induced by the laser field [123]. Eq. (5.2) explains qualitatively the fast oscillations of the population during the laser pulse due to the interfering term in $|c_2|^2$. We note that the rotating wave approximation is not valid if $\omega_l \gg \omega$. This time behavior shows that one can not completely remove the oscillation of the population and manipulate numerically completely the population transfer. However, one can change the time-profile with some manipulations during the interaction with a laser pulse (as we did by projecting out one of the coupled states). Alternatively, we have chosen the initial state as a superposition of the field free ground and first excited states to be reliable from experimental point of view. The initial contribution of the excited state changes the interference pattern by inducing an interference of the population of two states (similar to a two level system with $c_2(0) \neq 0$.). The change of the fast oscillations indicates that the type of the coupling and the type of the coherence is changed which opens an ionization channel from the second KH state. As can be seen, the intensity of the second peak is changed significantly for a large initial population of the excited state (i.e. $|c_{e_1}|^2 > 0.01$) and shows almost the same intensity like the first peak for $|c_{e_1}|^2 = 0.25$ in contradiction to the ratio of the initial populations. Moreover, from smaller cross section of photonabsorption of second KH state, one expects that the intensity of the corresponding peak must be smaller than the population ratio. The enhancement of the intensity of the second peak indicates that there is an open channel from the second KH state without interference. One can suppose that the destructive interference is cancelled out and the resulting ionization is added to the usual ionization (from the initial population) of this state. In addition, this figure shows that the ionization probability from the interfering paths is larger than the usual ionization which can be tested in the experiment.

5.3 Impact of the potential form

In all three cases the spectra (black) for the first four photoelectrons are compared with the same calculation when no state is projected out (blue). Although the power of the peak is smaller than the corresponding peak of the short range potential, it indicates the two coupled paths to the common continuum. In the case of a short range potential, although the power of the peak from the second KH state is suppressed significantly up to three photon numbers, it becomes larger than the peak from the third KH state after four photon numbers. First, according to multiphoton absorption and energy difference of final continuum from the threshold, the ionization probability decreases with increasing of the energy of the bound states. Second, the higher states show larger Rabi oscillation which means they are coupled to each other strongly and the related electron WP in this states spends more time in bound states consequently, the population in continuum states and final ionization probability decreases from the higher states. On the other hand, according to the two photon coupling ($\omega > I_P$) the probability of the ionization from the population transfer of two adjacent states (two paths) is higher than the ionization probability from the allowed population transfer. In the case of soft-Coulomb potential due to

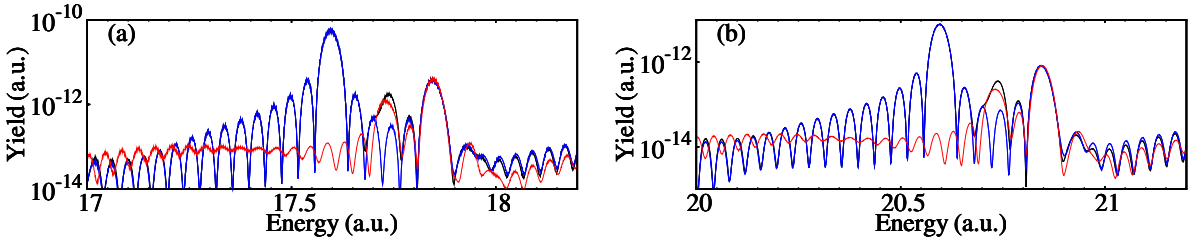

Figure 5.8: ATI spectra for the (a) 6^{th} and (b) 7^{th} photon absorption of a model atom with soft-Coulomb potential irradiated by a laser pulse of frequency $\omega = 3.0$ a.u. and electric field of $E = 25$. The laser pulse consists of 80 optical cycles with 5 cycle ramp. (red) The first and (black) the second KH state after the raising ramp are projected out, (blue) no state is projected out.

the infinite bound KH states the photoelectrons and continuum states couple stronger to the KH bound states compared with the short range potential. Therefore, not only the total ionization decreases with respect to the short-range potential, but also the power of the interfering peaks (ionized from the second KH state) are suppressed compared with the ionization from the third KH state. To prove this statement, the ATI spectra at 6 (Fig. 5.8(a)) and 7 (Fig. 5.8(b)) photoelectrons are calculated by projecting out the population of the first KH state (Fig. 5.8(red) and second KH state (Fig. 5.8(black) after the raising ramp of the laser pulse and compared with the spectra when no state is projected out (Fig. 5.8(blue)). In this figure the power of the peak corresponding to the ionization from the second KH state (second black peak and first red peak) enhances significantly with respect to the background, which shows that the higher continuum and related photoelectrons can weekly couple and recombine to the bound KH states during the interaction with the laser pulse.

Let us consider the time profile of the ionization during the constant part of the laser pulse. Due to the smaller energy difference of the higher KH states and bandwidth of the pulse, the higher KH states couple to each other with larger oscillation strength. The even states are populated at the beginning of the interaction with the laser pulse via build-up from the field free state. Therefore, the even-photon (two photon) transition couples to the even parity state (i.e $n_1 \longleftrightarrow n_3, n_1 \longleftrightarrow n_5, n_3 \longleftrightarrow n_5, \ldots$) with non-vanishing population. The states with different parity, however, couple (i.e $n_1 \longleftrightarrow n_2, n_1 \longleftrightarrow n_4, n_2 \longleftrightarrow n_3, n_2 \longleftrightarrow n_5, \ldots$) due to the higher order term of the potential. In addition the bandwidth of the laser pulse and the detuning, the allowed transitions have significant contribution to the couplings. The resulting couplings between the states induce the larger Rabi oscillation at higher bound states with the same parity and enhance the ionization probability from the forbidden transitions of the transferred WP. Therefor, the latter in the case of short range potential for the second KH is larger than the ionization from the third KH state due to the finite number of KH states. By projecting out the population of the third KH state after the raising ramp of the pulse, the corresponding peak vanishes (at the level of the background) in contrast to the population transfer to this state.

In addition to the photoelectrons ionized directly from the initially populated states via the build-up from the field free state, there is another photoelectron ionized from the population transfer. The latter shows larger probability for the forbidden transition when the channels are open.
The population, which contributes to the different ionization path to the final common continuum, oscillates between the states with a phase shift of half of an optical cycle.

5.4 Low frequency

In this section, we shortly discuss the considered effects of the drift, the bound population transfer and the interference in the ATI spectrum at intermediate frequencies $\omega \lesssim I_p$ when stabilization can still take place. The ATI spectra (spectral lines corresponding to single

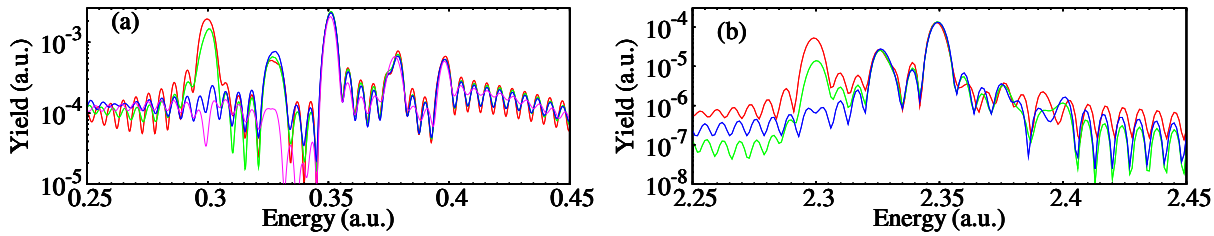

Figure 5.9: (a) 1^{st} and (b) 6^{th} peak in the ATI spectra of the model atom irradiated with a 80 cycle laser pulse with $E_0 = 2.4$, and $\omega = 0.4$. (red) all KH-states are included in the interaction within the flat part of the pulse, (green) first KH-state, (blue) first and second KH-state, (violet) first-third KH-state are projected out.

and six photon processes) for a model atom irradiated by a laser pulse with $\omega = 0.4$ and $E_0 = 2.4$, which is in the stabilization regime, are shown in Fig. 5.9. The peak positions correspond to the energies of the KH-states, the latter is indicated in Tab. 5.1. Note that the first peak results from the first two bound states as their energies are very close.

Table 5.1: Energy levels of the KH-states interacting with a laser pulse of $\omega = 0.4$ and $E_0 = 2.4$.

n	Energy	n	Energy	n	Energy
0	-1.033e-01	2	-7.348e-02	4	-2.449e-02
1	-1.021e-01	3	-5.215e-02	5	-2.745e-03

There is no distinct destructive interference as in the high frequency case. However, one can see the trace of this interference in the second peak of Fig. 5.9(a) and Fig. 5.9(b), noting the enhancement of the peak when projecting out the first two bound states. The latter means that the coherent population transfer is inefficient in the low frequency case. The time profile of the ionized WP is calculated and shown in Fig. 5.10. There

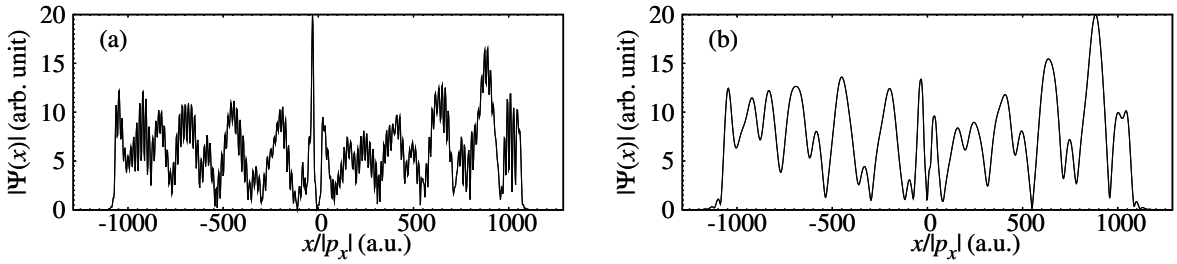

Figure 5.10: Time profile of the ionized WP with energy $\varepsilon = 4\omega$ for the same system as in Fig. 5.9. (a) $\sigma = 0.3$ and (b) $\sigma = 0.1$.

is enhancement of the ionization but they are decreasing in amplitude and are rather irregular. These features are probably connected with the higher ionization rate in the low frequency case, a large drift of the WP to one side during the rising ramp and comparable contributions to the ionization WP from many bound states. The population dynamics is shown in Fig. 5.11. From this figure, the trace of the drift induced population transfer can be seen which, however, is decreasing in amplitude and is irregular, similar to the ionization behavior of the WP. In the low frequency case $\omega < I_P$ the population dynamics of the KH states shows fast oscillations of ω in contrast to high frequency $\omega > I_P$. In fact in the low frequency case the population of the second or odd KH state can not be locked to $c_{e_1}(t_0)$ (t_0 here is the end of ramp) at a certain value which is necessary for the symmetric coupling with $c_{e_1}(0) = 0$. This is due to the DC part of the ramp with respect to the laser period in low frequency acting on the time evolution of the system.

5.5 Summary

The interferences on the photoelectron spectra at XUV lasers are studied. The quantum interference is complicated in the stabilization regime by formation and coupling of the

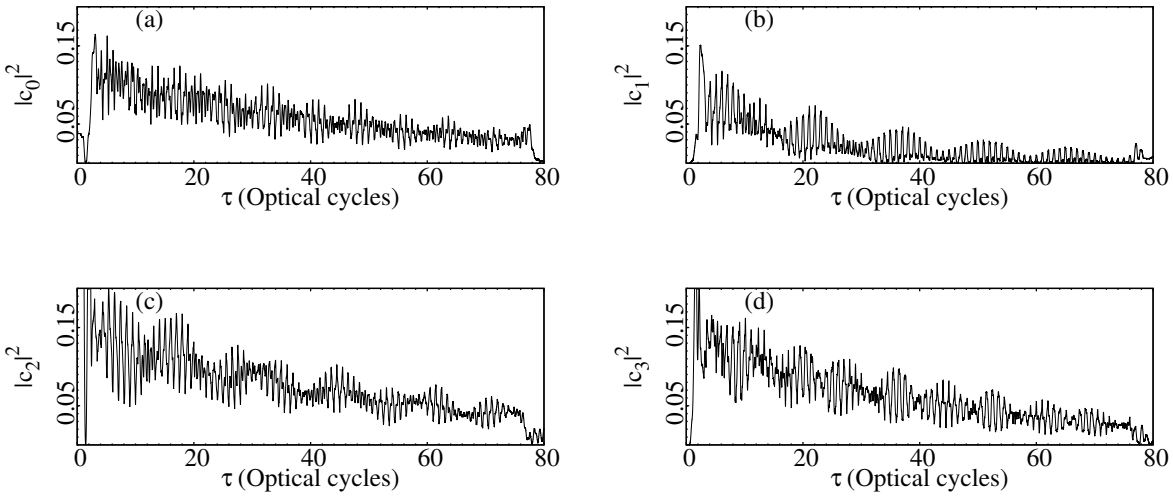

Figure 5.11: Time variation of the population dynamics of the bound KH-states. The peak electric field is $E_0 = 2.4$, the laser frequency $\omega = 0.4$ a.u. and the pulse length is 80 optical cycle including a 5-cycle ramp.

light induced states. In particular, a fine structure of a single ATI spectral line arises due to the interference of the ionization waves emitted at the rising and falling edges of a laser pulse in the stabilization regime. The low-energy continuous structure appears in the stabilization regime due to the ionization during the ramp of the pulse. It has been shown that there is a dramatic destructive quantum interference when the two adjacent KH states are coupled with an appropriate initial condition. The coupling of the KH states and the necessary conditions for the destructive interference happen when the frequency of the laser pulse is larger than the ionization potential.

Chapter 6

Conclusion

This work provided a systematic study of the fundamental quantum dynamics of atoms in high frequency laser pulses. Kinetic energy spectra of photo-electrons resulting from above-threshold ionization were calculated with high resolution for the model atoms for intensities from $10^{15}\,\mathrm{Wcm}^{-2}$ to $10^{20}\,\mathrm{Wcm}^{-2}$ at XUV laser frequencies which can be produced by free-electron laser facilities at Hamburg and Stanford. Our investigation was based on numerical solutions of the time-dependent Schrödinger and classical equations of motion. The main objective for these calculations is extracting the ionized electron wavepacket (quantum mechanically) or ionized trajectories (classically). In the quantum case the ionized wavepacket was obtained by a projection operator while in classical simulations ionized trajectories were identified by test of final energy of trajectories. In particular, we focused on strong field features of high intensity and high frequency ionization.

The first involves the comparison of ATI spectra at XUV lasers with its low frequency (IR) counterpart, when ionization processes are viewed from a tunnelling model. The tunnelling model is restricted to the low frequency laser field where a quasistatic assumption for the ionization is valid. The significant suppression of the ionization of the atoms at high frequency lasers has led to theories which suggest that the signatures known from the low-frequency domain are absent. However, there have not been clear and complete predictions of the rescattering and interferences at high frequency lasers where the ionization suppression in the stabilization regime would manifest itself as a dramatic suppression of the post-ionization dynamics. Our investigation, although for a model atom, clearly indicates the existence of a rescattering mechanism and its classical cut-off of ionized photoelectrons at XUV lasers, similar to the low-frequency tunneling domain. The classical trajectories are resolved for high energy photoelectrons similar to low frequency case. This similarity was proved by an energy-position phase space representation. The envelope of the ATI spectra, however does not show a plateau structure, which are thought to be caused by stabilization in high frequency lasers. Our simulation showed, moreover that the tail of Coulomb potential damps the rescattering probability in the ATI spectra.

Further calculation could increase our understanding of the detail of dynamics at high fre-

quency domain. A one dimensional model atom was taken in this work, more simulations of two and three dimensional model atoms would be desirable. While the energy spectra are expected to be rather insensitive to the dimensionality of the model, such advanced calculations could reveal differences in the angular distributions of the rescattered photoelectrons at XUV lasers and requires extensive three dimensional simulations. In addition, the degree of agreement could be more accurately tested with quantitative comparisons of electron yields in experiment. This would be an experimental and numerical challenge, but certainly within the realm of possibility.

The second focus of this work was on the time-analysis of ionization with certain resolution of kinetic energy spectra. An appropriate method was derived to reveal the temporal evolution of ionization during the interaction with a laser pulse. Our method relies on detailed analysis of the electron wave function at the end of the pulse. This work appears to be the first comprehensive, time resolved study of the ATI spectra in a high frequency laser field. We have used this time analysis from the final wavepacket as a general tool for studying the stabilization in a laser pulse with an arbitrary frequency within the wavepacket dynamic approach. The uncertainty principle, however, provides a fundamental limit to the time-energy resolution for quantum systems. Additionally, the time analysis of ionization shows a drift motion of the electronic wavepacket in the quantum mechanical ionization dynamics. It has also been shown by Grobe [120] that the stabilization in one dimension can be characterized by a drift motion of a single particle trajectory in the KH frame. This drift induces an oscillatory enhancement of ionization with a frequency equal to the energy gap between the first two KH states. Additionally, we proved this drift effect with an ensemble of particles via a Classical-Trajectory Monte Carlo simulation which represents a closer analogue to the quantum case than a single particle trajectory.

The stabilization of the atomic systems are still the subject of researches which recently was extended in two electron atom [124]. Our time analysis can be generalized as an evidence for the stabilization of few electron systems. In this work it has been shown that the dressed bound states at high frequency domain play significant role during the interaction. This manifests that the dynamics can be more complicated in two or few electron systems due to a correlated quantum dynamics. On the other hand the extraction of the photoelectron spectra from the final wavepacket with high resolution needs accurate representation of the man-body wavefunction during and at the end of interaction. However, this would be a theoretical challenge, which certainly needs a lot of effort.

The third part of this work was devoted to the interference of ionized photoelectrons from different channels at high frequency laser field in the stabilization regime. We used the time-analysis of ionization to investigate the interference in the stabilization regime in detail. In fact, the most interesting result of this investigation is a fully destructive interference between the ionization paths from the two lowest adjacent KH states. The two lowest KH states couple with Raman-type transition which induces two coupled ionization paths to the same continuum with a π difference in phases. This phase difference

induces a complete destructive interference. We introduced a numerical experiment to cancel this interference artificially and observe the ionized photoeletron from this channels. Our numerical experiment, however, can not be realized in laser laboratories, due to the fact that the light-induced states were artificially projected out. Further, we propose a realization of numerical experiment to show not only that there is this interference but also that this is a stimulated coupling. This can be done with an appropriate initial state preparation including the two lowest field free states with probability of 3:1.

As in low frequency case, above-threshold ionization and high-harmonic generation provide a unified picture of the competing processes of single electron dynamics in intense laser field. Altough these strong field processes are different, they can be used to understand the fine structure of the spectra resulting from the multiple bound-free state dynamics. As a complementing spectroscopic tool, investigation on the high harmonic emission will be helpful to explain the coherent coupling and resonances at high frequency regime where the calculation is easier than for ATI spectra especially for few-electron systems. In the case of HHG, the radiation spectra includes fine structure due to coupling of the bound states or correlated dynamics of few electron system. Additionally scaling of HHG at short wavelength (UV) lasers with photon energies in the range of 10-100 eV and available intensities ($10^{13} - 10^{22}\,\mathrm{Wcm}^{-2}$) is an objective of future work.

As most of the FEL pulses rely on self-amplification-spontaneous-emission (SASE) and have a chaotic structure, our study will be extended to simulations applying real experimental pulse shapes. The influence of the SASE FEL pulse shape on the harmonic yield shall be examined for different coherence times. Additionally, even harmonics will be examined with a SASE FEL pulse. As even harmonics need a coherent coupling of the light induced states in the stabilization regime and with a SASE pulse this may inhibit stabilization.

Bibliography

[1] T. H. Maiman, "Stimulated optical radiation in ruby," Nature (London) **187**, 493–494 (1960).

[2] P. A. Franken, A. E. Hill, C. W. Peters, and G. Weinreich, "Generation of optical harmonics," Phys. Rev. Lett. **7**, 118–119 (1961).

[3] D. Strickland and G. Mourou, "Compression of amplified chirped optical pulses," Opt. Commun. **56**, 219–221 (1985).

[4] A. McPherson, G. Gibson, H. Jara, U. Johann, T. S. Luk, I. A. McIntyre, K. Boyer, and C. K. Rhodes, "Studies of multiphoton production of vacuum-ultraviolet radiation in the rare gases," J. Opt. Soc. Am. B **4**, 595–601 (1987).

[5] X. F. L. G. M. M. Ferray, A. L'Huillier and C. Manus, "Multiple-harmonic conversion of 1064 nm radiation in rare gases," J. Phys. B **21**, L31 (1998).

[6] J. Arthur and *et. al*, *Linac coherent light source (LCLS): Conceptual design report*, SLAC-R-593, UC-414 (2002). http://www-ssrl.slac.stanford.edu/lcls/cdr, www-ssrl.slac.stanford.edu/lcls/cdr, http://hasylab.desy.de/facilities/flash/ http://www-xfel.spring8.or.jp/.

[7] G. S. Voronov and N. B. Delone, "Ionization of the xenon atom by the electric field of ruby laser emission," JETP **1**, 66 (1965).

[8] M. Göppert-Mayer, "You have full text access to this content über elementarakte mit zwei quantensprüngen," Ann. der Physik **9**, 273 (1931).

[9] P. Agostini, F. Fabre, G. Mainfray, G. Petite, and N. K. Rahman, "Free-free transitions following six-photon ionization of xenon atoms," Phys. Rev. Lett. **42**, 1127–1130 (1979).

[10] F. Krausz, "From femtochemistry to attophysics," Physics World **14**, 41 (2001).

[11] P. A. P. Saliéres, A. l'Huillier and M. Lewenstein, "Study of the spatial and temporal coherence of high-order harmonics," Adv. At. Mol. Opt. Phys. **41**, 83 (1999).

[12] P. J. Randerson, *Thesis, Fundamental Dynamics in High Intensity Laser Ionization* (The Ohio State University, 2005).

[13] A. M. Perelomov, V. S. Popov, and M. V. Terent'ev, "Ionization of atoms in an alternating electric field," Soviet Journal of Experimental and Theoretical Physics **23**, 924 (1966).

[14] N. B. D. M. V. Ammosov and V. P. Krainov, "Tunnel ionization of complex atoms and of atomic ions in an alternating electromagnetic field," Sov Phys JETP **64**, 1191–1194 (1986).

[15] M. Gavrila and J. Z. Kamiński, "Free-free transitions in intense high-frequency laser fields," Phys. Rev. Lett. **52**, 613–616 (1984).

[16] H. A. Kramers, "Collected scientific papers," North-Holland, Amsterdam p. 272 (1956).

[17] W. C. Henneberger, "Perturbation method for atoms in intense light beams," Phys. Rev. Lett. **21**, 838–841 (1968).

[18] M. Gavrila, "Atomic stabilization in superintense laser fields," J. Phys. B: At. Mol. Opt. Phys. **37**, R147 (2002).

[19] M. V. Fedorov, "Interference stabilisation of rydberg atoms in a strong laser field," Quantum Electronics **29**, 578 (1999).

[20] L. D. Noordam, H. Stapelfeldt, D. I. Duncan, and T. F. Gallagher, "Redistribution of rydberg states by intense picosecond pulses," Phys. Rev. Lett. **68**, 1496–1499 (1992).

[21] M. P. de Boer, J. H. Hoogenraad, R. B. Vrijen, R. C. Constantinescu, L. D. Noordam, and H. G. Muller, "Adiabatic stabilization against photoionization: An experimental study," Phys. Rev. A **50**, 4085–4098 (1994).

[22] Q. Su, J. H. Eberly, and J. Javanainen, "Dynamics of atomic ionization suppression and electron localization in an intense high-frequency radiation field," Phys. Rev. Lett. **64**, 862–865 (1990).

[23] V. C. Reed, P. L. Knight, and K. Burnett, "Suppression of ionization in superintense fields without dichotomy," Phys. Rev. Lett. **67**, 1415–1418 (1991).

[24] M. Gajda, J. Grochmalicki, M. Lewenstein, and K. Rzążewski, "Stabilization of atoms in ultrastrong laser fields: A classical approach," Phys. Rev. A **46**, 1638–1653 (1992).

[25] K. C. Kulander, K. J. Schafer, and J. L. Krause, "Dynamic stabilization of hydrogen in an intense, high-frequency, pulsed laser field," Phys. Rev. Lett. **66**, 2601–2604 (1991).

[26] L. You, J. Mostowski, and J. Cooper, "Suppression of ionization in one- and two-dimensional-model calculations," Phys. Rev. A **45**, 3203–3209 (1992).

[27] S. Geltman, "Comment on 'stabilization of a one-dimensional short-range model atom in intense laser fields'," J. Phys. B: At. Mol. Opt. Phys. **32**, 853 (1999).

[28] N. Yongfeng, *Thesis, From Strong Field Ionization to the Generation of Attosecond Laser Pulses* (FOM Institute for Atomic and Molecular Physics, 2006).

[29] S. Bauch, *Coulomb scattering and ionization processes in strong laser filds* (Universität zu Kiel, 2008).

[30] C. H. K. M. Protopapas and P. L. Knight, "Atomic physics with super-high intensity lasers," Rep. Prog. Phys. **60**, 389 (199).

[31] J. D. Jackson, *Classical Electrodynamics* (Akademic press, New York, 1999).

[32] H. B. V. L. van den Heuvell and H. G. Muller, *in Multiphoton Processes* (edited by S. J. Smith and P. L. Knight, page 25, Cambridge University Press, 1988).

[33] M. S. Z. Marlan O. Scully, *Quantum Optics* (Cambridge University Press, Cambridge, 1997).

[34] L. E. Ballentine, *Quantum Mechanics: A Modern Development* (World scientific, Singapore, 2000).

[35] L. V. Keldysh, "Ionization in the field of a strong electromagnetic wave," Soviet Physics JETP **20**, 1307 (1965).

[36] N. B. Delone and V. P. Krainov, "Ac stark shift of atomic energy levels," Phys.-Usp. **42**, 669 (1999).

[37] H. R. Reiss, "Limits on tunneling theories of strong-field ionization," Phys. Rev. Lett. **101**, 043002 (2008).

[38] G. Mainfray and C. Manus, "Multiphoton ionization of atoms," Rep. Prog. Phys. **54**, 1333 (1991).

[39] J. D.-R. P. Avan, C. Cohen-Tannoudji and C. Fabre, "Effect of high frequency irradiation on the dynamical properties of weakly bound electrons," Le Journal de Physique **37**, 993 (1976).

[40] N. V. Bordyung and V. P. Krainov, "Dynamic resonances in ultra-short laser pulses," Laser. Phys. Lett. **4**, 418 (2007).

[41] A. K. T. G. A. V. F. Markert, P. Würtz and H. Ott, "ac-stark shift and photoionization of rydberg atoms in an optical dipole trap," New J. Phys. **12**, 113003 (2010).

[42] P. Rosenbusch, S. Ghezali, V. A. Dzuba, V. V. Flambaum, K. Beloy, and A. Derevianko, "ac stark shift of the cs microwave atomic clock transitions," Phys. Rev. A **79**, 013404 (2009).

[43] V. Yanovsky, V. Chvykov, G. Kalinchenko, P. Rousseau, T. Planchon, T. Matsuoka, A. Maksimchuk, J. Nees, G. Cheriaux, G. Mourou, and K. Krushelnick, "Ultra-high intensity- 300-tw laser at 0.1 hz repetition rate," Opt. Express **16**, 2109–2114 (2008).

[44] L. F. DiMauro and P. Agostini, "Ionization dynamics in strong laser fields," Adv. At. Mol. Opt. Phys. **35**, 79 (1995).

[45] M. D. C. J. Joachain and N. Kylstra, "High-intensity laser-atom physics," Adv. At. Mol. Opt. Phys. **42**, 225 (2000).

[46] N. B. Delone and V. P. Krainov, *Multiphoton Processes in Atoms* (Springer-Verlag, New York, 1994).

[47] K. C. K. K. J. Schafer, "Theory of resonant multiphoton population transfer in xenon," Laser Phys. **7**, 740 (1997).

[48] R. R. Freeman, P. H. Bucksbaum, H. Milchberg, S. Darack, D. Schumacher, and M. E. Geusic, "Above-threshold ionization with subpicosecond laser pulses," Phys. Rev. Lett. **59**, 1092–1095 (1987).

[49] R. R. Jones and P. H. Bucksbaum, "Ionization suppression of stark states in intense laser fields," Phys. Rev. Lett. **67**, 3215–3218 (1991).

[50] D. B. D. B. Milosevic, G. G. Paulus and W. Becker, "Above-threshold ionization by few-cycle pulses," J. Phys. B: At. Mol. Opt. Phys. **39**, R203 (2006).

[51] H. G. Muller, "Tunneling excitation to resonant states in helium as main source of superponderomotive photoelectrons in the tunneling regime," Phys. Rev. Lett. **83**, 3158–3161 (1999).

[52] M. Razavy, *Quantum theory of tunneling* (World Scientific, Singapore, 2003).

[53] F. H. M. Faisal, "Multiple absorption of laser photons by atoms," J. Phys. B: At. Mol. Opt. Phys. **6**, L89 (1973).

[54] H. R. Reiss, "Effect of an intense electromagnetic field on a weakly bound system," Phys. Rev. A **22**, 1786–1813 (1980).

[55] S. Augst, D. Strickland, D. D. Meyerhofer, S. L. Chin, and J. H. Eberly, "Tunneling ionization of noble gases in a high-intensity laser field," Phys. Rev. Lett. **63**, 2212–2215 (1989).

[56] S. Augst, D. D. Meyerhofer, D. Strickland, and S. L. Chint, "Laser ionization of noble gases by coulomb-barrier suppression," J. Opt. Soc. Am. B **8**, 858–867 (1991).

[57] A. L'Huillier, P. Balcou, S. Candel, K. J. Schafer, and K. C. Kulander, "Calculations of high-order harmonic-generation processes in xenon at 1064 nm," Phys. Rev. A **46**, 2778–2790 (1992).

[58] H. Goldestein, *Classical mechanics* (Addison-Wesley, San Francisco, 2002).

[59] X. F. Li, A. L'Huillier, M. Ferray, L. A. Lompré, and G. Mainfray, "Multiple-harmonic generation in rare gases at high laser intensity," Phys. Rev. A **39**, 5751–5761 (1989).

[60] P. B. Corkum, "Plasma perspective on strong field multiphoton ionization," Phys. Rev. Lett. **71**, 1994–1997 (1993).

[61] K. J. S. K. C. Kulander and J. L. Krause, *in Super-intense laser-atom physics(SILAP III)* (edited by B. Piraux, volume 316, page 95, NATO,Plenum Press, New York, 1993).

[62] G. G. Paulus, W. Nicklich, H. Xu, P. Lambropoulos, and H. Walther, "Plateau in above threshold ionization spectra," Phys. Rev. Lett. **72**, 2851–2854 (1994).

[63] W. N. G. Paulus, W. Becker and H. Walther, "Rescattering effects in above-threshold ionization: a classical model," J. Phys. B: At. Mol. Opt. Phys. **27**, L703 (1994).

[64] B. Walker, M. Kaluza, B. Sheehy, L. F. DiMauro, P. Agostini, and M. Trahin, "Walker et al. reply:," Phys. Rev. Lett. **77**, 203 (1996).

[65] P. Hansch, M. A. Walker, and L. D. Van Woerkom, "Resonant hot-electron production in above-threshold ionization," Phys. Rev. A **55**, R2535–R2538 (1997).

[66] P. B. M. Hertlein and H. Muller, "Evidence for resonant effects in high-order ati spectra," J. Phys. B: At. Mol. Opt. Phys. **30**, L197 (1997).

[67] M. J. Nandor, M. A. Walker, L. D. Van Woerkom, and H. G. Muller, "Detailed comparison of above-threshold-ionization spectra from accurate numerical integrations and high-resolution measurements," Phys. Rev. A **60**, R1771–R1774 (1999).

[68] H. G. Muller and F. C. Kooiman, "Bunching and focusing of tunneling wave packets in enhancement of high-order above-threshold ionization," Phys. Rev. Lett. **81**, 1207–1210 (1998).

[69] H. Muller, "Non-sequential double ionization of helium and related wave-function dynamics obtained from a five-dimensional grid calculation." Opt. Express **8**, 417–424 (2001).

[70] J. Wassaf, V. Véniard, R. Taïeb, and A. Maquet, "Strong field atomic ionization: Origin of high-energy structures in photoelectron spectra," Phys. Rev. Lett. **90**, 013003 (2003).

[71] B. Sheehy, J. D. D. Martin, L. F. DiMauro, P. Agostini, K. J. Schafer, M. B. Gaarde, and K. C. Kulander, "High harmonic generation at long wavelengths," Phys. Rev. Lett. **83**, 5270–5273 (1999).

[72] J. Tate, T. Auguste, H. G. Muller, P. Salières, P. Agostini, and L. F. DiMauro, "Scaling of wave-packet dynamics in an intense midinfrared field," Phys. Rev. Lett. **98**, 013901 (2007).

[73] A. C. B. Shan and Z. Chang, "Tunable high harmonic generation with an optical parametric amplifier," Applied Physics B: Lasers and Optics **74**, s23 (2002).

[74] B. Shan and Z. Chang, "Dramatic extension of the high-order harmonic cutoff by using a long-wavelength driving field," Phys. Rev. A **65**, 011804 (2001).

[75] Petrissa Eckle *et al.*, "Attosecond angular streaking," Nature Physics **4**, 565 (2008).

[76] B. Schenkel, J. Biegert, U. Keller, C. Vozzi, M. Nisoli, G. Sansone, S. Stagira, S. D. Silvestri, and O. Svelto, "Generation of 3.8-fs pulses from adaptive compression of a cascaded hollow fiber supercontinuum," Opt. Lett. **28**, 1987–1989 (2003).

[77] G. Farkas and C. Toth, "Proposal for attosecond light pulse generation using laser induced multiple-harmonic conversion processes in rare gases," Phys. Lett. A **168**, 447 (1992).

[78] J. M. S. Harris and T. Hansch, "Atomic scale temporal structure inherent to high-order harmonic generation," Opt. Commun. **100**, 487 (1993).

[79] P. Antoine, A. L'Huillier, and M. Lewenstein, "Attosecond pulse trains using high–order harmonics," Phys. Rev. Lett. **77**, 1234–1237 (1996).

[80] M. Bellini, C. Lyngå, A. Tozzi, M. B. Gaarde, T. W. Hänsch, A. L'Huillier, and C.-G. Wahlström, "Temporal coherence of ultrashort high-order harmonic pulses," Phys. Rev. Lett. **81**, 297–300 (1998).

[81] M. B. Gaarde, F. Salin, E. Constant, P. Balcou, K. J. Schafer, K. C. Kulander, and A. L'Huillier, "Spatiotemporal separation of high harmonic radiation into two quantum path components," Phys. Rev. A **59**, 1367–1373 (1999).

[82] C. Lyngå, M. B. Gaarde, C. Delfin, M. Bellini, T. W. Hänsch, A. L' Huillier, and C.-G. Wahlström, "Temporal coherence of high-order harmonics," Phys. Rev. A **60**, 4823–4830 (1999).

[83] D. G. Lee, J.-H. Kim, K.-H. Hong, and C. H. Nam, "Coherent control of high-order harmonics with chirped femtosecond laser pulses," Phys. Rev. Lett. **87**, 243902 (2001).

[84] M. Ivanov, P. B. Corkum, T. Zuo, and A. Bandrauk, "Routes to control of intense-field atomic polarizability," Phys. Rev. Lett. **74**, 2933–2936 (1995).

[85] P. Antoine, D. B. Milošević, A. L'Huillier, M. B. Gaarde, P. Salières, and M. Lewenstein, "Generation of attosecond pulses in macroscopic media," Phys. Rev. A **56**, 4960–4969 (1997).

[86] D. G. Lappas and A. L'Huillier, "Generation of attosecond xuv pulses in strong laser-atom interactions," Phys. Rev. A **58**, 4140–4146 (1998).

[87] M. G. M. L. A. L. A. P. P. Antoine, B. Carr and P. Salires, "Gnration d'harmoniques d'ordre lev dans les gaz : rsultats rcents," Annales de Physique **22**, 45 (1997).

[88] O. Tcherbakoff, E. Mével, D. Descamps, J. Plumridge, and E. Constant, "Time-gated high-order harmonic generation," Phys. Rev. A **68**, 043804 (2003).

[89] Z. Chang, "Single attosecond pulse and xuv supercontinuum in the high-order harmonic plateau," Phys. Rev. A **70**, 043802 (2004).

[90] R. L.-M. et al., "Characterization of high-order harmonic radiation on femtosecond and attosecond time scales," Appl. Phys. B **78**, 835 (2004).

[91] K. J. Schafer and K. C. Kulander, "High harmonic generation from ultrafast pump lasers," Phys. Rev. Lett. **78**, 638–641 (1997).

[92] I. P. Christov, H. C. Kapteyn, and M. M. Murnane, "Comment on "sub-10-fs mirror-dispersion-controlled ti:sapphire laser" and "ultrabro adband ring oscillator for sub-10-fs pulse generation"," Opt. Lett. **22**, 1882–1883 (1997).

[93] M. D. et al., "X-ray pulses approaching the attosecond frontier," Science **291**, 1923 (2001).

[94] M. D. et al., "Attosecond metrology," Nature **414**, 509 (2001).

[95] A. B. et al., "Attosecond control of electronic processes by intense light fields," Nature **421**, 611 (2003).

[96] H. G. Muller, "Suppression of angular-momentum mixing in precision solutions of the schrödinger equation for photoexcitation of rydberg states," Phys. Rev. A **65**, 055402 (2002).

[97] S. A. Aseyev, Y. Ni, L. J. Frasinski, H. G. Muller, and M. J. J. Vrakking, "Attosecond angle-resolved photoelectron spectroscopy," Phys. Rev. Lett. **91**, 223902 (2003).

[98] S. Gasirowics, *Quantum Physics* (John Wiley and sons, Inc., 1996).

[99] H. R. Reiss, "Effect of an intense electromagnetic field on a weakly bound system," Phys. Rev. A **22**, 1786–1813 (1980).

[100] D. B. P. Mulser, *High Power Laser-Matter Interaction* (Springer, Berlin, 2010).

[101] S. V. Popruzhenko, G. G. Paulus, and D. Bauer, "Coulomb-corrected quantum trajectories in strong-field ionization," Phys. Rev. A **77**, 053409 (2008).

[102] D. G. Arbó, J. E. Miraglia, M. S. Gravielle, K. Schiessl, E. Persson, and J. Burgdörfer, "Coulomb-volkov approximation for near-threshold ionization by short laser pulses," Phys. Rev. A **77**, 013401 (2008).

[103] P. M. V.D. Rodrigueza and D. Arbo, "Resonant-enhanced above-threshold ionization of atoms by xuv short laser pulses," Nuclear Instruments and Methods in Physics Research Section B p. 334 (2009).

[104] R. Ramachandran and R. G. Griffin, "Multipole-multimode floquet theory in nuclear magnetic resonance," J. Chem. Phys. **122**, 164502 (2005).

[105] R. R. Freeman and P. H. Bucksbaum, "Investigations of above-threshold ionization using subpicosecond laser pulses," J. Phys. B: At. Mol. Opt. Phys. **24**, 325 (1991).

[106] V. O. N. L. Manakov and L. Rapoport, "Atoms in a laser field," Physics Reports **6**, 319 (1986).

[107] M. Gavrila, I. Simbotin, and M. Stroe, "Low-frequency atomic stabilization and dichotomy in superintense laser fields from the high-intensity high-frequency floquet theory," Phys. Rev. A **78**, 033404 (2008).

[108] H. G. Muller, "An efficient propagation scheme for the time-dependent schrdinger equation in the velocity gauge," Laser Phys. **9**, 138 (1999).

[109] D. Bauer, "Emergence of classical orbits in few-cycle above-threshold ionization of atomic hydrogen," Phys. Rev. Lett. **94**, 113001 (2005).

[110] R. S. Varga, *Matrix Iterative Analysis* (Prentice-Hall, Englewood Cliffs, N. J., 1962).

[111] J. A. F. M. D. Feit and A. Steiger, "Solution of the schrdinger equation by a spectral methodstar, open," Journal of Computational Physics **47**, 412 (1982).

[112] C. Bottcher, M. R. Strayer, A. S. Umar, and P.-G. Reinhard, "Damped relaxation techniques to calculate relativistic bound states," Phys. Rev. A **40**, 4182–4189 (1989).

[113] K. Toyota, O. I. Tolstikhin, T. Morishita, and S. Watanabe, "Siegert-state expansion in the kramers-henneberger frame: Interference substructure of above-threshold ionization peaks in the stabilization regime," Phys. Rev. A **76**, 043418 (2007).

[114] K. Toyota, O. I. Tolstikhin, T. Morishita, and S. Watanabe, "Slow electrons generated by intense high-frequency laser pulses," Phys. Rev. Lett. **103**, 153003 (2009).

[115] K. J. Schafer and K. C. Kulander, "Energy analysis of time-dependent wave functions: Application to above-threshold ionization," Phys. Rev. A **42**, 5794–5797 (1990).

[116] Y. I. S. *et al.*, "Relativistic high-power lasermatter interactions," Phys. Reports p. 41 (2006).

[117] I. C. P. R. Abrines, "Classical theory of charge transfer and ionization of hydrogen atoms by protons," Proc. Phys. Soc. **88**, 861 (1966).

[118] M. Gavrila, *Atoms in Intense Laser Fields* (Academic, New York, 1992).

[119] H. Miyagi and K. Someda, "Unified view of low- and high-frequency regimes of atomic ionization in intense laser fields," Phys. Rev. A **80**, 023416 (2009).

[120] R. Grobe and C. K. Law, "Stabilization in superintense fields: A classical interpretation," Phys. Rev. A **44**, R4114–R4117 (1991).

[121] M. Pont and M. Gavrila, "Stabilization of atomic hydrogen in superintense, high-frequency laser fields of circular polarization," Phys. Rev. Lett. **65**, 2362–2365 (1990).

[122] Z. Zhou and J. Yuan, "Fine structures of the harmonic and hyper-raman spectrum of the hydrogen atom in an intense high-frequency laser pulse," Phys. Rev. A **77**, 063411 (2008).

[123] P. B. C. M. Yu. Ivanov and P. Dietrich, "Coherent control and collapse of symmetry in a two-level system in an intense laser field," Laser Phys. **3**, 375 (1993).

[124] T. Birkeland, R. Nepstad, and M. Førre, "Stabilization of helium in intense xuv laser fields," Phys. Rev. Lett. **104**, 163002 (2010).

Acknowledgment

First of all, I express my gratitude to Prof. Christoph Keitel for giving me the opportunity to carry out this exciting research work in his group at Max-Planck-Institut für Kernphysik and for his tireless effort to provide ideal conditions for research.

Secondly, I would like to thank the members of my defense committee, Prof. Thomas Gasenzer, Prof. Selim Jochim and Prof. Klaus Pfeilsticker for their comments and advices.

In addition I would like to thank Prof. Ria Broer, Prof. Robert van Leeuwen and Dr. Paul de Boeij for their main contribution in my success within the field of physics.

Special thanks go to Peter Brunner for his support whenever needed, and to Markus Kohler, he was extremely helpful all the time.

I would like to thank Prof. Dieter Bauer, Dr. Jörg Evers, Prof. Piero Decleva, Dr. Erik Lötstedt for their important comments about theoretical techniques.

Also I thank Dr. Carsten Müller, Dr. Ben King, Dr. Matthias Ruf, Dr. Christian Buth, Benjamin Galow and Sven Augustin for thoroughly proofreading this thesis and their nice comments.

Moreover, I am especially grateful for the friendship of Dr. Octavian Postavaru and Dr. Bennaceur Najjari.

I acknowledge other colleagues and office-mates, especially Héctor Castañeda Cortés, Anis Dadi, Gabor Darvasi and Atif Shahbaz.

Last but not least, I would like to thank my parents that they provided everything for my education.

Erklärung

Diese Arbeit ist von mir selbstständig verfasst worden, und ich habe keine anderen als die angegebenen Quellen und Hilfsmittel benutzt.

Heidelberg, 18. April 2011 .....

Unterschrift